UNIVERSITY OF CAPE TOWN

DOCTORAL THESIS

Downstream evolution of ocean properties and associated fluxes in the Greater Agulhas Current System: Ad hoc Argo experiments and modeling

Author:
Tamaryn Morris

Supervisors:
Prof. Isabelle Ansorge
Prof. Juliet Hermes
Dr. Borja Aguiar González
Dr. Tarron Lamont

A thesis submitted in fulfillment of the requirements for the degree of Doctor of Philosophy

in the

Department of Oceanography

Declaration of Authorship

I, Tamaryn Morris, declare that this thesis titled, **Downstream evolution of ocean properties and associated fluxes in the Greater Agulhas Current System: Ad hoc Argo experiments and modeling**, and the work presented in it are my own. I confirm that:

- This work was done wholly while in candidature for a research degree at the University of Cape Town.
- Where I have consulted the published work of others, this is always clearly attributed.
- I have acknowledged all main sources of help.
- Where the thesis is based on work done by myself jointly with others, I have made clear exactly what was done by others and what I have contributed myself.
- I confirm that I have been granted permission by the University of Cape Town Doctoral Degrees Board to include the following publication(s) in my PhD thesis, and where co-authorships are involved, my co-authors have agreed that I may include the publication(s):

  Chapter 2: Morris T. and Lamont T. 2019. Using ocean robots on high-resolution profiling to capture the fast-flowing Agulhas Current. South African Journal of Science, 115 (1/2). DOI:10.17159/sajs.2019/5523

  Contributions:

  - Study idea: T.M. (80%), T.L.
  - Study design: T.M. (80%), T.L.
  - Data collection: T.M. (80%), T. L.
  - Data analysis: T.M. (75%), T.L.
  - Manuscript writing: T.M. (75%), T.L.
  - Manuscript revision: T.M. (60%), T.L.

  Chapter 4: Morris T., Aguiar González B., Ansorge I. and Hermes J. 2019. Lagrangian Evolution of Two Madagascar Cyclonic Eddies: Geometric Properties, Vertical Structure and Fluxes. Journal of Geophysical Research: Oceans, 124. DOI:10.1029/2019JC015090

  Contributions:

  - Study idea: T.M.
  - Study design: T.M.

- Data collection: T.M.
- Data analysis: T.M. (65%), B.A-G
- Manuscript writing: T.M. (70%), B.A-G
- Manuscript revision: T.M. (70%), B.A-G, J.H., I.A.

Chapter 5: Morris T., Aguiar González B., Ansorge I. and Hermes J. In Review.. Downstream evolution of hydrographic properties and fluxes of the Agulhas Current. Submitted to Journal of Geophysical Research: Oceans.

Contributions:

- Study idea: T.M. (50%), T.L.
- Study design: T.M. (50%), T.L.
- Data collection: T.M. (50%), T.L.
- Data analysis: T.M. (75%), B.A-G, T.L., J.H.
- Manuscript writing: T.M. (75%), B.A-G, T.L., J.H.
- Manuscript revision: T.M. (75%), B.A-G, T.L., J.H.

Signed: Signed by candidate

Date: 15 October 2020

"Life is not easy for any of us. But what of that? We must have perseverance and above all confidence in ourselves. We must believe that we are gifted for something and that this thing must be attained."

Marie Curie

Dedicated to

Haley, my inspiration
Mark, my motivation

Abstract

Downstream evolution of ocean properties and associated fluxes in the Greater Agulhas Current System: Ad hoc Argo experiments and modeling

Tamaryn Morris

The evolution of cyclonic eddies across the Southern Mozambique Chanel and the downstream evolution of the Agulhas Current was investigated using Argo floats, in combination with output from ocean general circulation reanalysis models. Two dedicated experiments were undertaken in April and July 2013, whereby eight floats were deployed within two separate cyclonic eddies. Floats were set to either daily and five-daily profiling from 1000 db to the surface, with park depths ranging from 300 db to 1000 db. The two cyclonic eddies propagated southwestward across the Mozambique Channel from southwest Madagascar to the KwaZulu-Natal Bight, a distance of approximately 1300 km, in approximately 130 days at a mean speed of 0.13 m s^{-1}. Estimates indicate the April (July) eddy showed mean trapped depths of 595 $\pm$ 294 m (914 $\pm$ 107 m), volume transport of 13.4 $\pm$ 5.2 Sv (21.2 $\pm$ 9.1 Sv), heat flux of -0.07 $\pm$ 0.06 PW (-0.2 $\pm$ 0.09 PW) and freshwater flux of 0.04 $\pm$ 0.04 Sv (0.09 $\pm$ 0.05 Sv). These results highlight the role of Madagascar cyclonic eddies as transporters of cooled and freshened source waters into the Agulhas Current.

During a third experiment, six floats were deployed in the Agulhas Current, and exited the current within 9 - 12 days at mean speeds of 0.51 – 0.76 m s^{-1}. An evolution of properties was shown from north to south for both Argo data and model output; for volume transport (16.76 – 38.18 Sv; 17.70 – 32.51 Sv), heat fluxes (0.85 – 1.79 PW; 0.99 – 1.91 PW) and salt fluxes (0.60 – 1.37 x 10^{12} kg s^{-1}; 0.63 – 1.17 x 10^{12} kg s^{-1}). This study illustrates the first near-real time survey of the Agulhas Current, and a potential method of quasi-synoptic surveys using Argo float technology.

These experiments highlight alternative methods of studying regions of turbulence by altering the mission parameters of Argo floats. Increased observations of eddies and Western Boundary Currents are critical to our understanding of the global oceans and impacts on the earths climate. Even more so for the understudied Indian Ocean.

Thesis publications at a glance

As a note to the examiners: While every effort was made to avoid repetition within the thesis, there exists some overlap of information around data, Argo deployments and methodology.

Paper 1 (Chapter 2): Using ocean robots on high-resolution profiling to capture the fast-flowing Agulhas Current.

Aim: Describe five ad hoc Argo float experiments on higher sampling resolution in the source region of- and within the Agulhas Current.

Method: Deployment of Argo floats on daily and five-daily sampling frequency with varying park depths.

Conclusions:

- The paper highlights detailed process studies undertaken on cyclonic (and anti-cyclonic) mesoscale eddies in the southern Mozambique Channel, and within the Agulhas Current.
- The studies increased Argo profiles in a traditionally understudied region.
- The studies suggest possible adaptations to future ocean observation strategies.

Paper 2 (Chapter 4): Lagrangian evolution of two Madagascar cyclonic eddies: Geometric properties, vertical structure and fluxes.

Aim: Improved understanding of the cyclonic eddy contribution of volume, heat and salt transport from south of Madagascar to the Agulhas Current.

Method: Deployment of Argo floats on daily and five-daily frequency with varying park depths in two unrelated cyclonic eddies spawned off the South-East Madagascar Current.

Conclusions:

- First study of the 3-D Lagrangian evolution of Madagascar cyclonic eddies
- Madagascar cyclonic eddies transport about 17.3 $\pm$ 7.9 Sv, with heat and freshwater fluxes of -0.1 $\pm$ 0.08 PW and 0.07 $\pm$ 0.05 Sv, per eddy
- Ad hoc Argo experiments provide valuable insight into the evolution of subsurface mesoscale dynamics

Paper 3 (Chapter 5): Downstream evolution of hydrographic properties and fluxes of the Agulhas Current.

Aim: Investigate the volume, heat and salt transport of the Agulhas Current in a near-real time synoptic survey.

Method: Deployment of six Argo floats on a daily park and profile mission off Port Edward, across the Agulhas Current.

Conclusions:

- First near-real time observations of the downstream evolution of hydrographic properties and fluxes of the Agulhas Current
- Good agreement between daily Argo profiles and model output
- Argo floats on daily profiling provide a valuable quasi-synoptic tool to study Western Boundary Currents

Acknowledgements

- Firstly, I need to thank my supervisors and co-authors on the publications stemming from this work: Dr. Borja Aguiar-González, Dr. Tarron Lamont, Prof. Juliet Hermes and Prof. Isabelle Ansorge.
- Prof. Michael Roberts for dancing the Argo Dance and coming up with the initial idea for this project.
- Argo floats were donated for this project by three institutions: Woods Hole Oceanographic Institution, the UK Met Office and the Euro-Argo ERIC MOCCA Project. The MOCCA project received funding from the European Maritime and Fisheries Fund (EMFF) under grant agreement No. EASME/EMFF/2015/1.2.1.1/SI2.709624.
- Argo floats were deployed from the Research Vessel *Algoa* on three separate research cruises. I would like to thank the Master(s), crew and scientific teams onboard these cruises for their assistance in getting floats in to the water.
- I feel one of the greatest achievements from this PhD is my skill development in terms of Matlab coding. This would not have been possible without the help (and endless patience) of Dr. Borja Aguiar-González, Dr. Charine Collins and Mr. Jethan d'Hotman.
- Funding in the form of University fees, publication costs and travel to present PhD results at conferences and meetings was received from the University of Cape Town (UCT), the South African Environmental Observation Network (SAEON) and the South African Weather Service (SAWS).
- With regards the work which has been published at the time of submission of the PhD, I would like to thank the anonymous reviewers and scientific journal teams for the assistance with the manuscripts.
- Finally, without the support, patience and dedication of my family, this PhD would never have become a reality. Over the time this thesis has taken, we lost our tiny nephew, our long-ill father and a dear uncle. But I made my husband an honest man, gained an extended family, gave birth to our daughter, and welcomed our nephew and niece to the world. Thank you for the sanity and realism. Mom, I danced and my crown is on straight, just like you xxx

Contents

List of Figures

List of Tables

List of Abbreviations

AAIW	**A**nt**a**rctic **I**ntermediate **W**ater
ACT	**A**gulhas **C**urrent **T**imeseries
ACEP	**A**frican **C**oelacanth **E**cosystem **P**rogram
ADCP	**A**coustic **D**oppler **C**urrent **P**rofiler
ADT	**A**bsolute **D**ynamic **T**opography
AHA	**A**vailable **H**eat **A**nomaly
AMOC	**A**tlantic **M**eridional **O**verturning **C**irculation
ASLOW	**A**rabian **S**ea **L**ow **O**xygen **W**ater
ASA	**A**vailable **S**alt **A**nomaly
AVHRR	**A**dvanced **V**ery-**H**igh-**R**esolution **R**adiometer
CTD	**C**onductivity **T**emperature **D**epth Instrument
EKE	**E**ddy **K**inetic **E**nergy
EMC	**E**ast **M**adagascar **C**urrent
ENSO	**E**l **N**iño **S**outhern **O**scillation
ICW	**I**ndian **C**entral **W**ater
KZN	**K**wa**Z**ulu-**N**atal
L-ADCP	**L**owered-**ADCP**
MC	**M**ozambique **C**hannel
NADW	**N**orth **A**tlantic **D**eep **W**ater
NEMC	**N**orth **E**ast **M**adagascar **C**urrent
NKZN	**N**orthern **K**wa**Z**ulu-**N**atal
PW	**P**eta-**W**att (10^{15} W)
RSW	**R**ed **S**ea **W**ater
ROMS	**R**egional **O**cean **M**odeling **S**ystem
SAMW	**S**ub-**A**ntarctic **M**ode **W**ater
SEC	**S**outh **E**quatorial **C**urrent
SEISAMW	**S**outh**e**ast **I**ndian **S**ub-**A**ntarctic **M**ode **W**ater
SEMC	**South E**ast **M**adagascar **C**urrent
SICC	**S**outh **I**ndian Ocean **Counterc**urrent
SICW	**S**outh **I**ndian **C**entral **W**ater
SLA	**S**ea **L**evel **A**nomaly
SSHA	**S**ea **S**urface **H**eight **A**nomaly
STSW	**S**ub-**T**ropical **S**urface **W**ater
Sv	**S**verdrup (1 Sv = 10^6 m^3 s^{-1})
SWIM	**S**outh-**W**est **I**ndian Ocean **M**odel
SWIO	**S**outh-**W**est **I**ndian Ocean **O**cean
THC	**T**hermo**h**aline **C**irculation
TSW	**T**ropical **S**urface **W**ater
UTR	**U**nderwater **W**ater **T**emperature Sensor
WBC	**W**estern **B**oundary **C**urrent
WMO	**W**orld **M**eteorological **O**rganisation
WOCE	**W**orld **O**cean **C**irculation **E**xperiment

Chapter 1

General Introduction

1.1 Introduction

The recent Intergovernmental Panel on Climate Change (IPCC) Assessment Report highlights that approximately 90% of the heat generated from global warming has been captured by the ocean (Rhein et al., 2013), which results in thermal expansion and sea-level rise. In addition to this, recent studies have shown the Indian Ocean to be warming basin-wide consistently over the last century (Roxy et al., 2014), with the tropical Indian Ocean increasing by more than 1° C at the surface. This surface warming at the tropics of the Indian Ocean is between 50 and 60% greater than other tropical regions and exceeds natural variability (Hu and Fedorov, 2019). A warm water pool dominates over the Eastern Indian Ocean, which has expanded over the last few decades (Roxy et al., 2014; Rao et al., 2012). Anomolous anticyclonic wind stress curl, triggered by anomolous easterlies and Indian Ocean Dipole events, results in downwelling oceanic Rossby Waves propagating across the Indian Ocean towards the west (Rao et al., 2012). This is turn results in a deeper thermocline and the advection of warmer waters in to the Greater Agulhas Current System (Rao et al., 2012). This system, which spans the currents' source water regions of the South West Indian Ocean, through arguably the strongest Western Boundary Current in the Southern Hemisphere, to the unique retroflection system south of South Africa, thus becomes of critical importance to global climatic systems (Fig. 1.1).

Subsurface, the Indian Ocean heat content in the upper 700 m has increased by 70% in the last decade (Lee et al., 2015). This is due to an increase in transport of warmer Pacific Ocean waters, making use of the Indonesian Throughflow as a conduit. The Indian Ocean has three dominant components to its circulation: influx through the Indonesian Throughflow of fresh warm waters (Lee et al., 2015; Desbruyeres et al., 2017), a vertical overturning circulation which connects upwelling in the north of the Indian Ocean to the inflow of mode waters from the south (Schott et al., 2009) and the subtropical gyre of the South West Indian Ocean which transports along its western boundary (the Agulhas Current), warm salty water to the South Atlantic, Southern and South Indian Oceans (Beal et al., 2011). This warm salty injection, into the South Atlantic in particular, contributes to the Atlantic Meridional Overturning Circulation (AMOC), (Beal et al., 2011). These waters are transported northwards in the upper portion of the water column, contributing to the Northern Hemisphere and regulating its climate (Frajka-Williams et al., 2019).

Given the importance the Indian Ocean plays in modulating global climate variability (Lee et al., 2015), and the critical role of the Greater Agulhas Current System within the Indian Ocean, understanding the evolution of mesoscale eddies

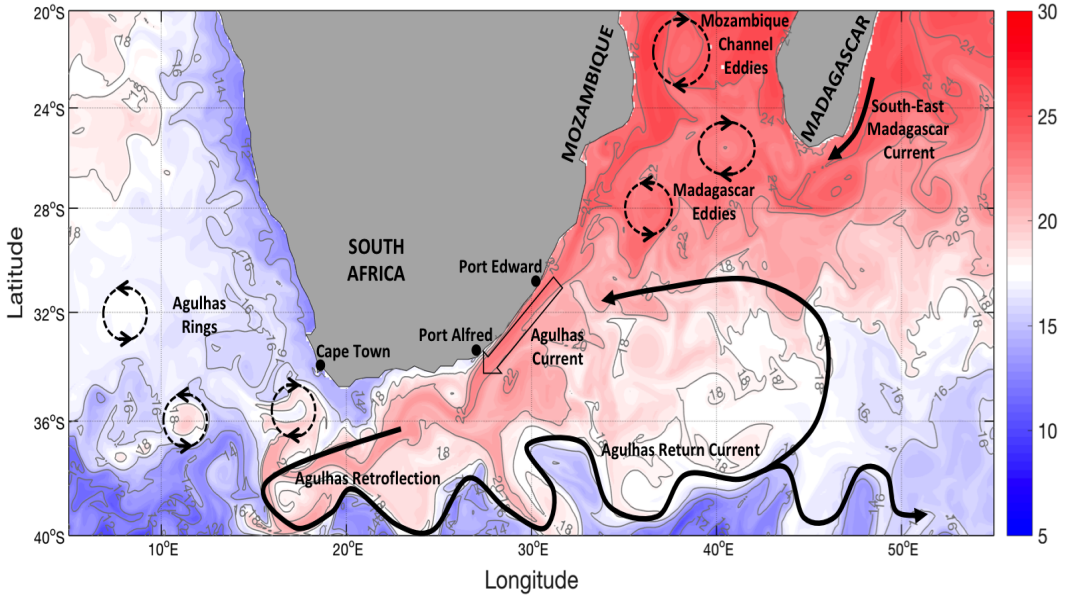

Figure 1.1: *Map of sea surface temperature (°C) for the greater Agulhas Current region for 10 August 2017 (day of float deployment). Highlighted along the east coast of South Africa, prominently between Port Edward and Port Alfred, is the Agulhas Current (black large arrow). Contributing to the Agulhas Current are mesoscale eddies (dashed ellipses) originating from the Mozambique Channel and spawned from the South-East Madagascar Current (solid black arrow) south of Madagascar. The Agulhas Current uniquely retroflects back on itself at the Agulhas Retroflection (black solid curve), forming the Agulhas Return Current (black solid curved line), which in turn contributes as a source to the Agulhas Current again. Finally, Agulhas Rings contributing heat and salt to the South Atlantic, are shed at the Agulhas Retroflection. Sea surface temperature data was obtained from Copernicus and the GLORYS12V1 Reanalysis product.*

that contribute to and the Agulhas Current itself, is essential for understanding thermohaline dynamics both locally and globally.

1.2 Literature review

The literature review is addressed in the following sections. First, the circulation of the South West Indian Ocean into the North East Madagascar Current and the South East Madagascar Current is presented in Section 1.2.1. A description of mesoscale eddies propagating southwards through the Mozambique Channel, westwards across the southern Mozambique Channel from South West Madagascar and the impact of mesoscale eddies on the Northern KwaZulu-Natal coast is given in Section 1.2.2. Next a description of the Agulhas Current is given in Section 1.2.3 and the South West Indian Ocean water masses in Section 1.2.4. Finally, a look at how Argo floats have been used to study mesoscale eddies is given in Section 1.2.5.

1.2.1 The South West Indian Ocean Circulation

The large scale circulation of the Indian Ocean is shown for the South West Monsoon period (July to August) in Figure 1.2 (Talley et al., 2011). The focus of this study is on the southern portion of the Indian Ocean. The northern circulation, along with its anomalies associated with monsoonal circulation reversals, will not be described further. Needless to say, the Indian Ocean is unique due in large to it being bounded by the Indian Sub-Continent to the north and the reversals in monsoons playing a large role on the northern Indian Ocean circulation patterns. Variability stemming from these monsoonal circulations do however extend in to the South Indian Ocean.

The subtropical anticyclonic gyre of the South Indian Ocean consists of three parts – the South Equatorial Current (SEC), the Agulhas Current down the east coast of South Africa which retroflects eastwards to form the Agulhas Return Current, and the South Indian Ocean Current (Fig 1.2) (Lutjeharms, 2006).

The SEC receives water from the subtropical gyre of the South Indian Ocean, and from the Indonesian Throughflow, thus an Indo-Pacific mixing of source waters (Schott et al., 2009). It starts as a broad band of flow east of 105° E, spanning from 7° S to 15° S, narrowing as it flows westwards to span between 10° and 20° S (Quadfasel and Swallow, 1986). The SEC bisects the Mascarene Plateau between 10° and 16° S, 60° E and at this stage is carrying between 50 and 55 Sv (1 Sv = 10^6 m^3 s^{-1} volume transport) of water (New et al., 2007). Once it interacts with the shelf off the east coast of Madagascar, it splits (between 18° and 20° S) to form the North East Madagascar Current (NEMC) and the South East Madagascar Current (SEMC).

North East Madagascar Current

The North East Madagascar Current (NEMC) is described as being 200 km wide, 1100 m deep and with current speeds on average around 0.5 m s^{-1} (Schott et al., 1988; Swallow et al., 1988). It also carries 30 Sv of water around the northern tip of Madagascar and propagates further westwards before splitting against the African east coast around 11° S in to the East African Coastal Current to the north and in to the Mozambique Channel to the south (Schott et al., 1988; Swallow et al., 1988). The volume transport estimate obtained using a regional model and satellite data of 38.93 Sv (Collins et al., 2014) is in good agreement with Schott et al. (1988) and Swallow et al. (1988). The NEMC, once it flows west of the northern tip of

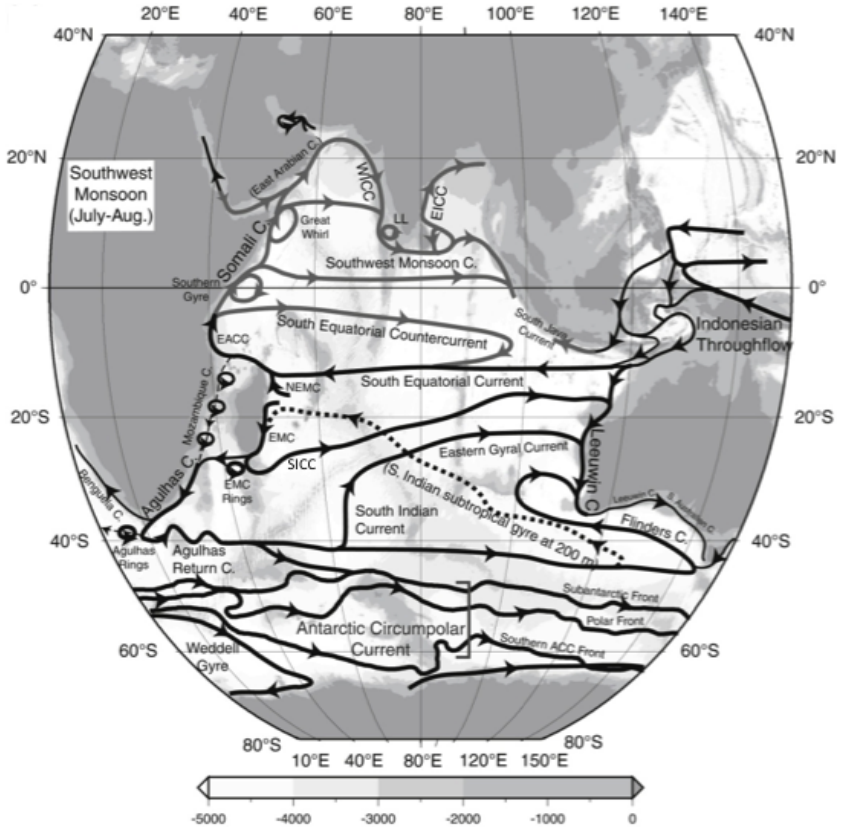

Figure 1.2: *Indian Ocean schematic surface circulation. Black lines show flows without seasonal reversals; gray lines show monsoonally reversing circulation, from Talley et al. (2011) (after Schott and McCreary (2001)). Abbreviations pertinent for the South West Indian Ocean: NEMC – North East Madagascar Current, EMC – East Madagascar Current (referred to in this study as the South East Madagascar Current), SICC – South Indian Ocean Countercurrent.*

Madagascar, generates anticyclonic eddies by associated barotropic instabilities (Collins et al., 2014). These then travel westwards across the Comoros Basin and into the Mozambique Channel. Cyclonic eddies are conversely generated off the northwest coast of Madagascar due to baroclinic instabilities (Collins et al., 2014).

South East Madagascar Current

The South East Madagascar Current (SEMC) is a deep (1100 m), short (650 km in length) Western Boundary Current with a width of 120 km and peak velocities within its core of $\sim$ 1.1 m s^{-1} (Quartly et al., 2006; Nauw et al., 2008). Various authors have described the volume transport of the SEMC at different locations along the east coast of Madagascar. At 20° S, the volume transport was shown to be less than 10 Sv (Donohue and Toole, 2003). At 23° S, the volume transport of the SEMC between 0 and 750 m is thought to be between 13 and 20 Sv (Schott et al., 1988). The volume transport close to the southern tip of Madagascar has been estimated at $\sim$ 35 Sv, illustrating an increase in volume transport with increasing latitude (Nauw et al., 2008). Using *in situ* mooring data collected at 23° S, a maximum (peak) volume transport of 50 Sv, with mean transport estimates of 18.3 $\pm$ 8.4 Sv was determined (Ponsoni et al., 2016), similar to that of Schott et al. (1988).

At the southern tip of the SEMC, the existence (or non-existence) of a retroflection of the SEMC current flowing eastwards in to the interior of the South Indian Ocean subtropical gyre, has been an ongoing debate for some time. The idea of a retroflection, similar to that existing south of Africa for the Agulhas Current, was first suggested based on the analysis of thermal imagery and drifter tracks (Lutjeharms, 1988). However the lack of a sustained eastward current, observed in either satellite imagery or *in situ* observations, is a critical argument against the existence of the retroflection (Quartly et al., 2006). A second theory proposed the SEMC acts as a free westward jet once it leaves the southern tip of Madagascar, which goes on to generate vortex eddy pairs (De Ruijter et al., 2004). The presence of mesoscale eddies propagating westwards along the latitudinal band $\sim$ 20° - 25° S complicates the issue of the existence of a retroflection further (Siedler et al., 2006; Donohue and Toole, 2003). The presence of a South Indian Counter Current (SICC) was described by using averages of altimetry data over longer periods of time, showing a narrow, shallow ($\sim$ 200 m) continuous band of flow in to the South Indian Ocean subtropical gyre (Siedler et al., 2006; Palastanga, 2007). Furthermore a large anticyclonic cell was suggested to exist between Madagascar and 75° E, bounded to the north by the SEC and in the south by the SICC (Palastanga, 2007), though only a small northward flow in the east, closing off this anticyclonic cell, could be shown (Siedler et al., 2006).

On analysis of 18 years of altimetry data on the SEMC and mesoscale eddy pair generation, the lack of a retroflection south of Madgascar, nor a free westward jet, was determined by Ridderinkhof et al. (2013). The authors also show that there is no connection between the SEMC and the SICC, thus suggesting that the SICC is an independent feature of the South Indian Ocean subtropical gyre.

1.2.2 Mesoscale eddies

In order to analyze mesoscale eddies throughout the world's oceans, 16 years of Sea Surface Height Anomaly (SSHA) data from two available altimetry sensors (one with a 10-day overpass and the second with a 35-day overpass) was used (Chelton et al., 2011). Mesoscale eddies are predominantly westward propagating with the exceptions of regions with strong eastward flow (e.g. Antarctic Circumpolar Current), with propagation speeds similar to long baroclinic Rossby waves (Chelton et al., 2011). These speeds were also found to be $\sim$ 20 % faster in the Southern Hemisphere compared to the north, but were also found to be $\sim$ 25 % slower globally than the westward propagation of features larger than mesoscale when analyzing the Sea Surface Height field (Chelton et al., 2011). Interestingly, cyclonic eddies were found to be more abundant in the Southern Hemisphere with average amplitudes greater than 10 cm and rotational speeds of 20 cm s^{-1} (Chelton et al., 2011).

Mesoscale eddies can be considered isotropic, thus fluid motion can be considered similar to solid-body rotation (Chelton et al., 2011). The most notable result described was that mesoscale eddies outside of the tropical band (20° N - 20° S) can be considered highly nonlinear, with fluid trapped within its core, where the metric U/c is greater than 1 ('U' being the rotational speed of the eddy and 'c' the translation speed of the eddy).

Flow through the Mozambique Channel and westward from southern Madagascar,

is dominated by mesoscale eddies (Halo et al., 2014b; Ullgren et al., 2012; De Ruijter et al., 2004; Ridderinkhof et al., 2013). While a special issue volume of Deep Sea Research has been published looking at the role eddies play within the Mozambique Channel from the physics through the food chain to top predators (Ternon et al., 2014), fairly little in comparison is known of eddies propagating westwards spawned from the South-East Madagascar Current (SEMC). Only two *in situ* surveys have been undertaken to date on mesoscale eddies in this region (De Ruijter et al., 2004; Barlow et al., 2017; Ockhuis et al., 2017; Noyon et al., 2018). While some modeling work is available (Ridderinkhof et al., 2013; Halo et al., 2014b), an in-depth dynamical assessment of these mesoscale eddies using *in situ* instruments is needed.

Mozambique Channel eddies

The relationship between the SEC and anticyclonic eddy formation at the northern tip of the Mozambique Channel was described by Backeberg and Reason (2010). Seasonal pulses propagating along the SEC are translated past the northern tip of Madagascar (assumedly along the NEMC) and impact the formation of anticylconic eddies, as described by Collins et al. (2014). This is significant, given eddies propagating southwards through the Mozambique Channel interact with the Agulhas Current which at its termination sheds warm salty water in to the South Atlantic and Southern Oceans. Thus a connection between the SEC and the Agulhas Retroflection could be postulated further.

The circulation of five individual eddy experiments in the Mozambique Channel was undertaken over a five year period (2005-2010), (Ternon et al., 2014). Mesoscale eddies formed in the northern Mozambique Channel migrate polewards along a western eddy corridor, adjacent to the African continent. Anticyclones were found to be the dominant mesoscale structure with current signatures apparent to 500 m in depth (Ternon et al., 2014). Cyclonic eddies, found to be the weaker structures in the Mozambique Channel, only had current signatures to 100 m (Ternon et al., 2014). However, this may not necessarily equate to the depth of influence the mesoscale eddies will have on surrounding water masses.

The water masses and structure across the northern Mozambique Channel where much of this eddy activity and formation takes place was studied by Ullgren et al. (2012). They show that more than 30% (40%) of salinity (temperature) variability within the Central Water range can be attributed to the large anticyclonic eddies propagating through this region. Thus anticyclonic eddies carry warm salty water water within their cores polewards (Ullgren et al., 2012).

Madagascar eddies

Madagascar eddies are generated as nonlinear dipole pairs from the SEMC (De Ruijter et al., 2004; Ridderinkhof et al., 2013). A deep-reaching jet southwest of Madagascar with velocities of 20 cm s^{-1} at 2000 m, with two contra-rotating eddies (one on either side of the jet) was surveyed in March 2001 (De Ruijter et al., 2004). The entire structure spanned $\sim$ 600 km; $\sim$ 250 km per eddy. The anti-cyclonic eddy showed water mass characteristics similar to the SEMC, while the cyclonic eddy had drawn water from the inshore side of the SEMC and was formed as a lee-eddy as the SEMC separated from the shelf (De Ruijter et al., 2004; Ridderinkhof et al.,

2013). As such, the cyclonic eddy had some Mozambique Channel water mass characteristics with the subsurface salinity maximum 0.1 psu larger in the upper layers than in the anticyclonic eddy (De Ruijter et al., 2004). From this observed dipole feature, a volume transport of 8 Sv was calculated to translate across the Mozambique Channel at a rate of 5 - 10 cm s^{-1} and contribute to the poleward flowing Agulhas Current (De Ruijter et al., 2004). Between four and six of these symmetric nonlinear dipole pairs are estimated to be shed each year from the SEMC, which break-up and interact with previously formed cyclones and anticyclones within the southern Mozambique Channel (Ridderinkhof et al., 2013). The total volume transport, calculated from *in situ* data, of $\sim 37 \pm 10$ Sv for the SEMC (Nauw et al., 2008), equates well to the volume transport estimate of the dipole surveyed (8 Sv), (De Ruijter et al., 2004) and the number of dipole pairs (4-6) calculated to occur each year (Ridderinkhof et al., 2013). *In situ* data in this region however remains sparse (Halo et al., 2014b).

Using 17 years of altimetry data and output from the South West Indian Ocean Model (SWIM) configuration of the Regional Ocean Modeling System (ROMS) model, the eddy generation, energy conversion and mean properties of mesoscale eddies south of Madagascar were described (Halo et al., 2014b). Dividing the area south of Madagascar into two distinct regions (Fig. 1.3) – South East (23-32° S, 45-51° E) and South West (23-32° S, 39-45° E), the authors found clear differences in the way in which eddies were being generated and their resultant characteristics. In the South East, eddies were generated by the barotropic instability of the mean flow of the SEMC with a total of 356 eddies for the over 17 years of data, 49 % being cyclonic and 51 % anticyclonic (Halo et al., 2014b). While in the South West, eddies were generated by a combination of barotrophic instabilities in the upper 300 m, and baroclinic instabilities in the upper 500 m and between 800 and 2000 m (Halo et al., 2014b). This resulted in a total of 394 eddies, 58 % cyclonic and 42 % anticyclonic. Furthermore, eddies generated in the South West had a maximum peak of non-linearity of less than 100 days compared to less than 30 days for eddies generated in the South East, suggesting that eddies generated in the South West only decay approximately 100 days after generation (Halo et al., 2014b) or roughly half way across the Mozambique Channel based on a cyclonic eddy surveyed along the east coast of South Africa (Morris et al., 2013).

Finally, all mesoscale eddies (in the South West and South East regions) generated were shown to be highly non-linear and effective trappers for biological material (Halo et al., 2014b). However, cyclonic eddies generated in the South West were considered to be the most abundant, had the strongest relative vorticity, were the most energetic and longest-lived and could travel the furthest distances (Halo et al., 2014b).

Mesoscale eddies impacting the Northern KwaZulu-Natal coast of South Africa

Previous studies off the Northern KwaZulu-Natal (NKZN) coast showed the impact of mesoscale eddies, primarily cyclonic eddies, on the shelf region. The first was a physical oceanographic study from 2001 to 2003 off Sodwana Bay, an embayment just south of the Mozambican border rich in coral reefs and associated marine biodiversity (Celliers and Schleyer, 2002). The study made use of a single seabed deployed Acoustic Doppler Current Profiler (ADCP) in 26 m of water and four Underwater Temperature Recorders (UTRs). The results, published as part of a

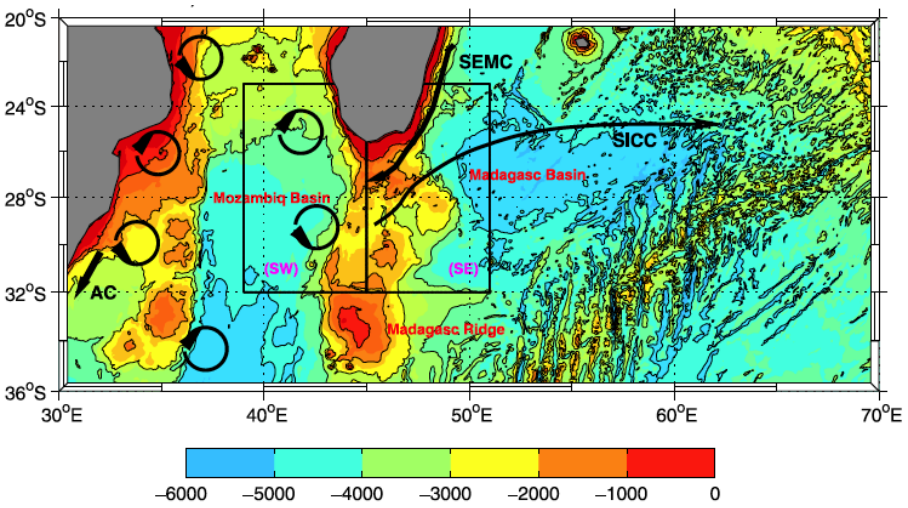

Figure 1.3: *Schematic of circulation around Madagascar, superimposed on GEBCO1 topography with 1000 m contour intervals. The boxes represent the division of region south of Madagascar used by Halo et al. (2014b) to study mesoscale eddy dynamics. Image reproduced from Halo et al. (2014b)*

Magister Technologiae dissertation (Morris, 2009), showed predominant southwestward currents associated with the Agulhas Current 73 % of the 30-month study period, with northeastward reversals the remaining 27 % of the study period. On several occasions, these reversals in current were associated with deep-sea mesoscale eddies originating from the southern Mozambique Channel.

The African Coelacanth Ecosystem Program (ACEP) from 2002 to 2006 undertook a study of Coelacanth (*Latimeria chalumnae*) habitat and associated environmental conditions, with particular emphasis on the deep canyons of the NKZN coastline where these prehistoric fish are found. A cyclonic eddy, bringing cold waters (a temperature decrease of $\sim 8^{\circ}$ C over four days) on to the narrow shelf region of NKZN, allowed the chance sighting of a coelacanth in February 2004 by Trimix SCUBA divers in 54 m of water; approximately 50 - 60 m shallower than the preferred depth range of these fish (Roberts et al., 2006).

A second ACEP study, surveyed a cyclonic eddy offshore of the NKZN coastline by means of Conductivity Temperature and Depth (CTD) casts and ship-borne ADCP, thereafter deploying a satellite tracked drifter within the eddy core (Morris et al., 2013). The eddy impacted the shelf within a month of the ship survey (as shown initially by the drifter track and thereafter satellite altimetry data) and caused upwelling onto the NKZN shelf, shown in the UTR data (a temperature decrease of $\sim 2^{\circ}$ C over four days) at Nine-Mile Reef, Sodwana Bay (Morris et al., 2013). Interaction over the shelf region between the cyclonic eddy and an anticyclonic eddy situated further offshore at the time of the survey, resulted in a colder upwelling event (a temperature decrease of $\sim 3^{\circ}$ C over four days) seven days after the first upwelling event, illustrating that both cyclonic, and their interaction with anticyclonic eddies, impact the NKZN shelf (Morris et al., 2013). It was also shown, through the UTR data coupled with satellite altimetry, that between two and five cyclonic eddies impact the shelf each year and like the cyclonic eddy surveyed for the paper, most originate off southeast Madagascar and travel westwards across the

southern Mozambique Channel (Morris et al., 2013).

1.2.3 The Agulhas Current

The Agulhas Current is sourced from three regions (Fig. 1.1) – the recirculation of Agulhas Current around the South West Indian Ocean sub-gyre and from mesoscale eddies propagating southwards through the Mozambique Channel and southwestwards from south Madagascar, and is fully constituted north of Durban (Lutjeharms, 2006). The Agulhas Current recirculation branch contributes $\sim$ 35 Sv to the overall flow, though this is based on the sparse hydrographic information available and should be considered an estimate only (Stramma and Lutjeharms, 1997). As stated above, the SEMC contributes $\sim$ 37 Sv (Nauw et al., 2008) or $\sim$ 8 Sv per dipole pair (4 - 6 dipoles per year), (De Ruijter et al., 2004; Ridderinkhof et al., 2013). The Mozambique Channel eddies contribute between 15 Sv (De Ruijter et al., 2002) and 20 Sv (Biastoch et al., 1999).

The northern Agulhas Current, defined to be between 27° and 34° S (Lutjeharms, 2006), has historically been described as a stable Western Boundary Current, most likely due to the steep continental slope (Ruijter et al., 1999) with mean speeds between 1.4 m s^{-1} and 1.6 m s^{-1}. After analysis of the Agulhas Current Time-Series (ACT) array of moorings deployed from the shelf to 300 km offshore at 34° S, and a 22-year proxy of the current using available altimetry data, the Agulhas Current was shown to be 219 km wide, 3000 m deep and with peak surface speeds of 1.8 m s^{-1} (Beal et al., 2015). The authors also developed an algorithm, which calculated the volume transport of the poleward current at each time step taken out to the maximum of the vertically integrated velocity, beyond the half-width of the mean jet. This was calculated to be 84 Sv $\pm$ 11 Sv (when taking in to account sampling and interval errors from the in situ instruments), (Beal et al., 2015). A volume transport of 70 Sv $\pm$ 22 Sv was calculated at 32° S (Bryden et al., 2005), which is 10 Sv less than Beal et al. (2015) showing a latitudinal increase of 2.4 Sv per 100 km and in agreement with what is predicted by Svedrup dynamics. Finally, they found the Agulhas Current to have a 25 % volume transport increase in summer from the winter minimum (Beal et al., 2015).

Beal and Bryden (1997) also showed a weak Agulhas Undercurrent at 1200 m below the core of the Agulhas Current, adjacent to the continental slope. The equatorward transport of this undercurrent was measured at 4.2 Sv (Bryden et al., 2005), and consists of modified Red Sea Water.

By comparison to the mesoscale source regions of the Agulhas Current, many more studies have been undertaken in this Western Boundary Current. These range from surveys (Leber and Beal, 2014; Lamont et al., 2016; Russo et al., 2019), moored assessments (Bryden et al., 2005; Beal et al., 2015) and process studies (Roberts et al., 2010). None have however made use of Argo floats on a high profiling frequency in an attempt at determining the evolution of the physical parameters of the current.

1.2.4 The South West Indian Ocean Water Masses

The water masses of the Indian Ocean have been described by a number of authors based on global data sets (e.g. International Indian Ocean Expedition), (Wyrtki, 1971; Tomczak and Godfrey, 1994), seasonal datasets coupled with a mixing model

(You, 1998) and by means of dedicated sampling expeditions (Beal et al., 2006). Figure 1.4 shows the source water regions of the major water masses of the Indian Ocean (Beal et al., 2006).

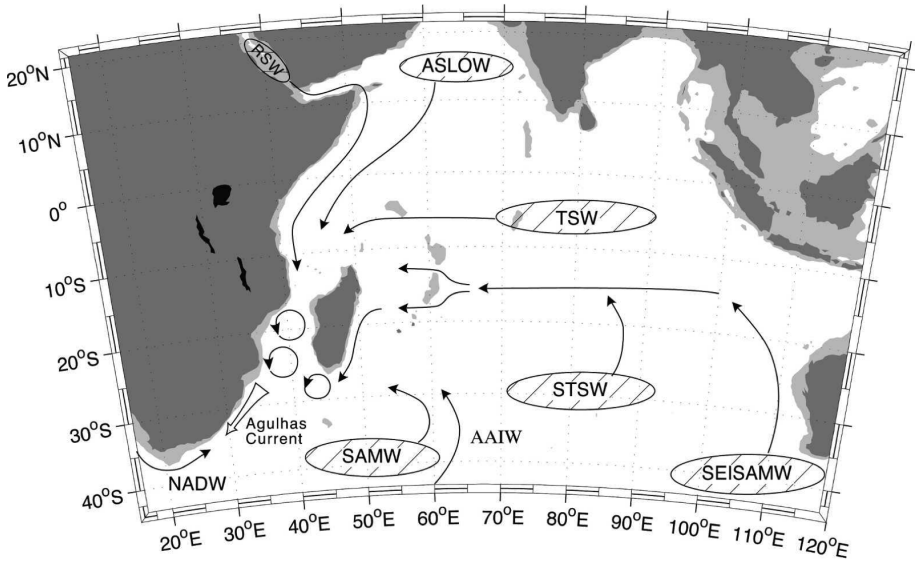

Figure 1.4: *Source water regions and pathways of water masses that converge in to the Agulhas Current. The water masses not circled, are sourced from outside the boundaries of the schematic. RSW – Red Sea Water, ASLOW – Arabian Sea Low Oxygen Water, TSW – Tropical Surface Water, SEISAMW – Southeast Indian Sub-Antarctic Mode Water, STSW – Sub-Tropical Surface Water, AAIW – Antarctic Intermediate Water, SAMW – Sub-Antarctic Mode Water, NADW – North Atlantic Deep Water. Taken from Beal et al. (2006).*

Upper Waters

The upper waters are those limited to above 500 m water depth, and are generally formed by excessive precipitation or evaporation or by convective overturning. Those common to the South West Indian Ocean include:

- **Tropical Surface Water (TSW)**
  TSW is formed in the central Indian Ocean along the equatorial band by means of excessive precipitation and evaporation in the tropics (Wyrtki, 1971), (Fig. 1.4). TSW propagates along the SEC, flowing in to the northern and southern branches of the East Madagascar Current as described in Section 1.2.1 (Swallow et al., 1988). The physical parameters of TSW are greater than 35.5 for salinity and with a neutral density of 25.5 kg m^{-3} (Beal et al., 2006), while a more specific range of 34.91 – 35.31 for salinity, and a range of 24.7° - 26.3° C for temperature is described by Donohue and Toole (2003).

- **Sub-Tropical Surface Water (STSW)**
  STSW is formed in the subtropical gyre of the South West Indian Ocean - 25° - 35° S, east of 90° E (Fig. 1.4) - and is found between 200 and 500 m (Wyrtki, 1971; Tomczak and Godfrey, 1994). It also propagates along the SEC and bifurcates around Madagascar along the northern and southern East Madagascar Current pathways. STSW is distinguished from TSW again with salinities greater than 35.5, but with neutral densities from 25.5 – 26.4 kg m^{-3} (Donohue and Toole, 2003).

- **Sub-Antarctic Mode Water (SAMW)**
  SAMW is formed at the subtropical convergence front (46° - 62° E) by means of deep winter cooling and convection to the south of the front itself (Fine, 1993). SAMW is further described at 28° S to be 13° C with a neutral density of 26.65 kg m^{-3}, and at 20° S to be 11° C with a neutral density of 26.8 kg m^{-3} (Donohue and Toole, 2003), highlighting the subduction northwards of SAMW within the thermocline.

- **Indian Central Water (ICW)**
  ICW, also known as South Indian Central Water (SICW), (Beal et al., 2006), is formed at latitudes 40 - 45° S by late winter convective overturning (You, 1998). It has a temperature range of 8° - 25° C, salinities of 34.6 – 35.8 (Emery, 2001; You, 1998) and a neutral density range of 26.4 – 27.0 kg m^{-3}.

Intermediate Waters

Intermediate water masses are found between 500 and 1500 m. Only two water masses are found commonly in the South West Indian Ocean:

- **Red Sea Water (RSW)**
  RSW is formed in the Red Sea through high evaporation processes, leaving high salinity water which enters the Gulf Of Aden and the Arabian Sea, subducting to depth fairly quickly suited to its neutral density of 27.25 kg m^{-3} (Tomczak and Godfrey, 1994). It enters the Mozambique Channel to the north and flows southwards to enter the Agulhas Current further south (Beal et al., 2006). RSW has a potential temperature range of 5° to 14° C and salinity range of 34.8 to 35.4, with a low oxygen core (Emery, 2001).

- **Antarctic Intermediate Water (AAIW)**
  AAIW is formed at the polar front in the South East Pacific and propagates eastwards along the Antarctic Circumpolar Current (Emery, 2001). At 60° E in the Indian Ocean, AAIW flows northwards in to the subtropical gyre (Fine, 1993), but never crosses the equatorial band (Tomczak and Godfrey, 1994). AAIW has a salinity range of 33.8 - 34.6, thus distinguishing it from RSW even though AAIW has a similar potential temperature range of 2° to 10° C (Emery, 2001).

1.2.5 Using Argo floats to study mesoscale eddies

The Argo program was initiated in 1999 as floats were deployed in the world's oceans with the objective to detect large-scale changes in the temperature and salinity distributions, how ocean circulation affects these distributions and climate variability on seasonal and decadal scales (Riser et al., 2016). In recent years, the reconstruction of the vertical structure of mesoscale eddies using Argo profiles and Sea Level Anomaly (SLA) satellite data has become possible with over 800 floats deployed within the world's oceans per year. At present there are over 3500 floats actively collecting data of the upper 2000 m of the water column every 10 days (http://www.argo.net).

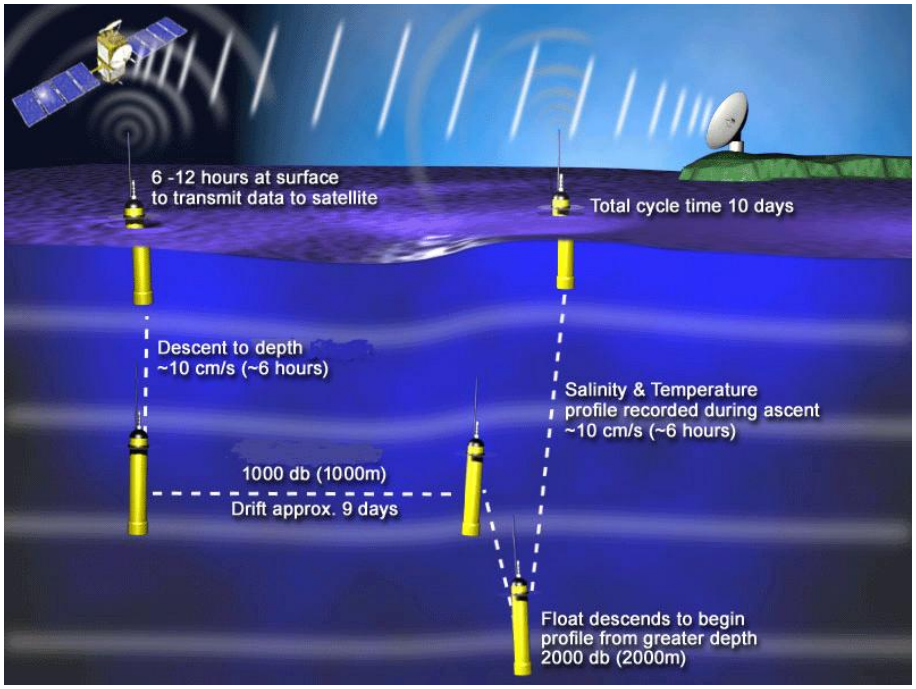

Figure 1.5: *Standard Argo program profile strategy of 10 days, with 9 days at park depth, and profiling from 2000 m depth (http://www.argo.net).*

Studies using Argo floats to investigate mesoscale eddies

The mesoscale vertical structure for the Peru-Chile Current System in the South Pacific Ocean was recreated using Argo floats (Chaigneau et al., 2011). This was done using 420 profiles from cyclonic eddies and 526 profiles from anticyclonic eddies, with core depths of $\sim$ 150 m, or within the density level 25.2 - 26.0 kg m^{-3}, for cyclonic eddies and $\sim$ 400 m (26.0 – 26.8 kg m^{-3}) for anticyclonic eddies

(Chaigneau et al., 2011). The varying mesoscale core depth can be attributed to the different formation mechanisms, with cyclonic eddies formed from instabilities of the equatorward surface current and anticyclonic eddies from instabilities in the poleward undercurrent of the Peru-Chile Current System (Chaigneau et al., 2011). The calculated maximum temperature and salinity anomalies from the eddy cores varied by $\pm$ 1° C and $\pm$ 0.1 respectively to the positive in anticyclonic eddies and to the negative in cyclonic eddies. The amount of water trapped within a mesoscale eddy was calculated using the ratio U/c (as per Section 1.2.2), (Chelton et al., 2011), with rotational speeds calculated at each depth by averaging the geostrophic velocity along the eddy-core edge, and an average eddy propagation speed of 4.3 cm s^{-1} for all the eddies used in the study (Chaigneau et al., 2011). This produced a vertical extent of 240 m for cyclonic eddies and 530 m for anticyclonic eddies. The authors do note that these depths will vary eddy by eddy, but was sufficient in calculating heat and salt transport anomalies of $\pm$ 1 – 3 x 10^{11} W and $\pm$ 3 – 8 x 10^{3} kg s^{-1} respectively, with a typical volume anomaly flux of $\pm$ 0.1 Sv (Chaigneau et al., 2011).

Souza et al. (2011) undertook a similar study for the Agulhas Rings propagating in to the South Atlantic from the Agulhas Current. Using SLA data every 7 days, and Argo profiles within 2 days (forwards or backwards in time) of the SLA image, 16 Agulhas Rings were reconstructed successfully from January 2005 to December 2008 with an eddy detection scheme described by Chaigneau et al. (2009). The Argo profile also needed to be within 2.5° ($\sim$ 270 km) of the Agulhas Ring core to be used for the reconstruction. Argo profiles that did not meet this criteria were linearly interpolated to where the Agulhas Ring core was assumed to be (Souza et al., 2011). The Argo data was further processed to normalize eddy amplitudes and diameters to account for the changes to temperature and salinity anomalies and distances respectively to allow for the ageing of the Agulhas Rings over time (Souza et al., 2011). Unlike Qiu and Chen (2005) who assumed the same vertical structure for each eddy surveyed in the Kuroshio Extension region in the North Pacific by all Argo profiles identified for that eddy, and thus ignoring variations over time. Souza et al. (2011) thus found mean annual volume transport of 9 $\pm$ 8 Sv, with a mean meridional heat flux across ring paths of 0.062 $\pm$ 0.012 PW (northwards). They also defined the water trapped within the Agulhas Rings (using the same ratio U/c) to be 800 $\pm$ 297 m for rings with a maximum propagation speed ($\sim$ 0.09 m s^{-1}) and 1133 $\pm$ 150 m for Agulhas Rings with a mean propagation speed (0.06 $\pm$ 0.02 m s^{-1}). Changes to the vertical structure of Agulhas Rings occurred at the surface due to surface fluxing with Agulhas Rings losing their core characteristics as they move away from the Agulhas Retroflection region (Souza et al., 2011).

Most studies resolving mesoscale dynamics using Argo floats use historical data on the standard Argo mission of profiling every 10 days from a depth of 2000 m and again parking at a depth of 1000 m until the next profile in 10 days time (Fig. 1.5). Few studies have modified the Argo float sampling structure and specifically deploy within mesoscale eddies to resolve these dynamics better. One such study has been carried out by the team at JAMSTEC / University of Tohoku in the Kuroshio Extension in the North Pacific Ocean (Inoue et al., 2016a; Inoue et al., 2016b; Kouketsu et al., 2016). The INBOX Project (Western North Pacific Integrated Physical-Biogeochemical Ocean Observation Experiment) builds on the SUPRFISH project (Studies on Prediction and Application of Fish Species Alternation) from the same region which showed possible subduction and frontal disturbance at

mesoscale eddy boundaries from Argo floats deployed on a 3-daily profiling mission (Inoue et al., 2016a). The INBOX project deployed 30 dissolved oxygen biogeochemical Argo floats on a 2-day sampling cycle in a 150 km x 150 km region centered around a biogeochemical mooring deployed at 30° N, 145° E (Inoue et al., 2016a). The first 18 floats deployed in the first phase of the project surveyed a cyclonic eddy as it was weakening (Kouketsu et al., 2016). Initial results showed enhanced primary production associated with the translation of eddies from their deployment site and the physical processes related to this blooming, and carbon dioxide fluxing at the air-sea interface (Inoue et al., 2016a). The ACE-INBOX project deployed a further 16 profiling floats from June 2012 to July 2013 within a warm-core anticyclonic eddy with similar float setups as the first phase of the project (Inoue et al., 2016b). The objective was to study the salinity minimum and its formation process in the Kuroshio-Oyashio mixed water region (Inoue et al., 2016b).

Argo floats with a higher sampling frequency were used to investigate anticyclonic subthermocline eddies related to the subduction of subtropical mode water in the North West Pacific Ocean (Zhang et al., 2015b). The floats were set up on a daily profiling frequency with a park depth of 500 m, profiling from 1000 m to the surface (Zhang et al., 2015b). Results revealed novel characteristics of subthermocline eddies supporting the potential of Argo floats to track and monitor eddies, particularly if on short repeating cycles (Zhang et al., 2015b). This work was expanded upon using all available historical data for 14 years to examine submesoscale eddy dynamics (Li et al., 2017).

Argo floats were not designed to study all the dynamical features of the ocean. However, they can be used to illuminate some poorly understood features in the vertical structure of the water column if they are used efficiently. For this reason, it was decided to use Argo floats in ad hoc experiments in an attempt to elucidate the dynamics of cyclonic mesoscale eddies shed from the South West Madagascar region, along with Agulhas Current dynamics, in terms of heat, salt and volume transport.

1.3 Key Questions

Using the experimental Argo float deployments (described further in Chapter 3), combined with available model data, this thesis aims to address the following key questions:

1) Can Argo floats be used to study mesoscale eddies in the southern Mozambique Channel and the Agulhas Current?

2) By using Argo floats on high-resolution profiling missions, can the knowledge of the vertical structure, geometric properties and fluxes of Madagascar cyclonic eddies be improved?

3) Can Argo floats be used to capture the downstream evolution of fluxes in the Agulhas Current?

4) What are the impacts and benefits of altered Argo mission parameters on data acquisition in the Indian Ocean?

The thesis is organized as follows.

- Chapter 2 describes the five Argo float experiments undertaken in the southern Mozambique Channel and Agulhas Current from 2013 - 2017 and highlights the value of high-resolution sampling as a technique for understanding turbulent regions.
- Chapter 3 details the technical aspects of the Argo float deployments which are used for this thesis specifically.
- Chapter 4 explores the Lagrangian evolution of two Madagascar cyclonic eddies using Argo floats as they propagate southwestwards across the Mozambique Channel.
- While Chapter 5 showcases the downstream evolution of hydrographic properties and fluxes of the Agulhas Current using Argo float technology.
- A general discussion and concluding remarks are given in Chapter 6.

Chapter 2

Using ocean robots on high-resolution profiling to capture the fast-flowing Agulhas Current

Preface:

This chapter highlights the value of high-resolution Argo float profiling in turbulent regions of intensive mesoscale activity and within Western Boundary Currents, such as the Agulhas Current. This chapter has been published in the South African Journal of Science as Scientific Correspondence, and the Chapter has been laid out in this format:

Morris T. and Lamont T. 2019. Using ocean robots on high-resolution profiling to capture the fast-flowing Agulhas Current. South African Journal of Science, 115 (1/2). https://doi.org/10.17159/sajs.2019/5523

This chapter addresses the first key question listed in Section 1.3:

Can Argo floats be used to study mesoscale eddies in the southern Mozambique Channel and the Agulhas Current?

The Argo programme was developed to provide near real-time observations of the ocean and contribute significantly to understanding the changes occurring in ocean temperature and salinity in the upper 2000 m. Riser et al. (2016) showed that, for profiles sampling both temperature and salinity to 1000 m or deeper, the Argo programme produced, in just under 16 years, three times as many profiles as all other shipboard observations in the past 100 years. Furthermore, Argo observations have occurred globally, albeit with higher resolution in regions where deployment opportunities were more prevalent. But what happens in particularly turbulent or fast-flowing current regions such as Western Boundary Currents and mesoscale eddies? Errors are reported to be high when Argo data are used to plot monthly and seasonal evolution of structures within turbulent Western Boundary Currents as a result of the lack of spatial resolution of Argo data (Riser et al., 2016). In an attempt to improve observations, the Argo Steering Team has suggested additional float resources be assigned to fast-flowing Western Boundary Current regions (Riser et al., 2016). While this addition may be sufficient for regions where deployment opportunities are numerous, in areas such as the Agulhas Current or the Mozambique Channel, where far fewer research cruises are conducted, another option is to set Argo floats to collect data at higher resolutions.

The Agulhas Current propagates along the east coast of South Africa at peak surface speeds of 1.8 $\mathrm{m\,s^{-1}}$ ($\sim$155 $\mathrm{km\,d^{-1}}$), (Beal et al., 2015), and is the fastest Western Boundary Current of the Southern Hemisphere. The Agulhas Current is considered stable from Durban in the north to Port Alfred in the south (Fig. 2.1), a distance of $\sim$570 km. Furthermore it is unique in that mesoscale eddies contribute to its source from east of Madagascar and the Mozambique Channel, and mesoscale eddies and Agulhas Rings are shed at the Agulhas Current termination as it retroflects back on itself into the Indian Ocean (Lutjeharms, 2006). The Agulhas Current is not accurately resolved in climate models (Renault et al., 2017) and thus forecasts used for the International Panel for Climate Change and similar misrepresent this feature, which is largely responsible for the transport of heat and salt from the Indian to Atlantic Oceans (Morris et al., 2017). Improved resolution *in-situ* measurements of this Western Boundary Current and its source regions are thus crucial for an accurate assessment of the contribution of the Agulhas Current and its sources to the transport of heat and salt.

Mesoscale eddies in the Mozambique Channel, originating usually in the narrows to the north of the Channel, extend to the full depth of the water column as found in in-situ measurements (De Ruijter et al., 2002; Halo et al., 2014a). Eddies originating from the South East Madagascar Current form in dipole pairs, around four to six per year (Ridderinkhof et al., 2013), with a strong jet found between the two lobes of the dipole propagating southwestwards (Ridderinkhof et al., 2013; De Ruijter et al., 2004). Halo et al. (2014b) showed that mesoscale eddies are indeed highly non-linear and capable of transporting material, such as biological organisms, between Madagascar and the African continent. But to what depths does this transport capability extend with particular emphasis on heat and salt input from the Indian Ocean interior into the Agulhas Current, especially given the significant decrease in velocities below 500 m in the limited in-situ data already available? In order to quantify this extent, dedicated research cruises undertaking extensive CTD (conductivity, temperature and depth) surveys across mesoscale eddies would be required - an incredibly expensive undertaking. A more affordable solution would be to deploy Argo floats profiling at higher resolution than that of

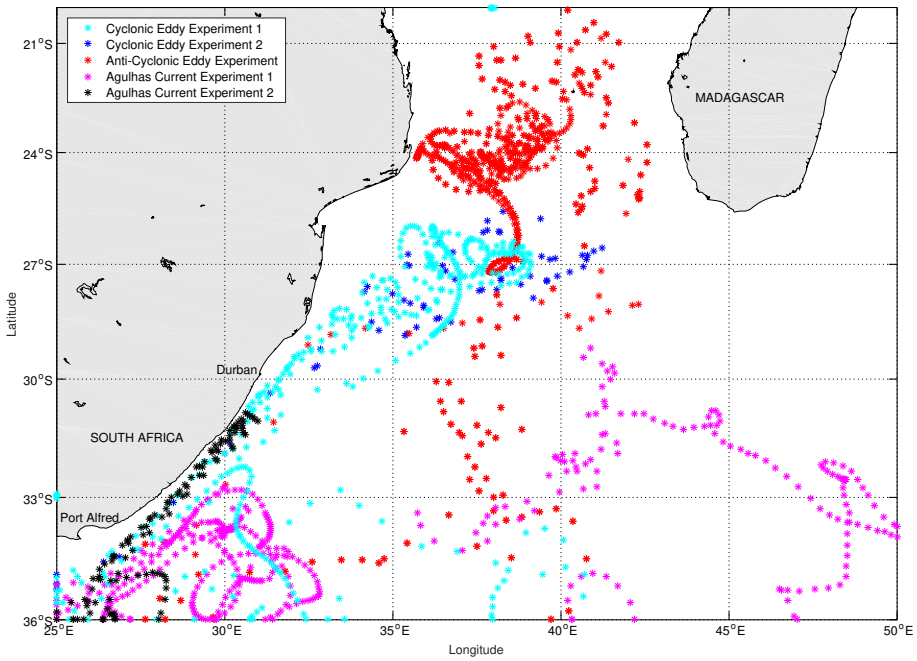

Figure 2.1: *Five high-resolution Argo profile experiments conducted between 2013 to 2017 in the Agulhas Current and its source regions. Cyclonic Eddy Experiment 1 (cyan) was deployed in April 2013 with five floats. Cyclonic Eddy Experiment 2 (blue) was deployed in July 2013 with four floats. The Anticyclonic Eddy Experiment (red) was deployed with two floats in December 2013, but the floats very quickly exited the eddy and became trapped in a Mozambique Channel cyclonic eddy. The two Agulhas Current Experiments (pink and black) were deployed in December 2013 with three floats and August 2017 with six floats respectively.*

the standard 10-day mission. Understanding what is being contributed to the Agulhas Current from its turbulent sources is imperative in order to validate coupled-climate models for better forecasting capabilities, to accurately assess physical dynamics impacting the coastal regions and critically track the transport of heat and salt, as well as pollutants such as microplastics (Morris et al., 2017; Nkwinkwa Njouodo et al., 2018).

Historically, scientific research cruises have been concentrated on the west and south coasts of South Africa because of the rich fisheries in these regions, whereas the east coast has had limited exposure to long-term studies of its powerful current. Intermittently deployed mooring arrays have been used to acquire data from the Agulhas Current (Beal et al., 2015; Morris et al., 2017; Bryden et al., 2005), and opportunistic surveys along the coast have been used to glean additional information whenever possible (Roberts et al., 2010; Leber and Beal, 2014). In contrast, much of the understanding of the Northern Hemisphere Western Boundary Currents comes from Argo float data and, when it is possible to deploy fairly regularly, a detailed picture can emerge (Riser et al., 2016). For the Agulhas Current, this paucity of *in-situ* data is further exacerbated by its relatively short length ($\sim$570 km) and with peak surface speeds of $\sim$155 km d^{-1}, an Argo float on the standard profiling of 10 days could miss the Agulhas Current completely in its propagation along the east coast.

With support of Argo teams from the USA, UK and Europe, South African researchers have begun using Argo floats with higher profiling frequencies (Argo, 2000), daily or five-daily as opposed to the standard 10-daily profiling mission, to understand this dynamic Western Boundary Current and the influence of mesoscale eddies from its source regions, as well as the fate of heat and salt transported by these features. The park and profile depths of these Argo floats were set to be shallower than the standard mission to ensure the floats were maintained within the features. Over the last 5 years, five experiments have been conducted on mesoscale eddies in the southern Mozambique Channel, and along the Agulhas Current (Figure 2.1). For the entire duration (2000 to 2017) of the Argo programme to date, 136 floats propagated along the east coast of South Africa have acquired 276 profiles within the Agulhas Current (Figure 2.2). For the 18 floats set to higher sampling frequencies for the five experiments, 199 profiles were collected (within the bounding box in Figure 2.2) – a number more than two thirds higher than that achieved by standard mission floats in close to 17 years, thus dramatically increasing the number of observations in this Western Boundary Current. For the southern Mozambique Channel, the increase in the number of observations is less obvious (Figure 2.3a and 2.3b) given that fewer high-resolution deployments were undertaken in this region. What is important to note is that, although there are more profiles per year on standard float missions in the southern Mozambique Channel, these floats are not profiling down the Agulhas Current as successfully (Figure 2.2b), and are thus not capturing the change in dynamics from a turbulent region into the Western Boundary Current.

With limited opportunities for dedicated research cruises in the Mozambique Channel to collect high-resolution CTD data, multidisciplinary cruises – such as that investigating a young cyclonic eddy spawned off south west Madagascar in July 2013 (Barlow et al., 2017; Ockhuis et al., 2017) – are crucial to further our understanding of these features. While it was possible to sample only a single high-resolution transect during the cruise (Barlow et al., 2017; Ockhuis et al., 2017), the deployment of Argo floats with higher profiling frequencies within that same eddy allowed for continuous sampling of water masses, heat, salt and volume transport of the eddy over a period of 4 months as the eddy moved from south west Madagascar to the Agulhas Current off South Africa (Refer to Chapter 4).

Arguably, high-resolution profiling is skewed to time periods when floats are deployed in these turbulent regions (Figures 2.2b and 2.3b); however detailed process studies have been made possible and these results will extend our understanding of the role of mesoscale eddies in the upstream dynamics of the Agulhas Current, and the structure and dynamics of the Agulhas Current itself. With the advances in satellite technology, it is now possible to reprogram the float so that once it leaves the high-resolution study region it can be set back to standard Argo profiling, thus extending the battery life of the float. Increased data profiling will increase data transmission costs and put additional strain on Argo data centres to validate data, but these advances should be considered similar to those of Deep-Argo, biogeochemical sensors on Argo floats and the increased float deployments in the equatorial regions. Argo floats were never designed to answer all the physical dynamics questions about the ocean, but given the massive cost of research vessels and dedicated *in-situ* sampling, obtaining detailed information on particularly turbulent regions to fill in at least some of the gaps should be undertaken in whatever way possible.

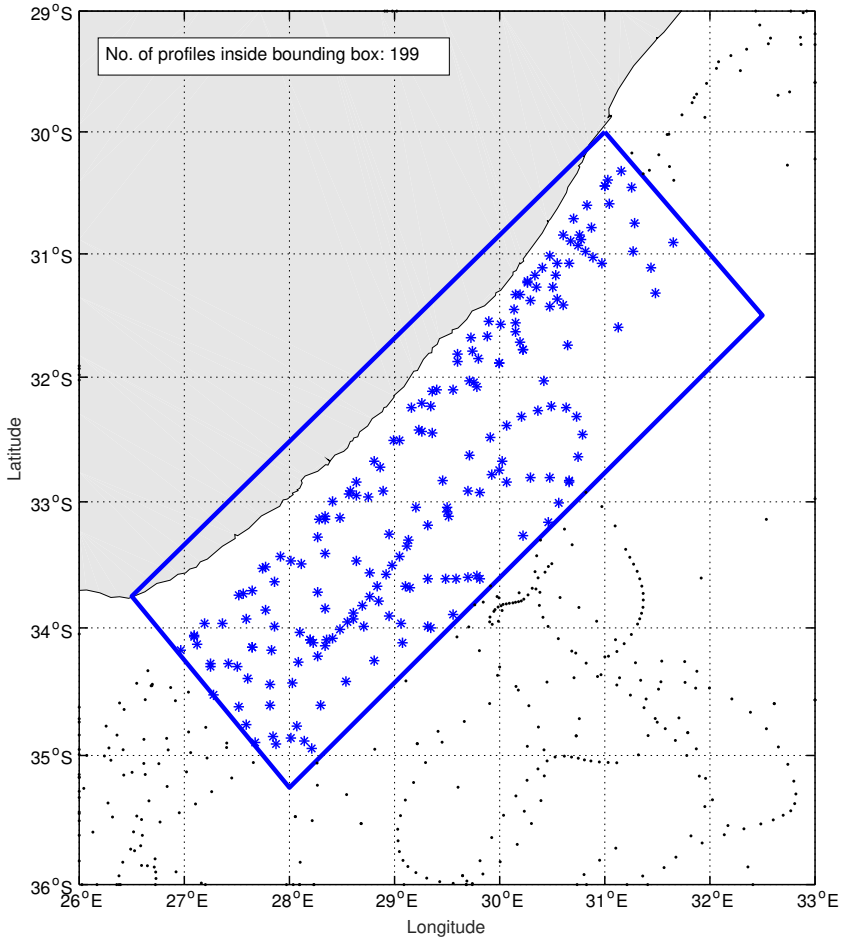

(a)

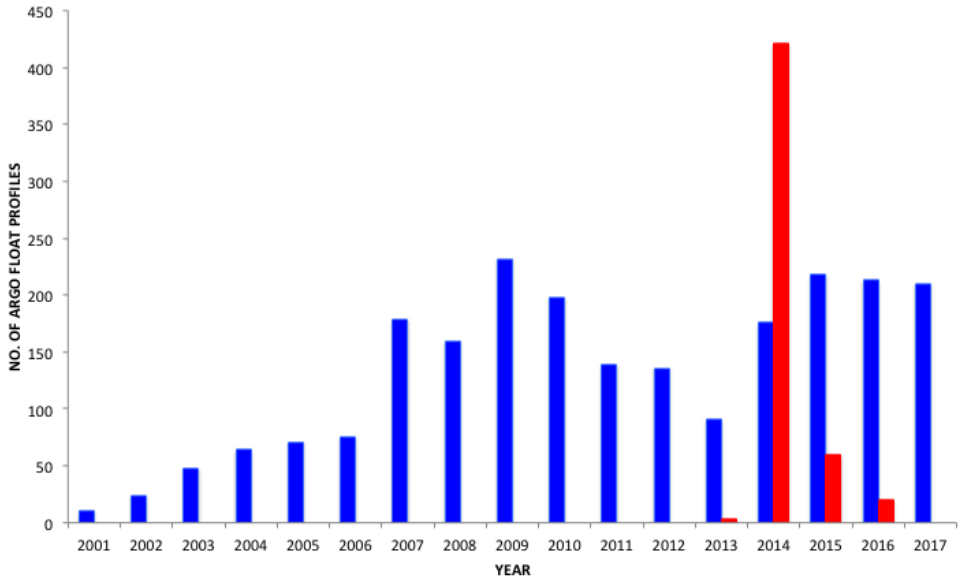

(b)

Figure 2.2: *(a) Map of the east coast of South Africa for the 18 high-resolution floats used in the mesoscale eddy and Agulhas Current experiments, with the Agulhas Current region depicted (as per Beal et al. (2015)) as a blue rectangle. (b) Histogram depicting, within the Agulhas Current bounding box, the profiles from standard profiling Argo floats (blue) and high-resolution Argo floats (red) per year.*

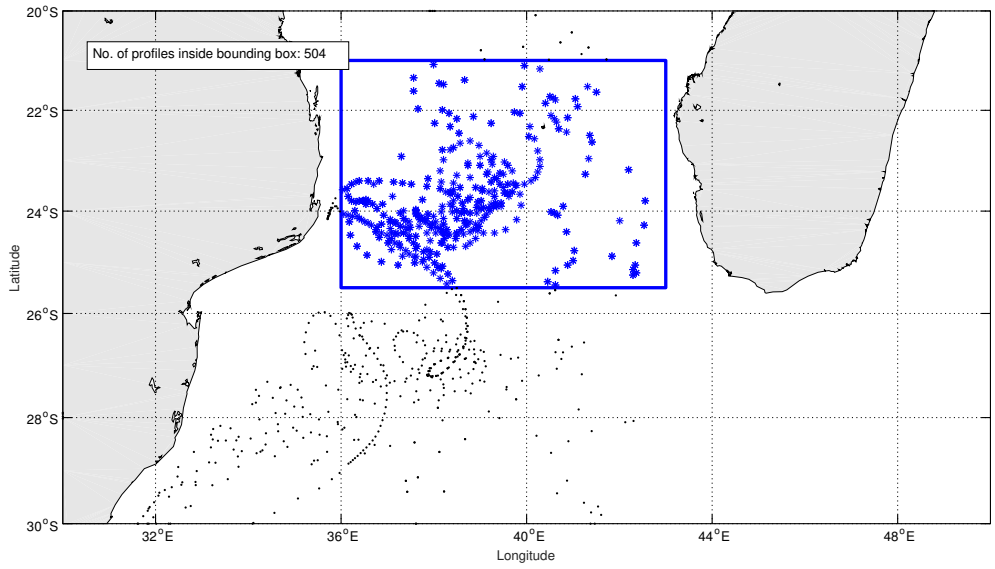

(a)

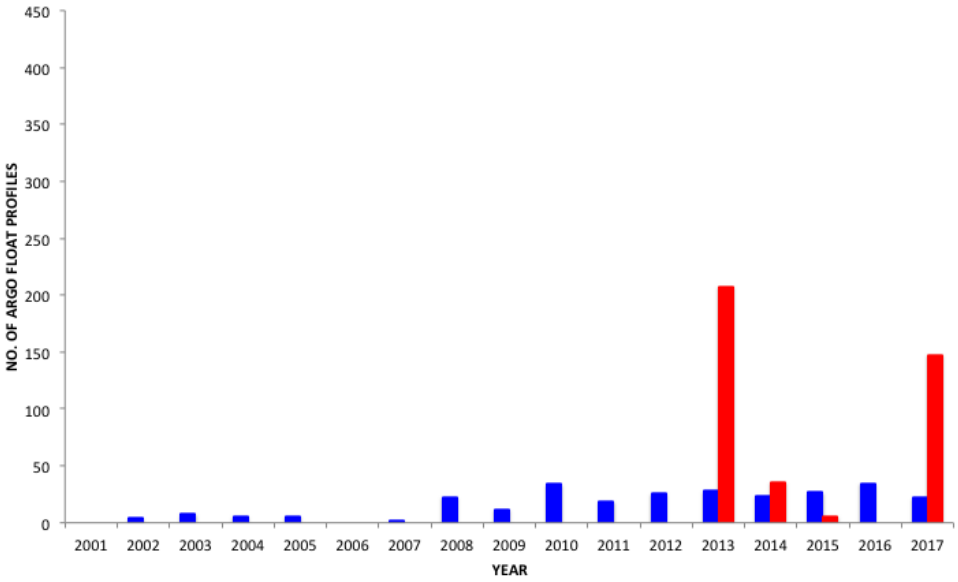

(b)

Figure 2.3: *(a) Map of the southern Mozambique Channel for the nine high-resolution floats used in the mesoscale eddy experiments, with the southern Mozambique Channel region depicted as a blue rectangle. (b) Histogram depicting, within the Mozambique Channel bounding box, the profiles from standard profiling Argo floats (blue) and high-resolution Argo floats (red) per year.*

Chapter 3

Technical description of high-resolution Argo float experiments

Chapter 2 has described the need for high resolution profiling of Argo floats in turbulent regions and within Western Boundary Currents. Chapter 3 details the three ad hoc experiments using Argo floats deployed on high frequency profiling which were undertaken in the Greater Agulhas Current Region and used for this thesis. The first two experiments, in April and July 2013, focused on cyclonic mesoscale eddies spawned off the South West coast of Madagascar, and eventually joined up with the Agulhas Current offshore of the KwaZulu-Natal Bight (Chapter 4). The final experiment was deployed to better understand the Agulhas Current and its evolution in terms of heat, salt and volume transport (Chapter 5). This experiment was deployed in July 2017. All deployments of Argo floats were opportunistically undertaken from the starboard side of the South African Research Vessel *Algoa* on various research cruises.

3.1 April 2013

This first of the cyclonic eddy experiments included the deployment of five Argo floats, provided by Woods Hole Oceanographic Institution (Fig. 3.1). Details of the cyclonic eddy development, evolution and structure are detailed further in Chapter 4, whereas this chapter focuses on the technical description. The deployments were targeted to span the centre of the cyclonic eddy in a west-east orientation, 10 nautical miles apart. The cyclonic eddy was tracked at sea with limited internet connectivity using available near-real time satellite imagery of sea surface heights. Upon analysis of both near-real time imagery and delayed time multi-mission products available recently through Copernicus Marine (http://marine.copernicus.eu), and used in Chapter 4, the floats were found not to have been deployed directly within the cyclonic eddy centre. However, they were sufficiently positioned to allow for an intensive subsurface study of the cyclonic eddy in question.

The five SOLO II Argo floats (WMO numbers: 1676, 1677, 1678, 1679 and 1680) were setup to profile daily from 1000 m to the surface, with park depths initially set for 300 m (Table 3.1). The floats were setup with an additional lithium battery pack and ballasted for the Indian Ocean to allow for longevity of the floats. Given the floats were equipped with Iridium two-way communication transmitters, the floats could be reprogrammed. Thus after the 17th profile, the park depths of the floats

were altered to determine how they may interact with the cyclonic eddy. Float 1676 and 1679 remained at 300 m, 1677 was changed to 500 m, 1678 to 650 m and 1680 to 1000 m.

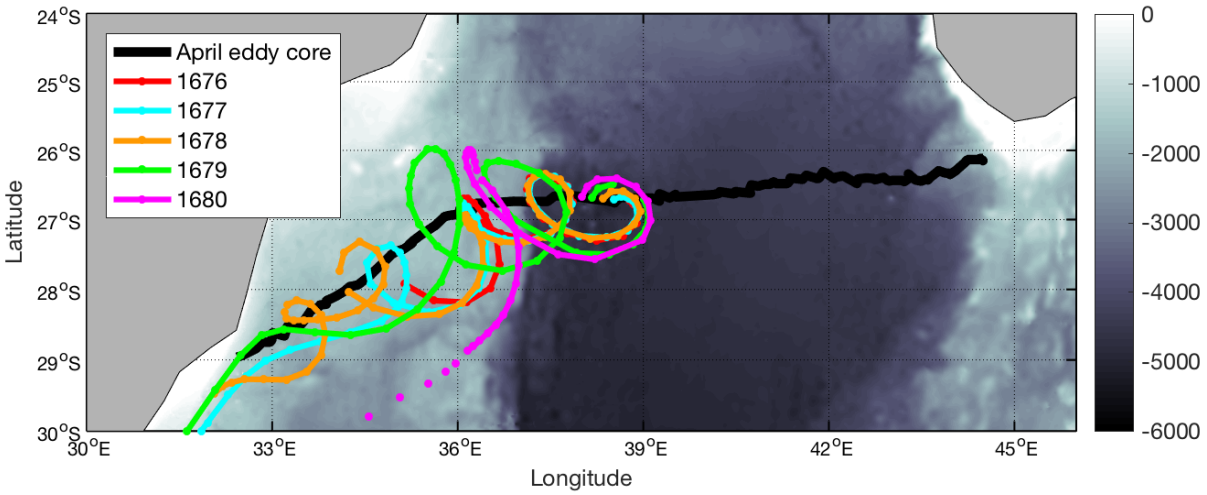

Figure 3.1: *April 2013 Argo float deployments and trajectories with the cyclonic mesoscale eddy track, obtained from an eddy detection and tracking scheme, overlaid as a thick black line*

After the floats exited the cyclonic eddy and the Agulhas Current, they were reprogrammed to continue on the standard Argo profiling mission of 10 days at park depths of 1000 m and profiling from 2000 m to the surface. Of the five floats, one lost communication after 33 profiles (1676), three of the four surviving floats propagated successfully with the cyclonic eddy in to the Agulhas Current southwards, while the last surviving float (1680) left the cyclonic eddy early and missed the Agulhas Current altogether. Detailed results of these two experiments are given in Chapter 4. The surviving four floats eventually propagated in to the western Indian Ocean via the Agulhas Retroflection and Agulhas Return Current.

3.2 July 2013

The second mesoscale eddy experiment deployed four Argo floats, provided by the UK Met Office, in a southwest – northeast transect across the cyclonic eddy (Fig. 3.2). The transect direction was due not to the orientation of the eddy, but rather the trajectory the research vessel was on to reach the southwest Madagascan shelf for sampling purposes. The centre of the cyclonic eddy was again determined at sea with available near-real time data, with actual results collocated with Copernicus Marine data (as above).

The four Apex floats (WMO numbers: 1309, 1310, 1311, 1312) were setup to profile every five days from a depth of 1000 m, parking at 500 m (Table 3.1). However, one of these floats (1312) failed after only four profiles and was removed from any further analysis in Chapter 4. The floats were also not equipped with Iridium transmitters, and thus could not be accessed to change their mission profiles.

For clarity to the reader, the Argo floats were deployed on differing profiling

frequencies (daily and five-daily profiling). This was as a result of the agreement made with the Argo float providers and the telecommunication systems the Argo floats were installed with. Unfortunately, for the July experiment, daily profiling was not possible for the UK MetOffice Argo floats as they could not reprogrammed (Argos-2 technology installed).

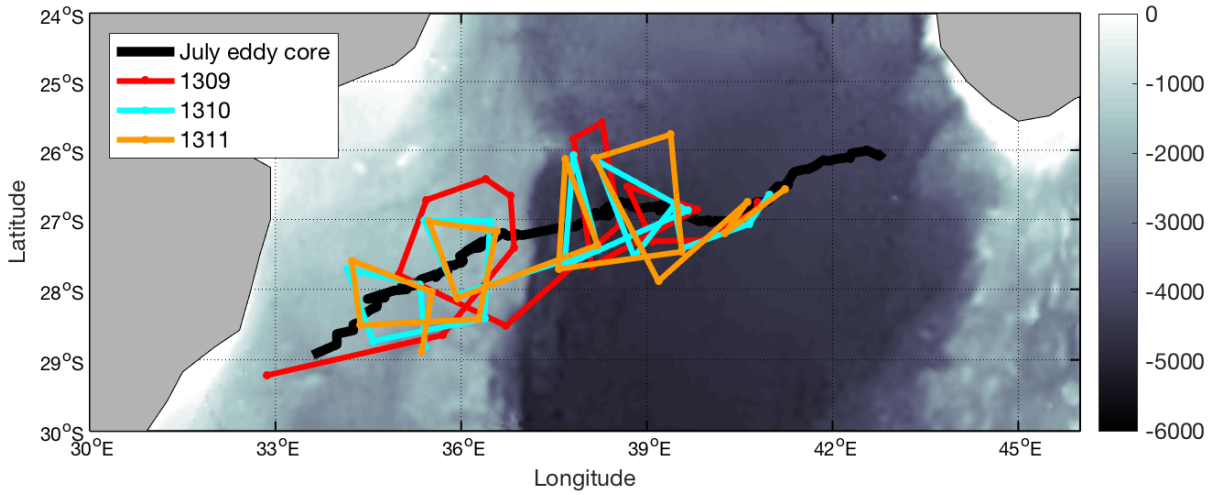

Figure 3.2: *July 2013 Argo float deployments and trajectories with the cyclonic mesoscale eddy track, obtained from an eddy detection and tracking scheme, overlaid as a thick black line*

3.3 August 2017

This final experiment was aimed at the Agulhas Current proper, with the Argo floats setup for deployment across the Agulhas Current offshore of Port Edward on the east coast of South Africa (Fig. 3.3). Six Apex floats (WMO numbers: 1912, 1913, 1914, 1915, 1916, 1917) were provided through the Euro-Argo ERIC MOCCA programme.

The floats were setup to profile daily from 1000 m to the surface with a park depth of 1000 m (Table 3.1). Given floats were deployed inside of, within and outside of the Agulhas Current, many downstream dynamics were captured and the fate of the floats varied between the South Atlantic, Southern and South Indian Oceans. Once the floats had exited the Greater Agulhas Current, the floats were set to the standard Argo mission via Iridium transmitters again.

Analysis of the float data through the stable portion of the Agulhas Current between Port Edward in the north and Port Alfred in the south are explored in Chapter 5.

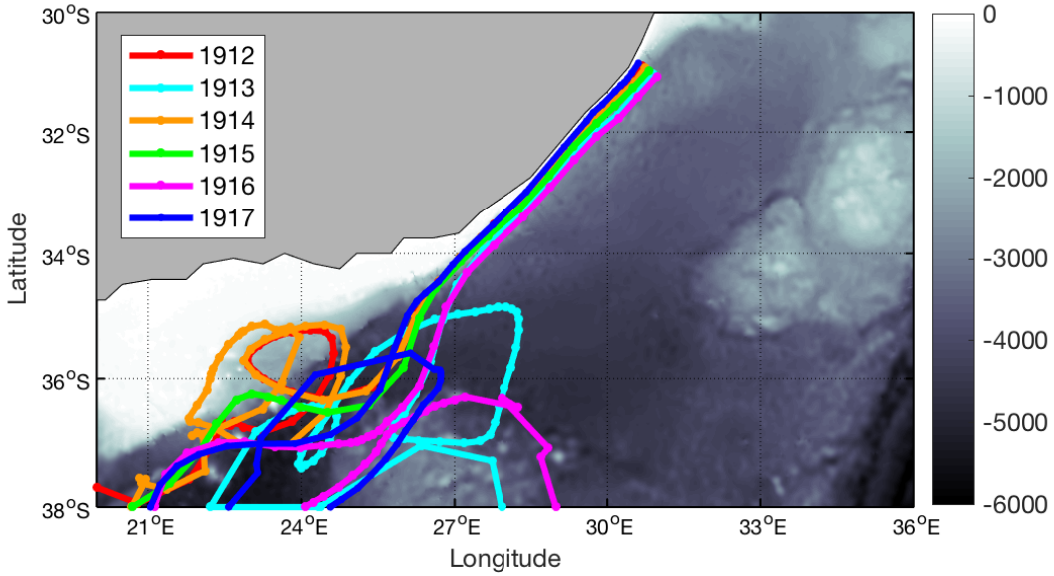

Figure 3.3: *August 2017 Argo float deployment and trajectories in the Agulhas Current.*

Table 3.1 summarizes the three Argo float experiments being investigated for this thesis and provides an efficient comparison of the key Argo float mission parameters and where changes were made.

Table 3.1: *Argo float experiment parameters*

Parameter	**April 2013**	**July 2013**	**August 2017**
Deployment date	12 April 2013	11 July 2013	10 August 2017
Float type	SOLO II	Apex	Provor
No. of floats	5	4 (1 failure)	6
Deployment region	Cyclonic eddy, southern Mozambique Channel	Cyclonic eddy, southern Mozambique Channel	Agulhas Current
Profiling frequency (initial)	Daily	5-daily	Daily
Park depth (initial)	300 m	500 m	300 m
Profile depth (initial)	1000 m	2000 m	1000 m
Profiling frequency (changes*)	1680 to 12 hourly, then 10-daily	none	none
Park depth (changes*)	1677 to 500 m, 1678 to 650 m, 1680 to 1000 m	none	none
Profile depth (changes*)	none	none	none
Battery type	Lithium	Alkaline	Lithium
Transmission system	Iridium	Argos	Iridium
Ballast	Indian Ocean	Indian Ocean	Indian Ocean
Fate of floats	South Indian Ocean	South Atlantic Ocean	South Indian, South Atlantic and Southern Ocean

* Changes to the mission during the experiment. Once outside of experiment bounds, changes to mission not pertinent to further analysis.

Chapter 4

Lagrangian evolution of two Madagascar cyclonic eddies: Geometric properties, vertical structure and fluxes

Preface:

This chapter explores the Lagrangian evolution of two cyclonic mesoscale eddies formed South West of Madagascar. The chapter explores the physical properties, the structure of the eddies and how they flux in terms of mass, heat and salt. This work represents the first such attempt at quantifying these mesoscale eddies, particularly using Argo float technology. This chapter has been published in the Journal of Geophysical Research: Oceans as a peer-reviewed paper, and the Chapter has been laid out in this format:

Morris T., Aguiar-González, B. Ansorge, I. and Hermes, J. 2019. Lagrangian evolution of two Madagascar cyclonic eddies: Geometric properties, vertical structure and fluxes. Journal of Geophysical Research, Oceans, 124. 8193–8218. https://doi.org/10.1029/ 2019JC015090

This chapter addresses the second key question listed in Section 1.3:

By using Argo floats on high-resolution profiling missions, can the knowledge of the vertical structure, geometric properties and fluxes of Madagascar cyclonic eddies be improved?

Abstract

The 3D Lagrangian evolution of two Madagascar cyclonic eddies based on *ad hoc* Argo experiments undertaken in April and July 2013 is investigated. Eight Argo floats were configured to measure temperature and salinity at high temporal resolutions (daily and five-daily experiments) and varying park depths (300 m, 500 m, 650 m and 1000 m) to test their performance with regards retention within the eddies described. Near-surface eddy properties are derived from an eddy detection and tracking algorithm applied to satellite altimetry data and a quasi eddy-resolving (1/4°) ocean general circulation model (GLORYS2v4). Both eddies propagated southwestward from southwest Madagascar (26°S, 40°E), where the South East Madagascar Current separates from the continental shelf. During a travel of about 130 days at an average speed of 11 km day^{-1}, the eddies experienced well defined growth, mature and decay phases, interacting with the Agulhas Current at the KwaZulu-Natal Bight (28°S, 34°E). Model-based estimates indicate the April (July) eddy showed mean trapping water depths of 595 $\pm$ 294 m (914 m $\pm$ 107 m), volume transport about 13.4 $\pm$ 5.2 Sv (21.2 $\pm$ 9.1 Sv), heat flux of -0.07 $\pm$ 0.06 PW (-0.2 $\pm$ 0.09 PW) and freshwater flux of 0.04 $\pm$ 0.04 Sv (0.09 $\pm$ 0.05 Sv). Peak estimates were found for both eddies during the mature eddy phase. These results highlight the role of Madagascar cyclonic eddies as transporters of cooled and freshened source waters into the Agulhas Current and illustrates the benefits of *ad hoc* Argo configurations for the study of 3D Lagrangian eddy dynamics in combination with a 'state-of-the-art' ocean model and remotely sensed data.

4.1 Introduction

Mesoscale eddies are shed southwest off the southern tip of Madagascar (Fig. 4.1), where the South East Madagascar Current (SEMC) detaches from the continental shelf and breaks up into a series of nearly symmetric dipolar vortex pairs at a frequency of four to six dipoles per year (Ridderinkhof et al., 2013). Based on model-based analyses of the energy conversion terms, Madagascar eddies have been suggested to be formed mainly in the upper ocean (0-300 m) by barotrophic instability and at intermediate depths (800-2000 m) by baroclinic instability (Halo et al., 2014b). These eddies tend to drift in a west- or southwestward direction across the southern Mozambique Channel (De Ruijter et al., 2004; Ridderinkhof et al., 2013) and interact with the southward eddy stream from the Mozambique Channel. Downstream, these eddies represent an important source of the flow and variability for the Agulhas Current (Schouten et al., 2002; De Ruijter et al., 2004; Ridderinkhof et al., 2013), the major Western Boundary Current of the South Indian Ocean (Beal et al., 2011).

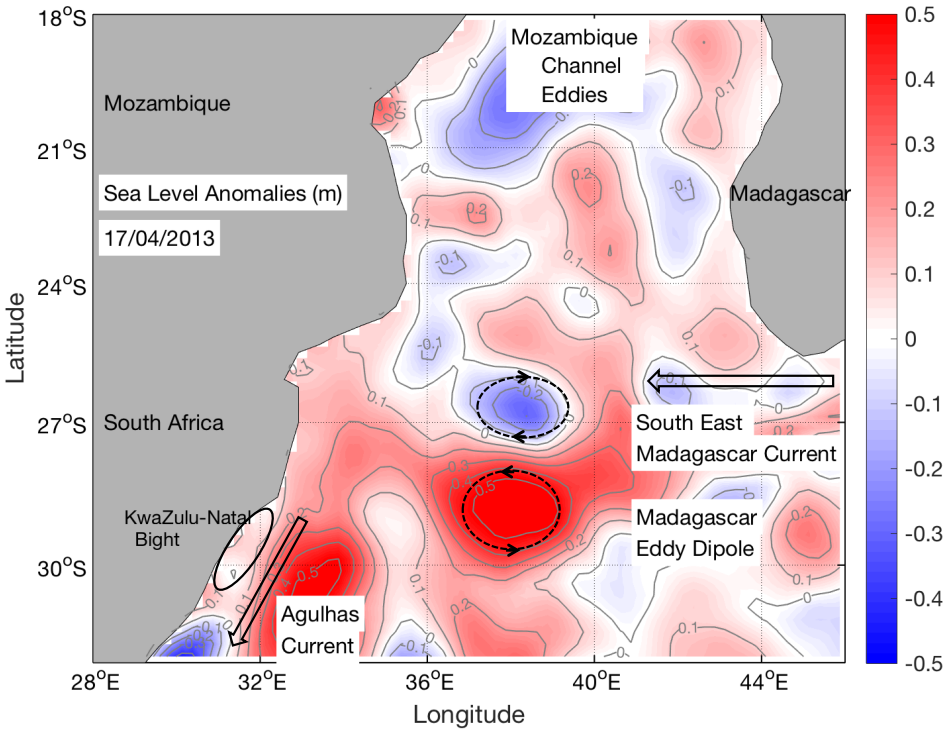

Figure 4.1: *Map of sea level anomaly (m) of the southern Mozambique Channel for 17 April 2013 showing the contribution of mesoscale features in to the Agulhas Current. These include the southwestward eddy stream from the Mozambique Channel and the Madagascar eddy dipolar structure, formed off of the South East Madagascar Current (black arrow). Highlighted against the South African east coast is the location of the KwaZulu-Natal Bight (ellipse) and the Agulhas Current (black arrow). Positive (negative) sea level anomaly represented by red (blue) shaded contours is indicative of anticyclonic (cyclonic) geostrophic circulation.*

Previous studies on eddies in the southern Mozambique Channel have provided information about their mean size, amplitude, propagation speed and seasonality (Quartly et al., 2006; Siedler et al., 2009; Halo et al., 2014b), yet a dedicated Lagrangian description of the eddy-driven volume, heat and salt anomalies which ultimately impact the Agulhas Current remains missing in the literature. Mesoscale eddies can also trap and transport organic and inorganic materials over long distances when they exhibit nonlinear properties, i.e. when the mean speed within the interior of the eddy or mean rotational speed exceeds the mean translation speed (McWilliams and Flierl, 1979; Robinson, 1983; Chelton et al., 2011). In line with this, a recent study has also provided corroborative evidence that suggests Madagascar cyclonic eddies have the potential to be important vectors of connectivity between Madagascar and KwaZulu-Natal, east coast of South Africa (Halo et al., 2014b). These results demand a better knowledge of the time-evolving capacity of Madagascar eddies to trap waters at their interior as they might contribute significantly not only to the heat and salt budgets of the Agulhas Current system but also to its marine ecosystems, carrying ocean properties which are representative of the Madagascar region.

Traditionally, Lagrangian studies of coherent vortices in the ocean are based on eddy properties derived from surface drifters and/or altimetry derived products (Lewis et al., 1989; Pérez, 2003; Sangrà et al., 2005; Beron-Vera et al., 2013; Haller and Beron-Vera, 2013); occasionally complemented with full water-column depth measurements undertaken specifically for a given time of their trajectories (Law et al., 2001; Van Aken et al., 2003; De Ruijter et al., 2004; Sangrà et al., 2007; Casanova-Masjoan et al., 2017). In this regard, the global network of Argo floats following a standard configuration can hardly assist, since having parking depths at 1000 m depth, floats are unlikely trapped over time within mesoscale eddies. This prevents a robust description of their generation and dissipation phases through the water column. The exception occurs when the core of mesoscale eddies reaches the Argo parking depths and the floats can remain trapped in the eddies (Pegliasco et al., 2015). Accordingly, the recent use of Argo floats following non-standard mission parameters allows higher resolution research and has proven successful in a handful of recent works (Riser et al., 2016; Inoue et al., 2016a; Inoue et al., 2016b; Kouketsu et al., 2016). Zhang et al. (2015b) used Argo floats with a high sampling frequency to investigate anticyclonic subthermocline eddies related to the subduction of subtropical mode water in the North West Pacific Ocean. The floats were set on a daily profiling frequency and a park depth of 500 m, profiling from 1000 m to the surface. Results revealed novel characteristics of subthermocline eddies supporting the potential of Argo floats to track and monitor eddies, particularly if on short repeating cycles. On a similar profiling strategy, the ACE-INBOX project (Inoue et al., 2016b) deployed 16 profiling floats from June 2012 to July 2013 within a warm-core anticyclonic eddy and used the data to investigate the salinity minimum and its formation process in the Kuroshio-Oyashio mixed water region.

In this Chapter, the 3D Lagrangian evolution of two Madagascar cyclonic eddies were investigated to improve the understanding of the cyclonic eddy contribution of volume, heat and salt transport from south of Madagascar to the Agulhas Current. To this aim two surveys were designed to deploy a series of Argo floats in the center of two non-concomitant cyclonic eddies using *ad hoc* Argo floats. The surveys were undertaken in April and July 2013, respectively, and non-standard

mission parameters were set up to test the trapping of floats by the cyclonic eddies as a function of their park depths and time-resolution profiling against the eddy core depth, nonlinearity and radius. These *in situ* hydrographic measurements from the Argo floats are combined with satellite altimeter data and the output of a quasi eddy-resolving (1/4°) ocean general circulation model. These diverse, but complimentary, data sources allow for the description of how two Madagascar cyclonic eddies evolve over time from South West Madagascar towards the African coastline carrying heat and salt anomalies which impact the Agulhas Current.

Recent studies based on data collected from one of the surveys described (July eddy) have already proven the advantages of the experimental design with *ad hoc* Argo floats (Barlow et al., 2017; Noyon et al., 2018). Barlow et al. (2017) presented a multi-disciplinary survey of the cyclonic eddy shed off South West Madagascar in July 2013. The authors investigated the capacity of Madagascar cyclonic eddies to transport biological material to the South African coast, and suggested that increased chlorophyll advected from the SEMC was entrained into the eddy. This was further explored by Noyon et al. (2018), who link enhanced mesozooplankton composition of the Madagascar shelf to the western edge of the eddy, potentially using the strong geostrophic flow south of the eddy as a conduit.

This analyses represents the first attempt in examining the spatio-temporal changes experienced in full depth by mesoscale eddies (specifically cyclonic) from their generation site towards a Western Boundary Current. The Chapter is organized as follows. Section 4.2 details the data and methods. Section 4.3 presents the results and discussion in subsections which address consecutively, the near-surface eddy properties, eddy vertical structure, retention capacity and associated volume, heat and salt fluxes of the two Madagascar cyclonic eddies of the study. The main findings and conclusions are summarized in Section 4.4, along with a synopsis on how to set up Argo floats for future mesoscale eddy experiments.

4.2 Data and Methods

Eight Argo floats were deployed in 2013 within the cores of two non-concomitant Madagascar cyclonic eddies as part of two experiments which aim to study eddy dynamics based on a combination of *ad hoc* Argo profiling, altimetry and model data. The Argo float deployments were described in Chapter 3. These experiments (and eddies) are named as the April and July experiments (eddies) following the month in which the floats were deployed. A detailed description of data and methods follows.

4.2.1 Argo-Based Observations

Five Argo floats were deployed on 12 April 2013 crossing a Madagascar cyclonic eddy along an east-west oriented transect, from its westernmost flank towards its center (Figure 4.2a). The five SOLO II Argo floats (WMO number: 1676, 1677, 1678, 1679 and 1680), provided by Woods Hole Oceanographic Institution, were setup to perform daily profiling from 1000 m to the surface with an initial park depth of 300 m and were equipped with Iridium transmitters. This allowed for two-way communication and thus changes to the profiling mission could be made after they were deployed. The floats were ballasted for the Indian Ocean with an additional lithium battery pack to compensate for the above float setup. Modifications of the park depths (listed in Table 5.1) were performed to evaluate the retention capability of the cyclonic eddy throughout the water column.

Three Apex Argo floats were deployed on 11 July 2013 within a Madagascar cyclonic eddy along a southwest-northeast transect crossing the eddy core (Figure 4.2b). The three profilers (WMO number: 1309, 1310, 1311), provided by the UK MetOffice, were setup to perform five-daily profiling from 1000 m to the surface with a park depth of 500 m to ensure battery life and data collection to the Argo data system. Floats were fitted in this experiment with Argos transmitters (i.e. two-way communication was not possible). Deployment of these floats took place while a multi-disciplinary survey of the cyclonic eddy was completed (Barlow et al., 2017; Noyon et al., 2018).

Mission parameters for each experiment are summarized in Table 5.1. All Argo data were collected and made freely available by the International Argo Program and the national programs that contribute to it (http://www.argo.ucsd.edu, http://argo.jcommops.org; (Argo, 2000)). The Argo program is part of the Global Ocean Observing System.

4.2.2 Altimeter Data

The Absolute Dynamic Topography (ADT) daily products produced by SSALTO / Duacs and distributed by Copernicus (http://www.copernicus.eu/) were used. These gridded altimetry products are computed using multimission data and are the same product as was previously distributed by AVISO+. The new version of SSALTO/Duacs product uses a 20-year reference period (1993–2010) of the sea level anomalies (SLA) with a 1/4° Cartesian grid resolution and projection for the global product (Duacs/AVISO, 2014). The ADT products are calculated using a new Mean Dynamic Topography (MDT), which uses the most recent geoid mean field (GOCE DIR-R4) and *in-situ* dataset, with an improved processing method (Duacs/AVISO, 2014).

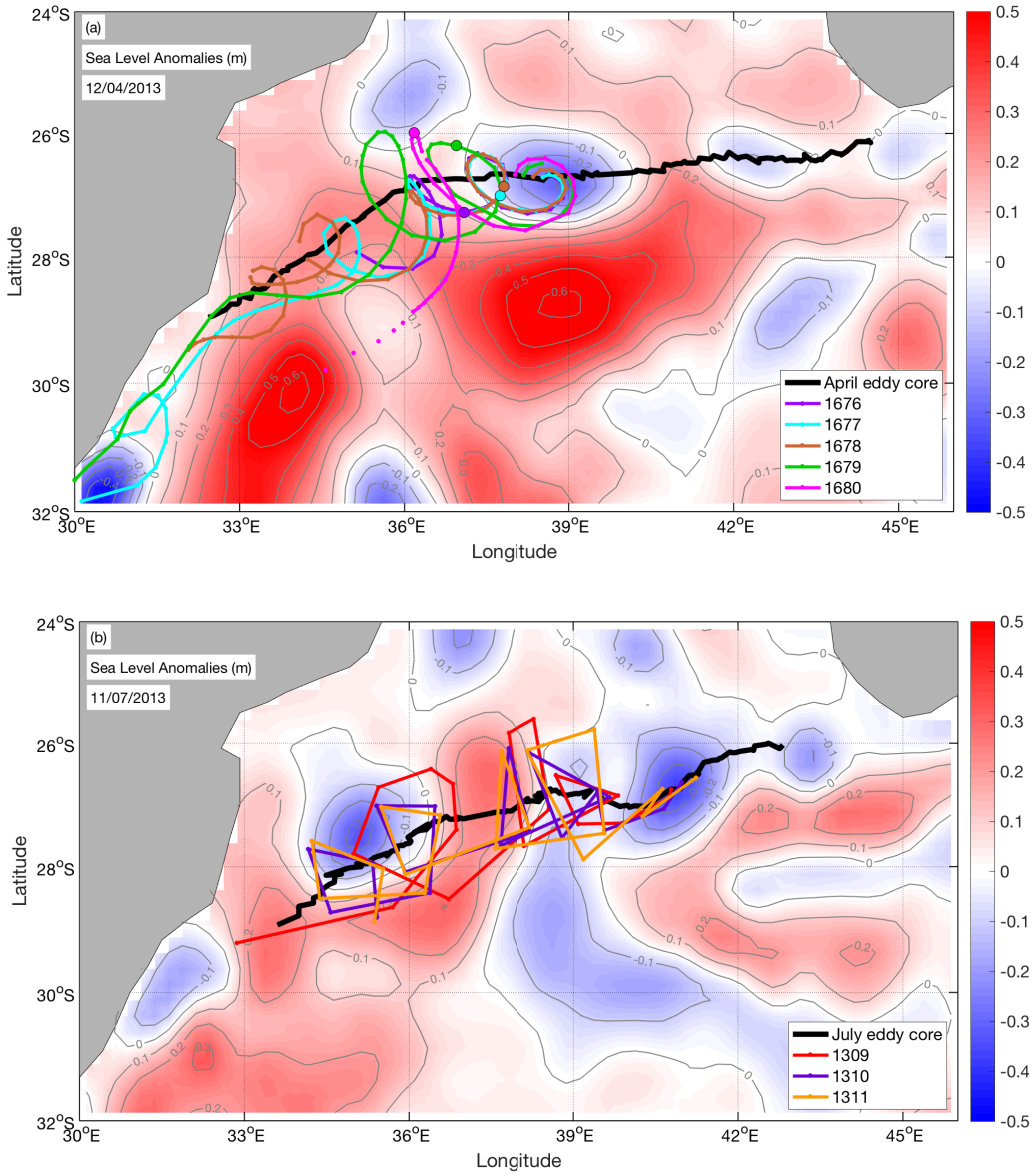

Figure 4.2: *Maps of Sea Level Anomaly (SLA, m) for the date of the Argo float deployments during the (a) April and (b) July experiments. Dates of deployments are 12 April and 11 July 2013, respectively. Float tracks for each panel end on the date the eddy was last detected in altimetry data: (a) 16 June and (b) 16 October. Positive (negative) SLA represented by red (blue) shaded contours is indicative of anticyclonic (cyclonic) geostrophic circulation. The thick black lines represent the altimeter-detected eddy core trajectories from the eddy-tracking scheme (Halo et al., 2014b). Float trajectories are overlaid with coloured lines (see legend for Argo float coding). Note the different time-resolution of Argo profiling: daily for the April experiment and 5-daily for the July experiment. During the April experiment park depths were changed after the 17th profile (29 April 2013) from 300 m after as follows: float 1676 and 1679 remained at 300 m, float 1677 was changed to 500 m, float 1678 to 650 m and float 1680 was changed to 1000 m. The 17th profile is highlighted with a larger circle over the float trajectories. The park depth during the July experiment remained constant at 500 m. Float parameters are summarised in Table 4.1*

Surface absolute (anomaly) geostrophic velocities derived from the altimetry data are based on the assumption of a geostrophic balance, i.e. a balance between Coriolis force and pressure gradient force. Accordingly, altimeter-derived absolute (anomaly) velocities are computed from maps of ADT (SLA) following the geostrophic relationship:

$$u = -g\frac{\partial h}{f\partial y} \qquad v = g\frac{\partial h}{f\partial x} \tag{4.1}$$

where x and y are the eastward and northward spatial coordinates, respectively; u is the zonal velocity (positive in the eastward direction); v is the meridional velocity (positive in the northward direction); h is the ADT (SLA); and g is the gravitational acceleration (9.80 m s^{-2}).

Table 4.1: *Setup parameters of Argo floats for the April and July experiments.*

Mission Parameter	**April Exp.**	**July Exp.**
No. of Floats	5	3
Communication	Iridium (2-way)	Argos (1-way)
Profiling Frequency	Daily	5-daily
Profiling Depth (m)	1000	1000
Initial Park Depth (m)	300	500
Park Depth after 17th Profile: Float Code (Depth, m)	1676 (300) 1677 (500) 1678 (650) 1679 (300) 1680 (1000)	1309 (500) 1310 (500) 1311 (500)

4.2.3 Numerical Model Output: GLORYS2V4

The GLORYS2V4 model was used to complement *in situ* and remotely sensed measurements and extend the analyses towards a 3D view of the thermohaline and horizontal velocity structure of the eddies. GLORYS2V4 is performed using the NEMOv3.1 ocean model in the ORCA025_LIM (1/4° resolution) configuration, and is forced by ERA-Interim atmospheric variables. The model has 75 vertical levels and spans over the period 1993–2015. A multi-data and multivariate reduced order Kalman filter technique, based on the Singular Extended Evolutive Kalman (SEEK) filter formulation, is applied to the assimilation of ocean observations to the ocean model. Ocean observations used for the assimilation include delayed-time along-track satellite Sea Level Anomalies (SLA), daily Reynolds 1/4° AVHRR-only Sea Surface Temperature (SST) satellite data, and *in situ* temperature and salinity profiles extracted from the Coriolis Ocean database for ReAnalysis (CORA) 4 database. These are obtained from all available types of profiling instruments, such as Argo floats, Conductivity, Temperature and Depth (CTD) profiles, Expendable Bathythermography (XBT) profiles and drifters, in both the surface and sub-surface (Cabanes et al., 2013). This reanalysis product (hereafter referred to as the model) is available for download from Copernicus at http://marine.copernicus.eu.

The first baroclinic Rossby radius of deformation for the southern Mozambique Channel ranges from 40 km in the south to 60 km in the north (Chelton et al., 1998; Halo et al., 2014b), while eddies with radii beyond the first baroclinic Rossby radius of deformation have been regularly observed in this region from both *in situ* and satellite altimetry data (De Ruijter et al., 2004; Quartly and Srokosz, 2004; Nauw et al., 2008; Ponsoni et al., 2016). This supports the suitability of the model resolution to resolve the mesoscale variability in the region south of Madagascar. Furthermore, a number of studies have already shown the value of this model in capturing the mesoscale dynamics of the South West Madagascar Coastal Current (Ramanantsoa et al., 2018b; Ramanantsoa et al., 2018a) and the South Indian Ocean Countercurrent (Menezes et al., 2016).

4.2.4 Eddy Identification and Tracking Scheme

An eddy detection and tracking scheme developed by Penven et al. (2005) and modified by Halo et al. (2014a) was used. The algorithm is based on both the closed contour (i.e. geometric criteria) and Okubo-Weiss methods of eddy detection. The closed contour method (Chelton et al., 2011) identifies mesoscale eddies as closed loops of sea surface height (SSH), given an eddy-length scale small enough to exclude gyres. The Okubo-Weiss method (Okubo, 1970; Weiss, 1991) finds regions in the ocean where the mesoscale vorticity dominates the strain (i.e. the Okubo-Weiss parameter (W) is negative).

Results in Halo et al. (2014b) suggest a hybrid eddy detection and tracking scheme is more robust at detecting eddies when compared to using only one of the methods independently of the other. The cyclonic eddies of this study were tracked with reference to their cores, and have specified thresholds to ensure minimal subjectivity of their identification. These thresholds include a 2 cm interval between closed contours, a maximum closed loop of 600 km to avoid gyre-sized anomalies and the number of passes of the Hanning filter equal to two (Halo et al., 2014b). These three parameters were also shown not to have a highly sensitive effect on the number of eddies detected, which proved the hybrid method to be the most suitable for eddy detection in the southern Mozambique Channel region (Halo et al., 2014a).

4.3 Results and Discussion

4.3.1 Near-Surface Eddy Properties

In this section the time-evolution and statistics of the April and July eddy properties derived from the SLA altimetry data are discussed. First, an overview of mean eddy properties exhibited along the pathway from South West Madagascar towards the western boundary current (Section 4.3.1) is provided; second, the Lagrangian evolution of eddy properties is described (Section 4.3.1).

The Pathway from South West Madagascar to South East Africa

The April and July eddies propagated westward, with a slight poleward deflection, from South West Madagascar (∼26°S, 43–44°E), where the SEMC separates from the Madagascan continental shelf. The altimeter-derived track of each eddy core is shown in Figure 4.2 as a black solid line. Both eddies interacted with the Agulhas Current at the KwaZulu-Natal Bight (∼29°S, 32–34°E), separately in time, after a travel of 130–137 days (ca. 5 months) at an average propagation speed of 13–15 cm s^{-1} (Figure 4.2).

The mean propagation speed of the April and July eddies was about two times the phase speed of nondispersive baroclinic Rossby waves for the range of latitude of Madagascar eddies (5–6 cm s^{-1} at 25–30° S), thus exceeding the prediction from theories for nonlinear vortices (McWilliams and Flierl, 1979; Cushman-Roisin, 1994; Chelton et al., 2011). The observed high propagation speeds of the April and July eddies being advected in the southern Mozambique Channel were attributed to the consistent background currents present in this region. Nevertheless, this mean propagation speed was still much less than the mean rotational speed of both eddies (57 cm s^{-1} for the April eddy and 69 cm s^{-1} for the July eddy). This is important as the ratio of the rotational speed, U, to the propagation speed, c, provides a measure of nonlinearity, indicating that both eddies of study were strongly nonlinear (i. e. the nonlinearity ratio exceeds 1). This aspect will be further examined in Section 4.3.3, where the ratio of nonlinearity through the entire water column is computed to determine the trapping depths (and associated volume, heat and salt fluxes) of each eddy evolving in time and space.

The propagation speeds and directions described above agree well with previous works on Madagascar eddy census. A study based on altimeter data for the period April 1995–December 2000 found that Madagascar eddies propagate generally in west- and southwestward directions at speeds between 5 and 10 cm s^{-1} (De Ruijter et al., 2004). The sizes of the cyclones and anticyclones were roughly equal when paired, ranging between 50 and 200 km over their lifespan, and the amplitudes of their anomalies about 31–35 cm. The mean radii of the eddies within the study fell within these ranges although with smaller amplitudes: the April (July) eddy with a mean radius and amplitude of 65 km (89 km) and 16 cm (27 cm), respectively.

Halo et al. (2014b) investigated eddy dynamics south of Madagascar using 17 years of altimetry data (1992–2010) and output from the South West Indian Ocean Model (SWIM) configuration of the Regional Ocean Modeling System (ROMS). The authors found that Madagascar cyclonic eddies were the most abundant and longest-lived (approximately 4 months) when compared to Madagascar anticyclones. Accounting that only a 10 percent of the global eddy population are

long-lived structures with lifetimes $>$ 4 months (Chelton et al., 2011), Madagascar cyclonic eddies stand out as suitable candidates to evolve in time through the growth, mature and decaying phases before dissipation against the Western Boundary Current system.

Lagrangian Evolution

The Lagrangian evolution of altimeter-derived eddy parameters (radius, amplitude, rotational and daily propagation speed) are analyzed for the April and July eddies as presented in Figure 4.3 from application of the eddy identification and tracking scheme. For simplicity the eddy amplitude in absolute value are plotted, but recall here that cyclonic eddies were identified as a low in the topography field, i.e. negative SLA. A summary of eddy characteristics is presented in Table 4.2, along with values similarly derived from the model data; the comparison between both data sources will be addressed in Section 4.3.3 to support the use of the model for further analyses. Furthermore, key events of the life cycle of each eddy are illustrated in Figure 4.4, where a sequence of altimeter-derived absolute geostrophic velocity maps follow the evolution of the April Eddy (panels a-d) and the July Eddy (panels e-h) on selected dates. These dates respond to days over which the April and July eddies interacted with other mesoscale features (labelled on each panel) or against the Western Boundary Current.

Generally, the life cycle of an oceanic mesoscale eddy may be summarised as follows. The eddy evolves along its growth phase from a relatively small initial size towards a mature stage, when the eddy growth slows down and its radius remains nearly stable over time. The mature stage ends when the eddy starts to decrease and approach its initial size along the so-called, decay phase (Zhang et al., 2015a; Samelson et al., 2014). In Figure 4.3, black dashed vertical lines are used to indicate the end and start of the eddy growth and decay phases based on the first and last peaks of the eddy radius, as suggested in Zhang et al. (2015a). At arrival to the Western Boundary Current, both eddies had evolved through well delimited growth, mature and decay stages.

The April eddy was first detected on 31 January at 26.12° S, 44.49° E, with an initial radius and amplitude of 36 km and 4 cm, respectively; while the July eddy was first detected on 14 June at 26.03° S, 42.82° E with a larger initial radius of 49 km and similar amplitude of about 5 cm (Figure 4.3). Interestingly, the April eddy evolved towards a mature stage faster than the July eddy; the growth phase lasted for 26 days for the April eddy and 42 days for the July eddy. This might be a response to the time the July eddy, of a larger initial size, required to evolve and reach its peak dimensions.

Through the mature and decay stages, some general similarities were observed (Figure 4.3). The April eddy collided against the KwaZulu-Natal Bight on 16 June after a total travel of 137 days. As a mature feature (76 days), it propagated with peak dimensions of about 91 km and 30 cm amplitude, decreasing and approaching its initial size of 33 km and 8 cm amplitude along the decay phase (34 days). Roughly, the July eddy experienced an analogous path and arrived at the KwaZulu-Natal Bight on 16 October after a total travel of 123 days. As a mature eddy (39 days), it propagated as a larger feature than the April eddy, having a peak

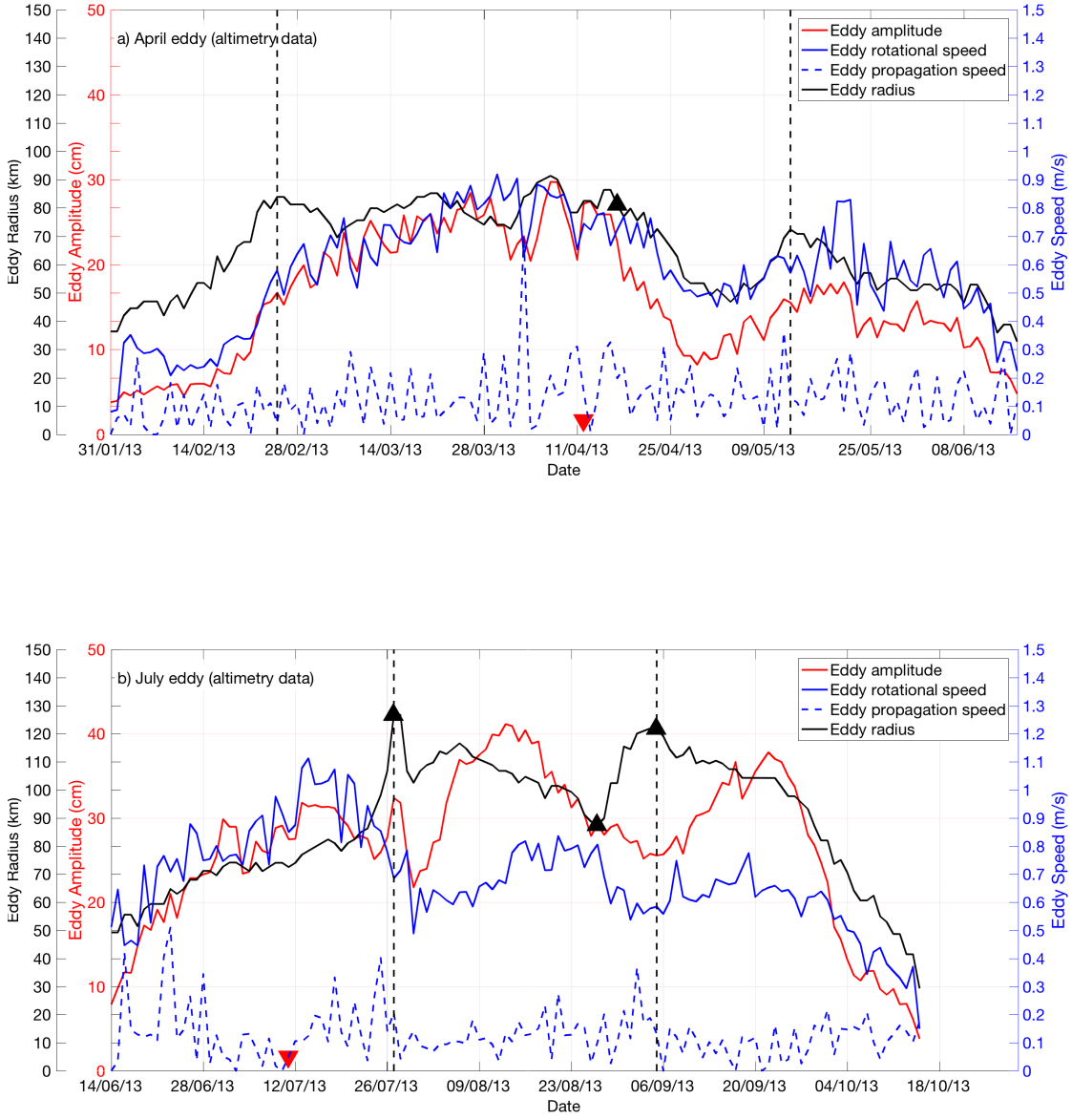

Figure 4.3: *Lagrangian evolution of altimeter-derived eddy radius (km, black line), eddy amplitude (cm, red line), eddy rotational speed ($\mathrm{m\,s^{-1}}$, blue line) and daily eddy propagation speed ($\mathrm{m\,s^{-1}}$, blue dashed line) for the (a) April eddy and (b) July eddy as estimated from applying the eddy tracking scheme (Halo et al., 2014b) over SLA fields. Note that the eddy amplitude is shown in absolute values although cyclonic eddies are identified as a low in the topography field, i. e. negative SLA. The black dashed vertical lines indicate the end and start of the eddy growth and decay phases, respectively (the mature stage evolves between both lines). The red inverted triangles indicate the date when Argo floats were deployed. Black triangle symbols along the radius indicate the start date of the cyclonic eddy merging with adjacent cyclonic anomalies, described further in the text.*

Table 4.2: *Eddy characteristics of the April and July eddies as derived from applying the automated eddy identification and tracking scheme through the satellite altimetry and model data. 'S' stands for satellite altimetry data, 'M' stands for model data and 'CE' stands for cyclonic eddy. Statistics of a given parameter are presented as the mean ± standard deviation. The number and nature of eddy interactions with other mesoscale features is noted after visual inspection of the full time-series of surface horizontal maps from altimetry data.*

	April E. (S)	**April E. (M)**	**July E. (S)**	**July E. (M)**
Generation at SW Madagascar	26.12° S 44.49° E	26.26° S 43.46° E	26.03° S 42.82° E	26.24° S 42.90° E
Dissipation at KwaZulu-Natal Bight	28.96° S 32.43° E	27.98° S 33.91° E	28.93° S 33.60° E	29.38° S 32.80° E
Lifespan mm/dd (days)	31/01–16/06 (137)	21/02–02/06 (101)	14/06–16/10 (123)	02/06–30/10 (130)
Radius (km)	65.43 ± 15.05	74.53 ± 10.28	88.67 ± 22.39	78.66 ± 15.84
Amplitude (cm)	15.81 ± 7.11	13.44 ± 6.33	26.77 ± 8.71	22.12 ± 7.90
Prop. Speed (cm s^{-1})	12.8 ± 9.78	13.7 ± 8.3	14.6 ± 15.01	13.0 ± 8.93
Rot. Speed (cm s^{-1})	57 ± 19	42 ± 19	69 ± 17	62 ± 14
Peak Radius, (km) (Date)	91 (7 April)	89 (23 April)	126 (27 July)	107 (7 Sept.)
Peak Ampl., (cm) (Date)	30 (7 April)	26 (8 March)	41 (13 Aug.)	34 (2 Aug.)
Peak Rot. Speed, cm s^{-1} (Date)	92 (30 March)	87 (7 March)	111 (14 July)	102 (30 July)
Eddy Interact.	1 CE	1 CE	3 CEs	3 CEs

size of about 126 km and 41 cm amplitude. However, the July eddy also decreased its size approaching its initial dimensions along the decay phase (55 days), with a final size of 30 km and 4 cm amplitude.

On closer inspection, each eddy resembled varying structures given the occasional fluctuations of the eddy radius in response to interactions with other mesoscale features. The eddy radius was taken as reference of the eddy evolution and compared to its trend against the amplitude and rotational speed curves in Figure 4.3. This allowed a better account for eddy interactions and merger events, highlighting the complexity of studying lagrangian properties in dynamically active areas. To ease the interpretation, the relationship between eddy radius, amplitude and rotational speeds was referenced. The eddy amplitude relates to rotational speeds following Eq. 4.1. A prominent low in SLA is suggestive of a

strong cyclonic geostrophic circulation, while the opposite occurs with a prominent high, pointing to a strong anticyclonic circulation. The stronger the spatial gradient of SLA becomes in Eq. 4.1, the stronger the rotational speeds of the eddies are. According to this, one finds strengthening of eddy rotational speeds when, for a given eddy radius, the associated low (or high) in SLA intensifies; analogously, eddy rotational speeds slow down when the low (or high) in SLA weakens. The same applies to lows and highs in ADT and the associated absolute geostrophic velocity field.

In principle, the relationship between the eddy radius, amplitude and rotational speed holds tight in parallel while the eddy propagates without complex interactions with other mesoscale features and / or physical boundaries. This is the case of the April eddy, whose evolution of the eddy radius, amplitude and rotational speed followed each other closely through the growth, mature and decay phases. Along its lifespan only one merger to another relatively small cyclonic eddy was detected, which originated in the Mozambique Channel. The date when this interaction started is highlighted in Figure 4.3a with a black triangle. The interaction with this second cyclonic eddy started on 17 April with the elongation of the feature to the northwest (Figure 4.4a), showing a more complete merger by 29 April (Figure 4.4b). During the merger, the April eddy decreased both in size and amplitude, while rotational speeds also weakened (Figure 4.3a). By 13 May the merger was complete (Figure 4.4c) and the April eddy exhibited a moderate strengthening just before starting its decay phase (Figure 4.3a). This occurred about one month prior to collision against the Agulhas Current, when the April eddy represented a smaller, weaker cyclonic eddy entering the KwaZulu-Natal Bight from the north and disappearing from the eddy detection and tracking scheme on 16 June 2013 (Figure 4.4d).

Differently, the July eddy evolved as a larger mesoscale vortex with parameters exceeding those reached by the April eddy (see Table 4.2) and the tight relationship between the trends of the radius, amplitude and rotational speed was only clear during the growth and decay stages (Figure 4.3b). During the mature stage, three noticeable disruptions occurred matching in time the interaction of the July eddy with other smaller cyclonic features to the north and east of it. The dates when these interactions started are indicated with black triangles in Figure 4.3b and are tracked through a sequence of maps in Figure 4.4. Two smaller cyclonic eddies were evident to the east and west on 27 July and 27 August, respectively, which eventually merged with the July eddy (Figure 4.4e, f). Towards the end of the July eddy track, further interactions with cyclonic features to the north were also evident on 5 September (Figure 4.4g), prior to interaction against the Western Boundary Current on 22 September (Figure 4.4h).

As advanced in the previous section, the mean propagation speed of the April and July eddies suggests both features propagated as strongly nonlinear vortexes. This is shown in Figure 4.3 noting that the propagation speeds of both eddies ranged most of their lifespan at rather weaker values than the rotational speeds (compare blue dashed and solid lines in panels a and b).

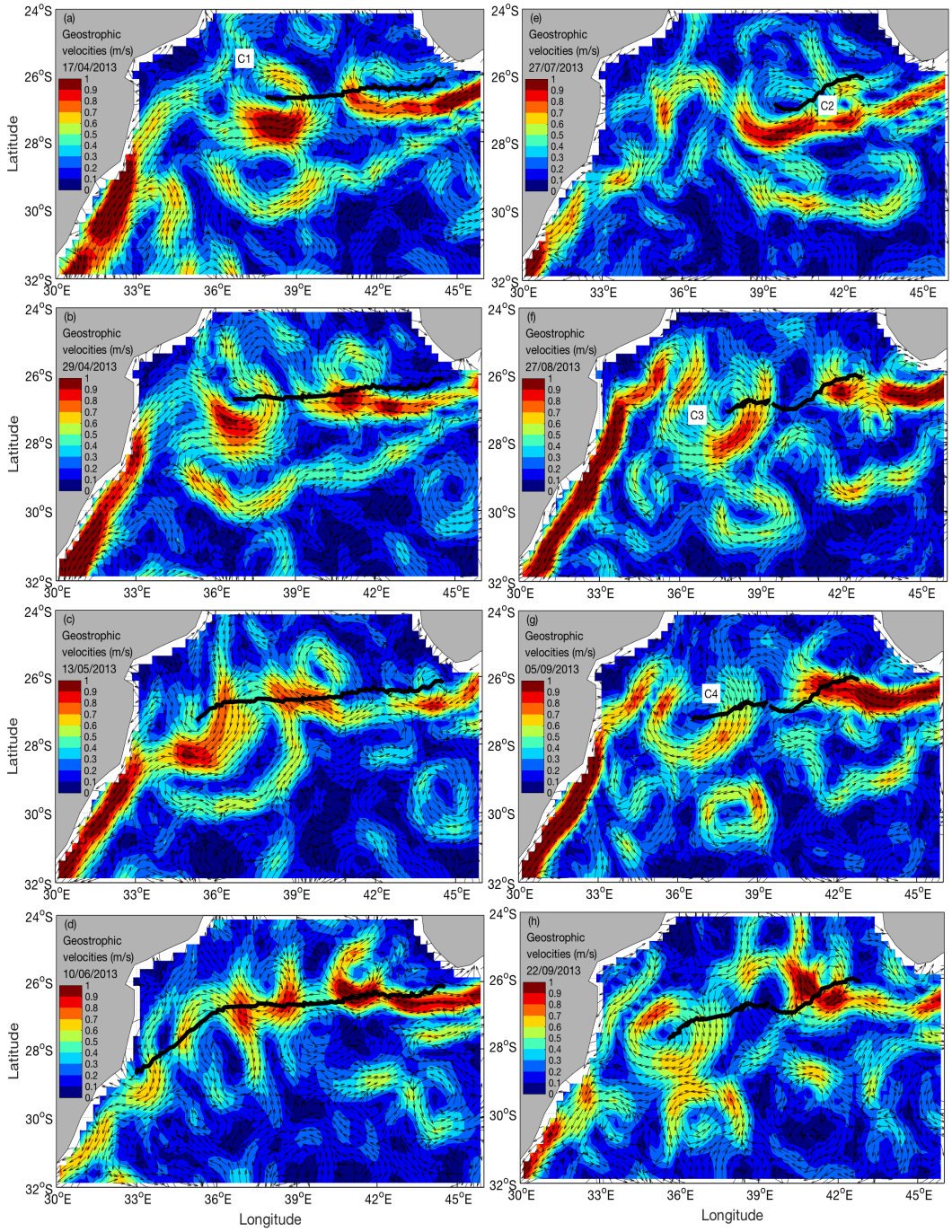

Figure 4.4: *Evolution of the April (a-d) and July (e-h) eddies as seen from a set of altimeter-derived geostrophic velocity maps at selected dates. Shades of colors are speed in units of cm s^{-1}. Arrows represent unit vectors parallel to the vector velocity field. The selected dates refer to key events discussed in the text: a) 17 April, b) 29 April, c) 13 May, d) 10 June, e) 27 July, f) 27 August, g) 05 September, h) 22 September. The eddy core trajectories are shown as thick black lines. Labels with white background overlying the velocity field, and noted as C1–C4, stand for numbered cyclonic features interacting with the April and July eddies.*

4.3.2 Eddy Retention and Vertical Structure based on Observations

As explained in the *Introduction*, Argo floats in this study followed non-standard configurations aiming to test the capability of capturing eddy dynamics if park depths fall within the eddy vertical extent for trapping waters, thus preventing floats from leaving the eddy along their lifespan.

In this section the success of Argo floats on being retained within the eddies as they propagated southwestward across the Mozambique Channel based on Argo float trajectories and altimeter-derived eddy properties is evaluated (Sections 4.3.2 and 4.3.2). Furthermore, a number of Argo floats sampling the April and July eddy cores and eddy flanks were selected to investigate the Lagrangian evolution of temperature and salinity properties carried by the eddies over time and space (Section 4.3.2). Given that floats do not remain stationary or evenly spaced within the eddies, the observational view presented here is complemented with further analyses based on model data in subsequent sections.

Eddy Retention: the April Eddy

The April eddy was surveyed on 12 April with five Argo floats deployed from its western edge towards the core, when the eddy was located roughly in the middle of the southern Mozambique Channel, centered at 26.73° S, 39° E, and loosely paired to an anticyclonic eddy as part of a dipolar structure (Figure 4.2a; see the color code for floats in legend). A dipole structure is two counter-rotating eddies, once cyclonic and one anticyclonic, forming a jet current where the two eddies connect. Over the deployment date, the eddy was about 71 days old, evolving through its mature phase (see the inverted red triangle in Figure 4.3a).

While Argo floats during the April experiment were all setup to perform daily profiling from 1000 m to the surface with an initial park depth of 300 m, the initial distances for float deployments ranged among floats from 70 km to 15 km off the eddy core. According to the float trajectories in Figure 4.2a, the time-varying distance of each float to the altimeter-derived eddy core (see the color code for floats in legend) is presented in Figure 4.5a. The inset shows the full lifespan of the eddy radius as per reference to Figure 4.4.

The most prominent feature during the April experiment was the zigzagging of float distances, suggesting the floats were systematically travelling by subsequent times, first, towards the eddy edge and, then, back towards the eddy core. This pattern was followed by all floats for about one month of daily profiling (Figure 4.5a). A secondary circulation within the eddy may be accounting for this phenomenon, driving the convergence of floats towards the eddy core and divergence towards the eddy edges according to the time the floats spent drifting both at surface and at the park depths. This pattern also suggests the altimeter-derived eddy radius might be either an underestimation of the actual eddy radius or that the eddy dynamics still have a strong influence in surrounding waters beyond the eddy edges; otherwise, it is hard to account for the systematic convergence of Argo floats back towards the eddy core once they have exceeded the eddy radius in several dozens of kilometers from the eddy core.

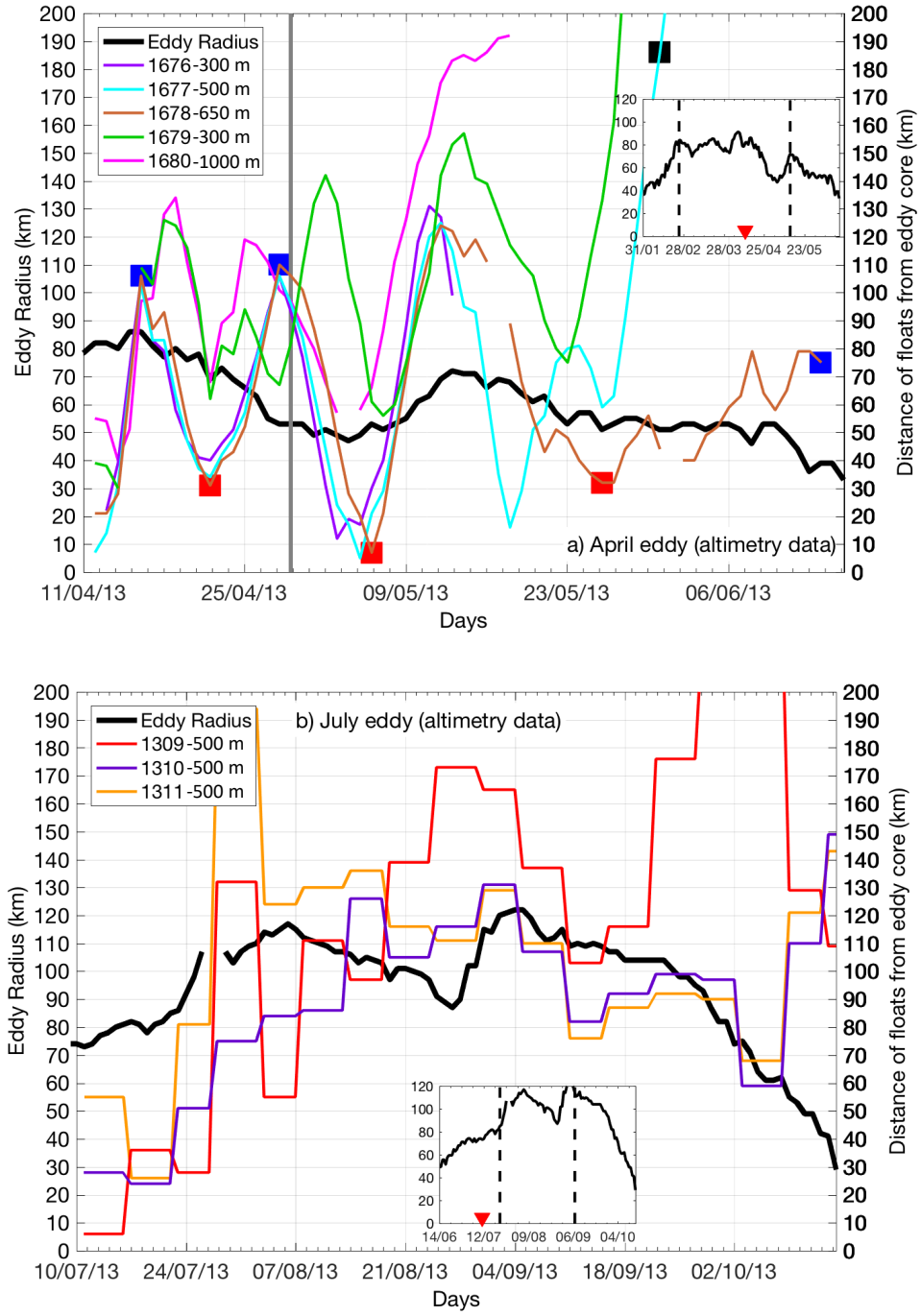

Figure 4.5: *Argo float retention within (a) the April eddy and (b) the July eddy as seen from time-evolving distance to the eddy core (see legend for Argo float coding). The time evolution of the eddy radius (thick black line) is shown as indicative of the eddy size. The insets show the full lifespan of the eddy radius evolution, as per Figure 4.3. Within (a), the blue squares represent the profiles farthest away from the eddy core shown in Figure 4.6, while red squares show the profiles closest to the eddy core. The black square represents the profile for float 1677 which enters the Agulhas Current before the eddy, as per Figure 4.6. The grey solid line in (a) highlights the 17^{th} profile where mission parameters were altered.*

At the 17^{th} profile (29 April) after deployment during the April experiment, the park depth of the floats were changed from 300 m as follows: float 1676 and 1679 remained at 300 m (the former stopped communicating after 33 profiles); float 1677 was changed to 500 m, float 1678 to 650 m and float 1680 was changed to 1000 m (see a summary of mission parameters in Table 4.1). The merger of the April eddy to another (smaller) cyclonic eddy, as described in Section 4.3.1 (Figure 4.4a-c), occurred coincidentally to the park depth changes made to the floats. Large coloured circles along the float tracks in Figure 4.2a highlight the float positions where the park depths were modified. In Figure 4.5a, the 17^{th} profile is also indicated (see gray vertical line). As explained in the *Introduction*, these changes were configured to assess the effectiveness of Argo floats on capturing eddy dynamics depending on different park depths.

Figure 4.5a highlights that before the 17^{th} profile, all floats were retained by the eddy dynamics, suggesting 300 m as park depth was a suitable choice. One week after the 17^{th} profile, the float 1680 (1000 m park depth) left the eddy, increasing in time its distance to the eddy core until end of communication. This suggests that 1000 m as park depth might actually fall out of the range of eddy trapping depths. All other floats (park depths between 300–650 m) remained under the influence of the April eddy for at least one extra month (29 April–23 May); except the float 1676 (300 m as park depth), which stopped communicating about two weeks after the 17^{th} profile while still zigzagging from the eddy edge towards the eddy core.

The floats 1677 and 1679 (500 m and 300 m as park depths) left the April eddy and started their propagation towards the Western Boundary Current around 23–27 May, one month after the 17^{th} profile. This occurred while the floats were circulating around an enlarged merged cyclonic eddy (Fig. 4.4c), likely hampering its return travel towards the eddy core and favouring its exit. These floats reached the Western Boundary Current soon afterwards and, propagating along the Agulhas Current, increased quickly their distance from the April eddy core (see cyan and green lines in Figure 4.2a and Figure 4.5a). Interestingly, the float 1678 (650 m as park depth) remained within the eddy to the end of its lifespan, upon arrival to the Western Boundary Current.

Eddy Retention: the July Eddy

The July eddy was surveyed with three Argo floats deployed during the eddy growth phase, when the eddy was 27 days old on 11 July (Figure 4.2b and Figure 4.3b). The floats were deployed from southwest to northeast crossing the eddy center and falling within a range of 60 km from the eddy core. All floats were setup to perform five-daily profiling from 1000 m to the surface with a park depth of 500 m, which was not modified after deployment as it occurred during the April experiment.

Interestingly, the float deployed closest to the eddy core (float 1309; red line in Figure 4.2b and Figure 4.5b) eventually moved the furtherest away, while the other two (floats 1310 and 1311) remained closely associated with the eddy radius to the end of the eddy's lifespan. However, it is worthwhile noting the exit of the float 1309 occurs after two months of the instrument being under the influence of the eddy dynamics, thus further supporting the suitability of 500 m as Argo park depth for the float to be retained within the eddy. Similar to what was observed

from the Argo float distances to the April eddy core (Figure 4.5a), the Argo float distances to the July eddy core were observed zigzagging in space and time around the eddy edges, although the lower time resolution of the Argo profiling during this experiment hampers a clear visualization of the phenomenon.

Results in Sections 4.3.2 and 4.3.2, based on Argo float trajectories and altimeter-derived eddy properties, suggest that the most suitable configuration (among tested options) to capture eddy dynamics of Madagascar cyclonic eddies was daily profiling with park depths between 300–650 m. On the one hand, the park depth at 1000 m tested during the April experiment seemed to exceed the vertical extent of the eddy while shallower park depths resulted in floats drifting over longer periods of time within the eddies. On the other hand, the five-daily profiling of the July experiment appears to miss details of the apparently rapid secondary circulation patterns suggested by the convergence/divergence of the floats towards/from the eddy core, and which demand further investigation. In Section 4.3.3 the vertical extent of the April and July eddies were assessed as they evolve in time and space based on model data, supporting further the suitability of Argo park depths between 300–650 m following estimates of nonlinearity through the water column (a measure of eddy retention) and associated eddy trapping depths.

Vertical Structure

To illustrate the evolution of the vertical structure of a prototypical Madagascar cyclonic eddy as seen from Argo profiling, a series of vertical profiles of (a) conservative temperature, (b) absolute salinity and (c) potential density from float 1678, which remained with the April eddy the longest at daily profiling is presented in Figure 4.6. Results in Figure 4.5a were used to select the profiles of interest according to its spatial closeness to the eddy core and eddy flanks, respectively, so that differences in properties carried by the eddies over time and space could be assessed separately. The selected profiles falling close to the eddy edges are shown with blue squares in Figure 4.5a, while profiles close to the altimeter-detected eddy core are shown with red squares. Also in Figure 4.5a, the black square along the curve for float 1677 indicates an Argo profile which sampled the Agulhas Current 15 days before float 1678 sampled nearly the same location (29.5°S, 32.1–32.3°E), while still retained within the April eddy before it interacted with the Agulhas Current (see legend in Figure 4.6). The comparison between these two Argo profiles from different floats (1677 and 1678) allows an estimation of the magnitude of temperature and salinity anomalies carried by the April eddy upon interaction with the Agulhas Current (Figure 4.6d, e). Based on all the Argo profiles described above, the variability of water masses is presented following the θ/S_A diagram in Figure 4.6f.

Among the profiles sampled within the April eddy (both the core and flanks), surface waters displayed the highest variability as a consequence of direct and rapid ocean-atmosphere interactions modifying the upper ~100 m of the water column, where Tropical Surface Water (TSW: σ_Θ<25.5 kg m^3; Beal et al. (2006)) becomes cooler and saltier over time as the eddy propagates southwestward (Figure 4.6a–c, f). At 150–200 m, all eddy profiles presented a subsurface salinity maximum approaching 35.65, characteristic for Subtropical Surface Water, (STSW Gründlingh et al. (1991)); and, below, a rather less variable domain of South Indian

Central Water between 300–900 m (SICW: 8–14°C, 34.6–35.4 g kg^{-1}; Emery (2001)). Deeper than 900 m, eddy profiles showed a progression from diluted Red Sea Water (RSW) towards Antarctic Intermediate Water (AAIW) signals. The RSW signal, originated further north, opposes to the AAIW signal, originated further south, on that the latter was characterised by salinities lower than 34.6 g kg^{-1} while RSW was found commonly saltier than 34.6 g kg^{-1}. The progressive decrease in diluted RSW and increase in AAIW as the floats travelled southwestward suggests the eddy capability to retain temperature and salinity properties over time along its pathway to the African coastline might not reach beyond 900 m. Above this depth level and up to 100 m, all eddy profiles followed each other remarkably closely as the eddy evolved in time and over space. Especially profiles sampling the eddy core, which was suggestive of the retention capability of ocean properties of the eddy. The description of water masses characterising the April eddy agreed well with that reported in De Ruijter et al. (2004), focused on the first 400 m of the water column, and based on direct measurements of temperature and salinity surveying a Madagascar cyclonic eddy in the middle of the southern Mozambique Channel.

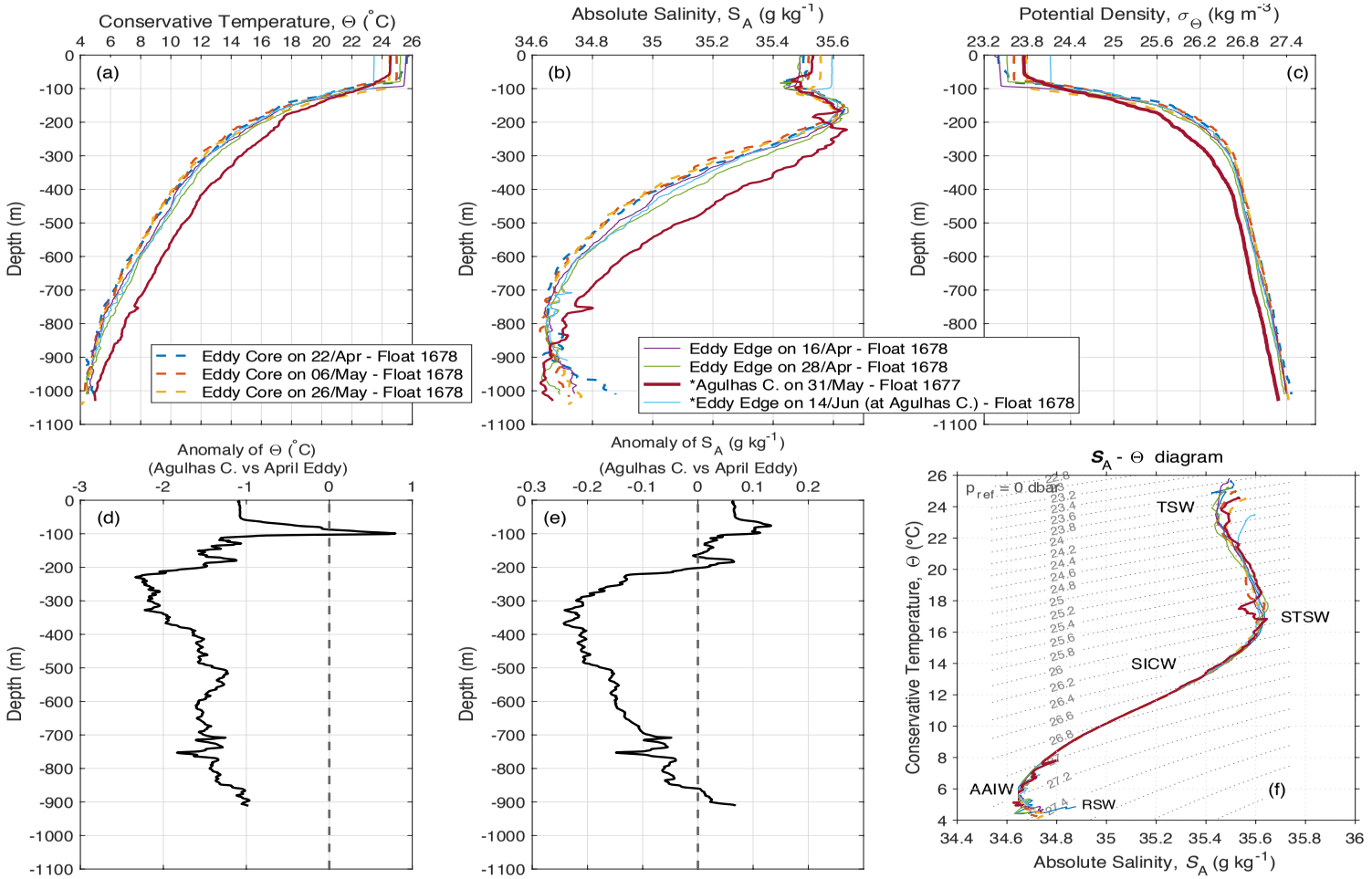

Figure 4.6: *Argo-based vertical profiles of (a) conservative temperature, (b) absolute salinity and (c) potential density (kg m^{-3}) representative of properties along the eddy edge (solid lines) and within the eddy radius (dashed lines) as identified by blue and red squares, respectively, in Figure 4.5a (see float 1678, brown line, sampling the April eddy). The anomaly of (d) conservative temperature and (e) absolute salinity was calculated from comparison between a profile from float 1677 sampling the Agulhas Current and a profile from float 1678 sampling the cyclonic eddy while interacting with the Agulhas Current at nearly the same location (29.5°S, 32.1–32.3°E) but 15 days apart. (f) Conservative temperature vs absolute salinity diagram with indication to water masses: Tropical Surface Water (TSW), Subtropical Surface Water (STSW), South Indian Central Water (SICW), Antarctic Intermediate Water (AAIW), Red Sea Water (RSW).*

When compared to the Argo profile which sampled the Agulhas Current (dark red lines in Figure 4.6a–c, f), the eddy profiles exhibited a distinctive cooler and fresher vertical distribution of ocean properties highlighted as negative temperature and salinity anomalies which extended through the water column down to 900 m, except for a relatively shallow and weak positive salinity anomaly within the upper 200 m (Figure 4.6d, e). These negative temperature and salinity anomalies were as large as -2°C (0–900 m) and -0.2 g kg^{-1} (200-900 m), respectively. These results support the potential of Madagascar cyclonic eddies to transport large temperature and salinity anomalies effectively from Madagascar to southeast Africa, from the surface down to about 900 m.

In the next section model data is used to provide first estimates of the volume, heat and salt fluxes associated to the April and July eddies down to their time-varying trapping depth as they propagated towards the western boundary, thus evaluating how these fluxes may change in time according to the growth, mature and decay phases of the eddies.

4.3.3 Vertical Structure, Eddy Retention and Fluxes based on Model Data

In this section the observational view in previous sections are complemented and extend the analyses supported on model data to examine, first, the time-evolving vertical structure of the April and July eddies through their growth, mature and decay phases (Section 4.3.3); second, their time-varying retention capacity and associated volume, heat and freshwater fluxes (Section 4.3.3). The aim is to assess the major changes which characterise the Lagrangian evolution of these features upon interaction with the Agulhas Current.

Vertical Structure

Figure 4.7 shows the Lagrangian evolution of near-surface eddy properties of the April and July eddies calculated using the eddy detection and tracking scheme of Halo et al. (2014b) over model data. These eddy properties are model eddy radius (black line), amplitude (red line), rotational speed (solid blue line) and the daily eddy propagation speed (dashed blue line) for both the April and July eddies (panels a and b, respectively). The same axis limits are applied (particularly with reference to time) that are used in Figure 4.3 (altimeter-derived properties) to ease comparison between data sources, for which a summary is also provided in Table 4.2.

As compared to the altimeter-derived Lagrangian evolutions, the model April eddy was detected later in the eddy tracking scheme (21 February), further west (26.26° S, 43.46° E), and disappeared sooner (02 June), slightly north of the KwaZulu-Natal Bight (27.98° S, 33.91° E), lasting 101 days in total (Table 4.2). Regarding the model July eddy, its detection was slightly later (22 June) in a very similar position as the altimetry July eddy, but lasted longer (30 October), and dissipated similarly off of the KwaZulu-Natal Bight. The above differences being noted, the overall comparison of spatial and time scales of the model April and July eddies showed a good agreement with eddy statistics of the altimeter-derived properties in Table 4.2, and their corresponding Lagrangian evolution in Figure 4.3. This encourages the extension of the analyses further based on the model data.

Following the model-derived Lagrangian evolution of the April and July eddies in Figure 4.7, presented in Figure 4.8 is a set of horizontal maps of surface velocity (m s^{-1}) for selected dates. These dates were representative of the eddy growth, mature and decay phases of each eddy. These maps are used, first, to describe the eddy evolution at surface; and second, to identify the latitudes over which to extract zonal transects to investigate the time-varying vertical structure of the eddies as they propagate towards the Western Boundary Current.

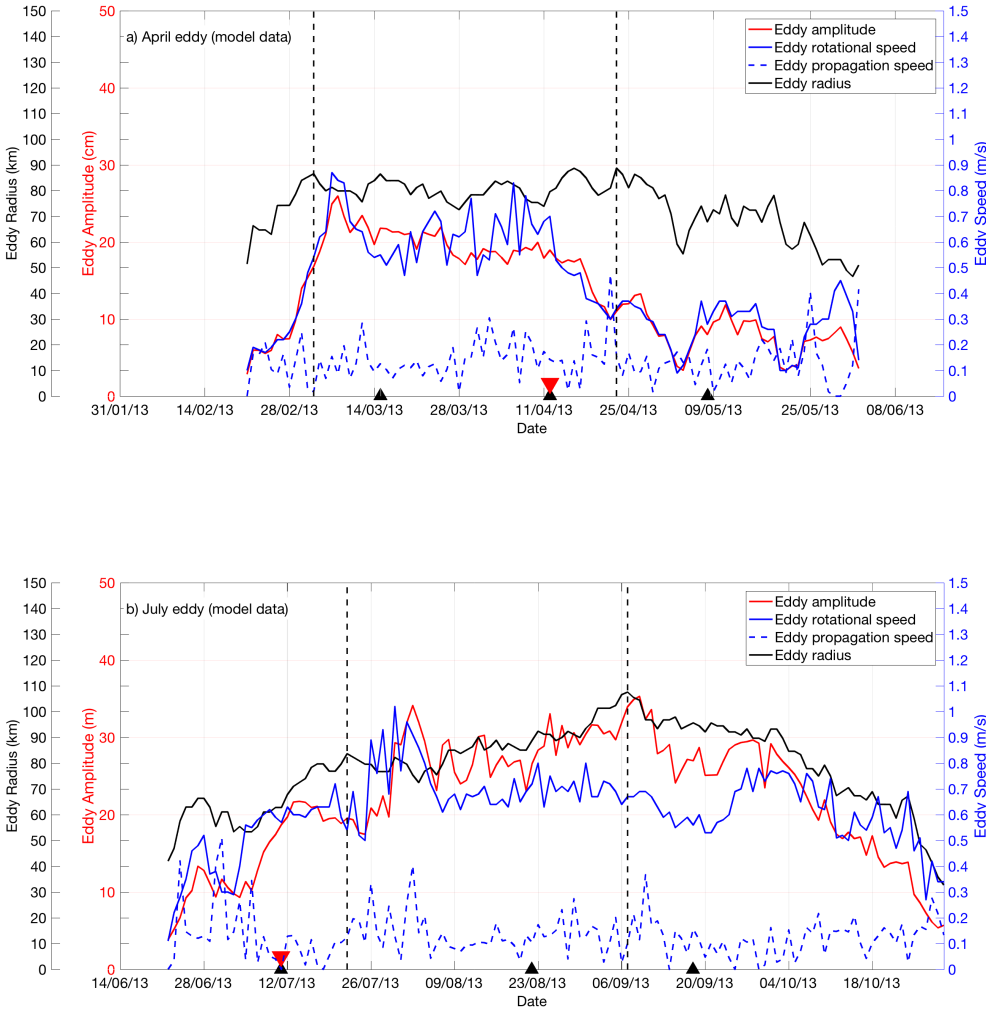

Figure 4.7: *Lagrangian evolution of modelled-derived eddy radius (km, black line), eddy amplitude (cm, red line), eddy rotational speed* ($\mathrm{m\,s^{-1}}$, *blue line) and daily eddy propagation speed* ($\mathrm{m\,s^{-1}}$, *blue dashed line) for the (a) April eddy and (b) July eddy as estimated from applying the eddy tracking scheme (Halo et al., 2014b) over model. The red inverted triangles indicate the deployment of floats within the eddies. The black dashed vertical lines indicate the end and start of the eddy growth and decay phases, respectively (the mature stage evolves between both lines). Black triangle symbols indicate the the dates of the non-linear profiles plotted in Figure 4.11.*

Figure 4.8 a and d show at the surface a recently formed Madagascar cyclonic eddy, paired to an anticyclonic eddy as part of a dipolar structure. The dates are 3 March and 11 July, respectively, and captured the April and July eddies during their growth phase. Next, panels b (12 April) and e (22 August) show the eddies while crossing the southern Mozambique Channel during their mature phase, propagating southwestward as well developed and dynamically strong mesoscale features. Lastly, panels c (8 May) and f (19 September) capture the eddies as decaying features prior to interaction with the Agulhas Current.

On each panel of Figure 4.8, two black solid lines are overlaid. The zonal lines indicate the location of the zonal transects extracted from the model to illustrate the spatio-temporal evolution of the vertical structure of the April and July eddies (Figures 4.9 and 4.10). The meridional lines indicate the intersecting location of the eddy center, shown as a dashed vertical line in Figures 4.9 and 4.10 to highlight the position of the April and July eddies, respectively. These vertical sections present the conservative temperature, absolute salinity, potential density and meridional velocity anomalies along a sequence of zonal cross-channel transects which intersect the April and July eddies as they progressed across the southern Mozambique Channel.

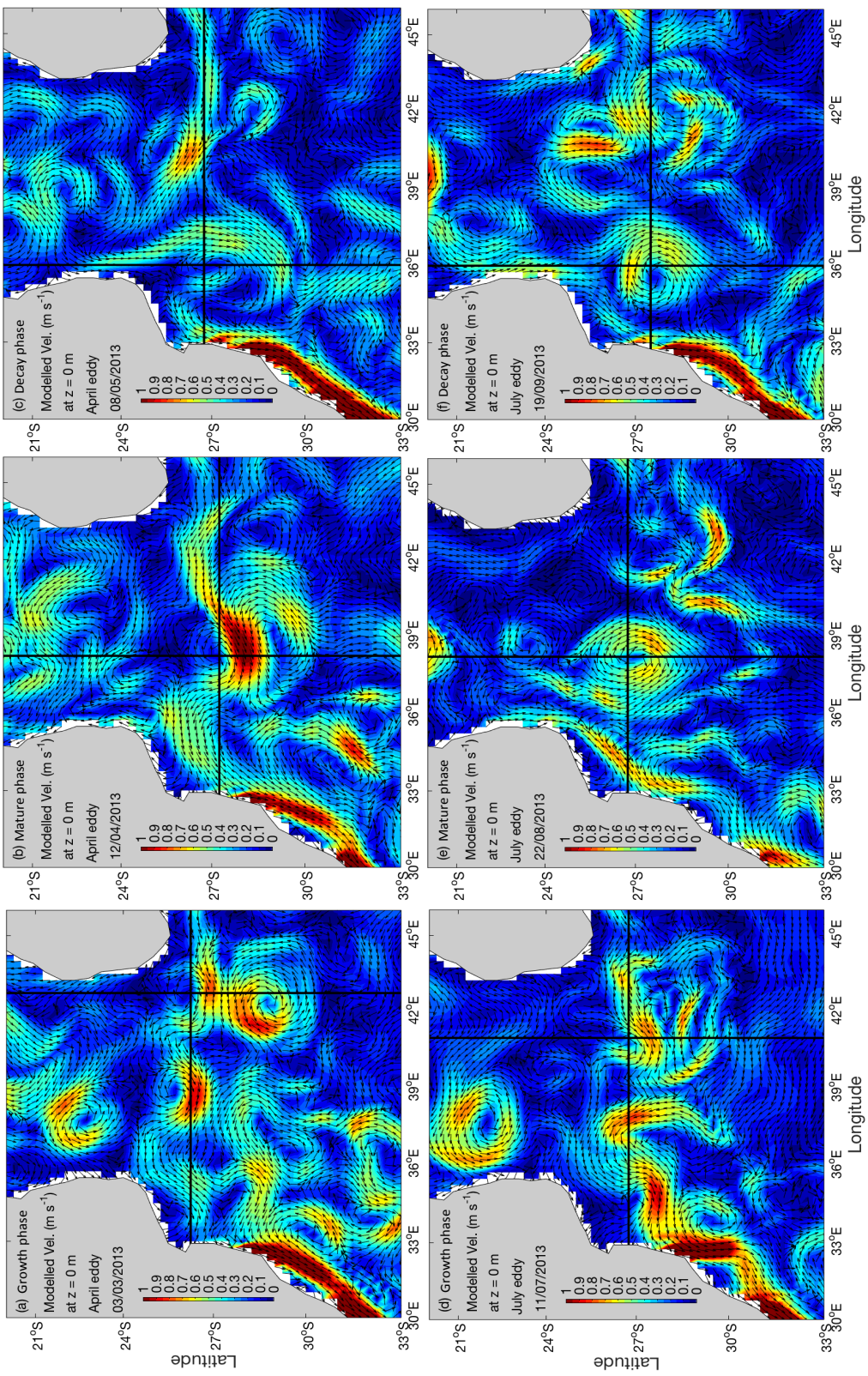

Figure 4.8: *Horizontal maps of modelled surface velocity (m s^{-1}) at selected dates which capture the growth, mature and decay phases of the April eddy respectively. For the April eddy the selected dates are: (a) 3 March, (b) 12 April and (c) 08 May. For the July eddy the selected dates are: (d) 11 July, (e) 22 August and (f) 19 September. Overlaid on to the core of the cyclonic eddy of study are the zonal transects selected for each date, as shown in Figures 4.9 and 4.10.*

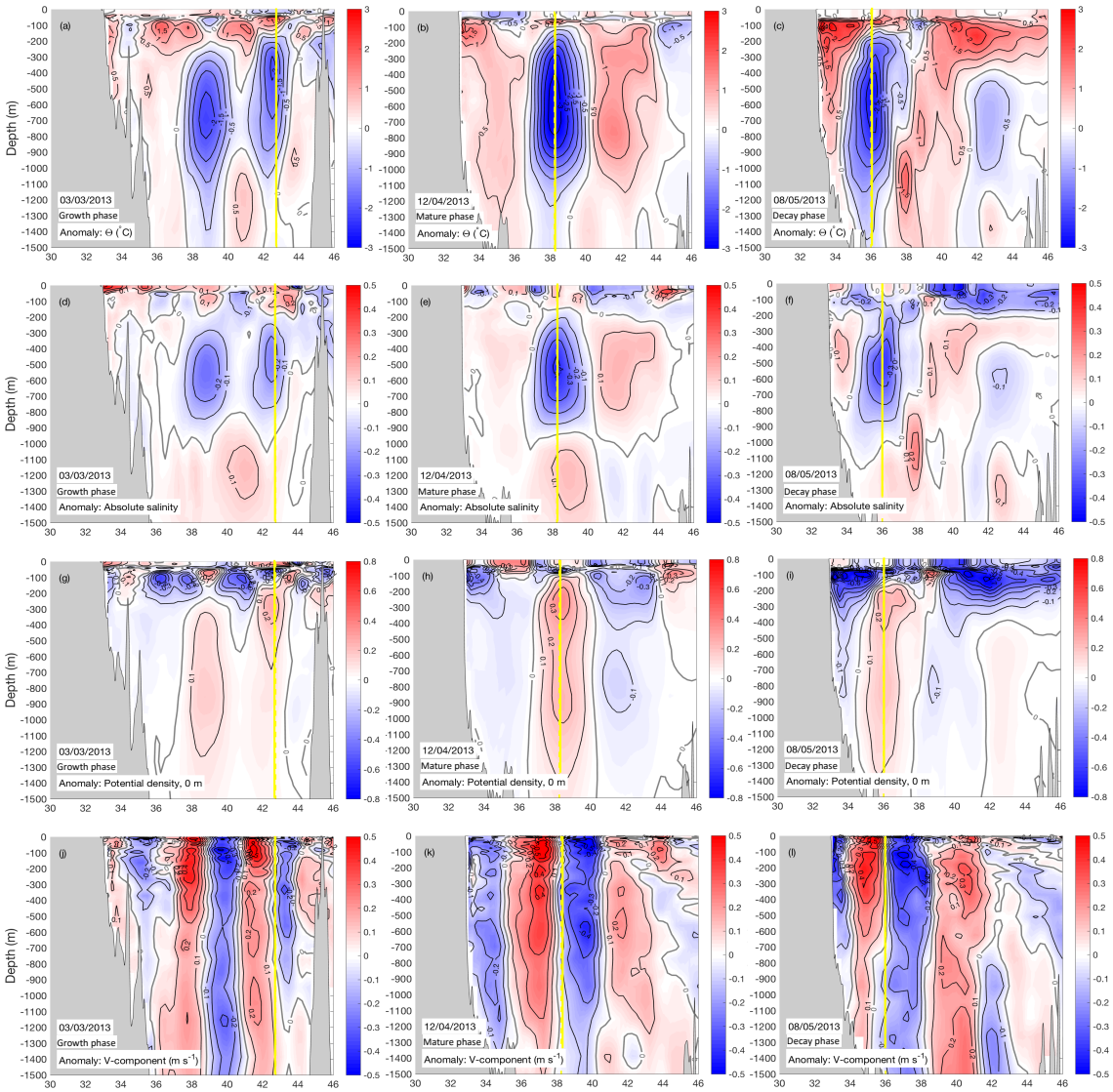

Figure 4.9: *Lagrangian evolution of the April eddy as seen from zonal sections crossing the southern Mozambique Channel at different latitudes according to the position of the eddy core at selected dates: 15 March, 12 April and 08 May 2013. These dates capture the eddy growth, mature and decay phases, respectively, and highlight the time-evolving anomalies of conservative temperature (a–c), absolute salinity (d–f), potential density (g–i) and meridional velocity (j–l). Positive (negative) shades of colors for velocity denote equatorward (poleward) velocities. See Figure 4.8 for location of each corresponding zonal transect, represented here by the yellow dashed vertical lines.*

Generally, the April and July eddies exhibited an analogous evolution of the vertical structure with only a few differences. The April eddy presented a subsurface negative anomaly of temperature from 200 m down to 1100 m during its growth phase, with a relatively shallow positive anomaly from the surface down to 200 m (Figure 4.9a). As the eddy evolved towards a mature stage across the southern Mozambique Channel, the subsurface negative anomaly increased and extended to just below 100 m down to 1500 m, squeezing the positive anomaly to a lens-like structure (Figure 4.9b). This structure was maintained upon arrival to the Western Boundary Current through the decay phase of the eddy. The subsurface negative anomaly strengthened vertically with the positive lens-like anomaly seemingly joining up with a positive anomaly adjacent to the African coastline (Figure 4.9c). The vertical structure of the anomaly temperature field for the July eddy followed an analogous evolution to that found for the April eddy but no lens-like positive anomaly at the surface was apparent (Figure 4.10a–c).

A similar structure of subsurface negative anomaly with a positive anomaly above evolving in time was also evident for the salinity field of the April and July eddies (Figure 4.9d–f and 4.10d–f). The subsurface negative anomaly, which extended from 200 m to about 1000 m, also strengthened vertically through the growth, mature and decay phases. According to the above pattern, both eddies carried a vertically elongated positive anomaly of potential density, which strengthens in time. This positive anomaly extended from 150 m down to 1500 m for the April eddy, with a lens-shaped negative anomaly above (Figure 4.9g–i); while the July eddy did not present such a surface negative anomaly (Figure 4.10g–i). Remarkably, the vertical sections of meridional anomaly velocities for the April and July eddies showed relatively high and deep-reaching rotational speeds, suggesting these eddies were strongly nonlinear through the water column (Figure 4.9j–l and 4.10). Peak rotational speeds were as high as 0.4–0.5 m s^{-1} and extended down to 700–1000 m during the mature phase in both eddies, and shallower depths of 300–500 m during the growth and decay phases.

The dynamic vertical structure of the modelled April and July eddies described so far agrees well both in qualitative and quantitative terms with the eddy vertical structure of rotational speeds presented in De Ruijter et al. (2004), showing deep reaching strong velocities around 0.3–0.4 m s^{-1} down to 750–1000 m. Also, the vertical structure of negative temperature and salinity anomalies in the modelled eddies agreed well with Argo-based anomalies reported in the previous section, although the model data showed slightly higher anomalies than those derived from the Argo profiles with peak anomalies reaching -2°C between 0–900 m and -0.2 g kg^{-1} between 200-900 m. These results encourage the further examination of the eddy retention capacity and associated fluxes based on model data.

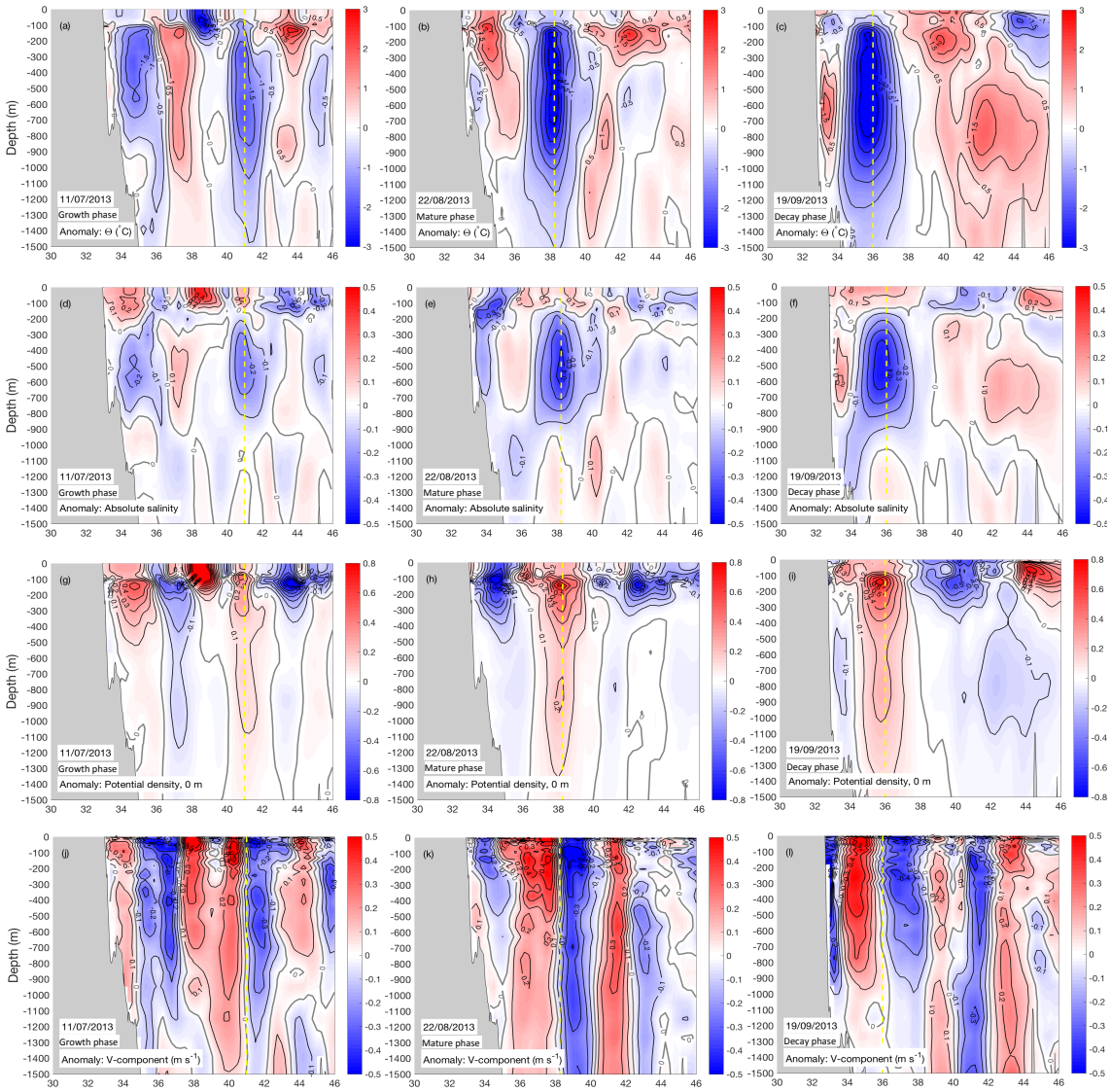

Figure 4.10: *Lagrangian evolution of the July eddy as seen from zonal sections crossing the southern Mozambique Channel at different latitudes according to the position of the eddy core at selected dates: 11 July, 22 August and 18 September 2013. These dates capture the eddy growth, mature and decay phases, respectively, and highlight the time-evolving anomalies of conservative temperature (a–c), absolute salinity (d–f), potential density (g–i) and meridional velocity (j–l). Positive (negative) shades of colors for velocity denote equatorward (poleward) velocities. See Figure 4.8 for location of each corresponding zonal transect.*

Eddy Retention and Associated Volume, Heat and Freshwater Fluxes

As advanced in Section 4.3.1, mesoscale eddies are capable of trapping water within their cores if the ratio between rotational speed, U, and propagation speed, c, is greater than one (McWilliams and Flierl, 1979; Robinson, 1983; Chelton et al., 2011). Where this ratio exceeds five, the eddy can then be considered highly non-linear as per Chelton et al. (2011). This relationship is denoted in Figure 4.7 by

comparing the rotational eddy speed (blue solid line) to the daily propagation speed (blue dashed line). Rotational speed through the water column was extracted from the modelled velocity maps as a vertical profile at the location of maximum speed (Ning et al., 2019) within the eddy contours detected by the eddy identification and tracking scheme. The eddy was considered non-linear where the eddy rotational speed was above the daily propagation speed, which occurred for the majority of the time for both the April and July model eddies.

Based on the model vertical sections selected in Figures 4.9 and 4.10 to capture the growth, mature and decay phases of the April and July eddies, the time-varying nonlinearity ratio with depth of the April and July eddies through the water column at those same dates is presented in Figure 4.11. The degree of nonlinearity was conservatively estimated at each date and eddy by confronting the mean averaged rotational speed at every depth level (U) against the mean propagation speed (c) estimated over the dates of interest. Also, the eddies were assumed to move as bulk entities at all levels taking the propagation speed constant along the vertical. The vertical distributions of the nonlinearity derived in this manner allow the estimation of the depths over which the eddy has retention capability to transport ocean properties along its lifespan.

Notably, both eddies exhibited a similar time-varying evolution of nonlinearity with depth, although the model July eddy presented overall greater trapping depths than the model April eddy, likely as a consequence of its larger size and stronger rotational speeds. Thus eddy retention increased from initially shallow values to deepest trapping depths as the eddy grew and reached its mature stage, when rotational speeds were stronger and deep-reaching. Towards the decay phase of the eddies, trapping depths decreased accordingly. Following this pattern, the model April eddy showed trapping depths from the surface to 373 m during its growth phase, evolving to 928 m during the mature phase and, again, shallower trapping depths about 483 m during the decay phase (Figure 4.11a). Analogously, the model July eddy presented an increase of trapping depths from 905 m during the growth phase to 1026 m during the mature phase and 812 m through its decay (Figure 4.11b).

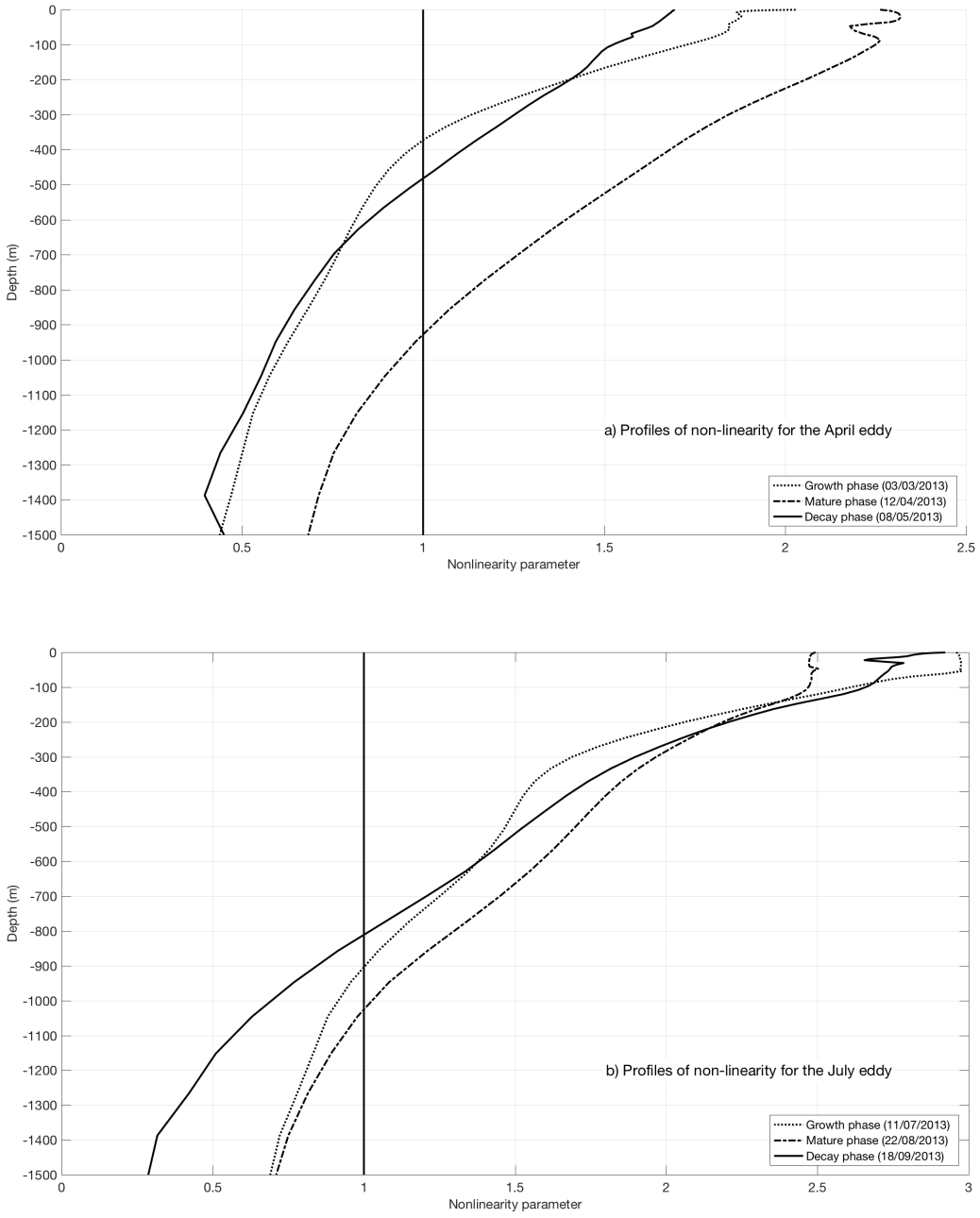

Figure 4.11: *Profiles of non-linearity (unitless) with depth (m) for the growth (blue line), mature (red line) and decay phases (black line) of the (a) April and (b) July eddies as they cross the southern Mozambique Channel (see legend). The black vertical lines indicate a nonlinearity ratio of 1. Depths exceeding this value respond to the vertical extent over which the eddy is capable of transporting water effectively.*

Results from Section 4.3.1 suggested Madagascar cyclonic eddies have the ability to advect mass, heat and freshwater in distinct depth layers, depending on the ratio between their rotational and propagation speeds. The estimates of time-varying trapping depths for the model April and July eddies were taken and combined with the temperature and salinity anomalies shown in Figures 4.9 and 4.10 through the growth, mature and decay phases to calculate the available heat and salt contents (AHA, ASA) following (Barceló-Llull et al., 2017; Dilmahamod et al., 2018):

$$AHA = \int_{z_{trap}}^{0} \int_{0}^{Rc} \rho_0 \, C_p \, \Theta' \, (2 \, \pi \, r) \, dr \, dz \tag{4.2}$$

$$ASA = \int_{z_{trap}}^{0} \int_{0}^{Rc} \rho_0 \, S'_A \, (2 \, \pi \, r) \, dr \, dz \tag{4.3}$$

where z is the vertical coordinate (depth, m), z_{trap} is the trapping depth (m), ρ_0 is the mean upper ocean density (1026 kg m^{-3}), C_p is the specific heat capacity (4000J kg^{-1} °C^{-1}), r is the eddy radius (m). Then temperature and salinity anomalies (Θ' and S'_A respectively) are calculated comparing model daily fields of the selected dates of study against the corresponding multi-year averaged monthly field over the period 1993–2015. Θ' and S'_A are integrated over the eddy-core area by assuming a circular symmetrical shape, and then vertically integrated over the eddy vertical extent for each eddy phase (from the surface down to the trapping depth). The eddy centre to the eddy-core radius was integrated radially, with Rc being the eddy radius. A 0.001 factor is used for ASA so as to convert salinity to salinity fraction (kg of salt per kg of seawater). The calculations were complemented with estimates of the associated volume, heat and salt fluxes following (Dong et al., 2014; Dilmahamod et al., 2018):

$$V_e = c \int_{z_{trap}}^{0} 2 \, r \, dz \tag{4.4}$$

$$Q_{eh} = c \int_{z_{trap}}^{0} \rho_0 \, C_p \, \Theta' \, (2 \, r) \, dz \tag{4.5}$$

$$Q_{es} = c \int_{z_{trap}}^{0} \rho_0 \, S'_A \, (2 \, r) \, dz \tag{4.6}$$

where V_e is eddy-driven volume transport in units of Sverdrups (1 Sv=10^6m^3 s^{-1}), Q_{eh} is eddy-driven heat flux in Watts, Q_{es} is eddy-driven salt flux and in kg s^{-1} and c is the mean eddy propagation speed. The vertical integral is computed by discrete summation over interpolated vertical levels. c is calculated as the mean of five days centered around the selected date (e. g. 10–14 April for 12 April). Also, c is taken as a positive so that the sign in fluxes reveal the nature of the temperature and salinity anomalies they transport. Lastly, salt fluxes are discussed in terms of freshwater fluxes (unit: Sv), with Q_{fw} = - $Q_{es}/(\rho_0 \, S_o)$, where S_o = 35 psu (salt mass fraction) is the mean upper ocean salinity. The resultant property contents and fluxes associated with the April and July eddies are presented in Table 4.3, where positive (negative) heat fluxes mean eddy-driven warming (cooling) and positive (negative) freshwater fluxes mean eddy-driven freshening (salt contribution).

Table 4.3: *Vertical extent, eddy radius, propagation speed, volume, volume transport, thermohaline contents and associated heat/freshwater flux of the April and July eddies through their growth, mature and decay phases.*

Property	**Growth Phase April Eddy** 3 March	**Mature Phase April Eddy** 12 April	**Decay Phase April Eddy** 7 May	**Growth Phase July Eddy** 11 July	**Mature Phase July Eddy** 22 August08	**Decay Phase July Eddy** 18 September
Vertical extent (m)	373	928	483	905	1026	812
Radius (km)	86.45	79.59	67.83	62.80	88.83	94.46
Propagation speed (m $s^{-}1$)	0.14	0.13	0.18	0.13	0.17	0.11
Volume (10^{12} m^3)	8.75	18.46	6.98	11.21	25.43	22.76
Volume Transport (Sv)	9.02	19.20	11.92	14.54	31.53	17.48
AHA (10^{18} J)	-19.35	-133.85	-23.09	-55.19	-196.32	-203.63
Heat Flux (PW)	-0.02	-0.1	-0.04	-0.07	-0.2	-0.2
ASA (10^{10} kg)	-12.80	-321.48	-102.22	-122.58	-404.63	-483.02
Freshwater Flux (Sv)	0.003	0.09	0.04	0.04	0.14	0.10

The mean estimates of cross-sectional volume transport (Equation 4.4) of the April and July eddies were about 13.4 $\pm$ 5.2 and 21.2 $\pm$ 9.1 Sv, respectively, taking as reference estimates from the three eddy phases (Table 4.3). These estimates compared well with the cyclonic eddy observed in De Ruijter et al. (2004), which accounts for a cross-sectional volume transport of about 14.4 Sv from the surface down to 1000 m given an eddy radius of 120 km and a propagation speed of 6 cm s^{-1}. As derived from L-ADCP observations, these authors reported a larger mean volume transport of about 33 Sv from the flow around the cyclonic eddy, taken from the surface down to 1000 m. At a rate of four to six dipole structures per year, De Ruijter et al. (2004) and Ridderinkhof et al. (2013), one could expect from these estimates for a mean decaying cyclonic eddy between 58.8–88.2 Sv reaches the Agulhas Current per year with SEMC waters entrapped (a mean decay eddy transports $\sim$14.7 Sv with reference to values in Table 4.3).

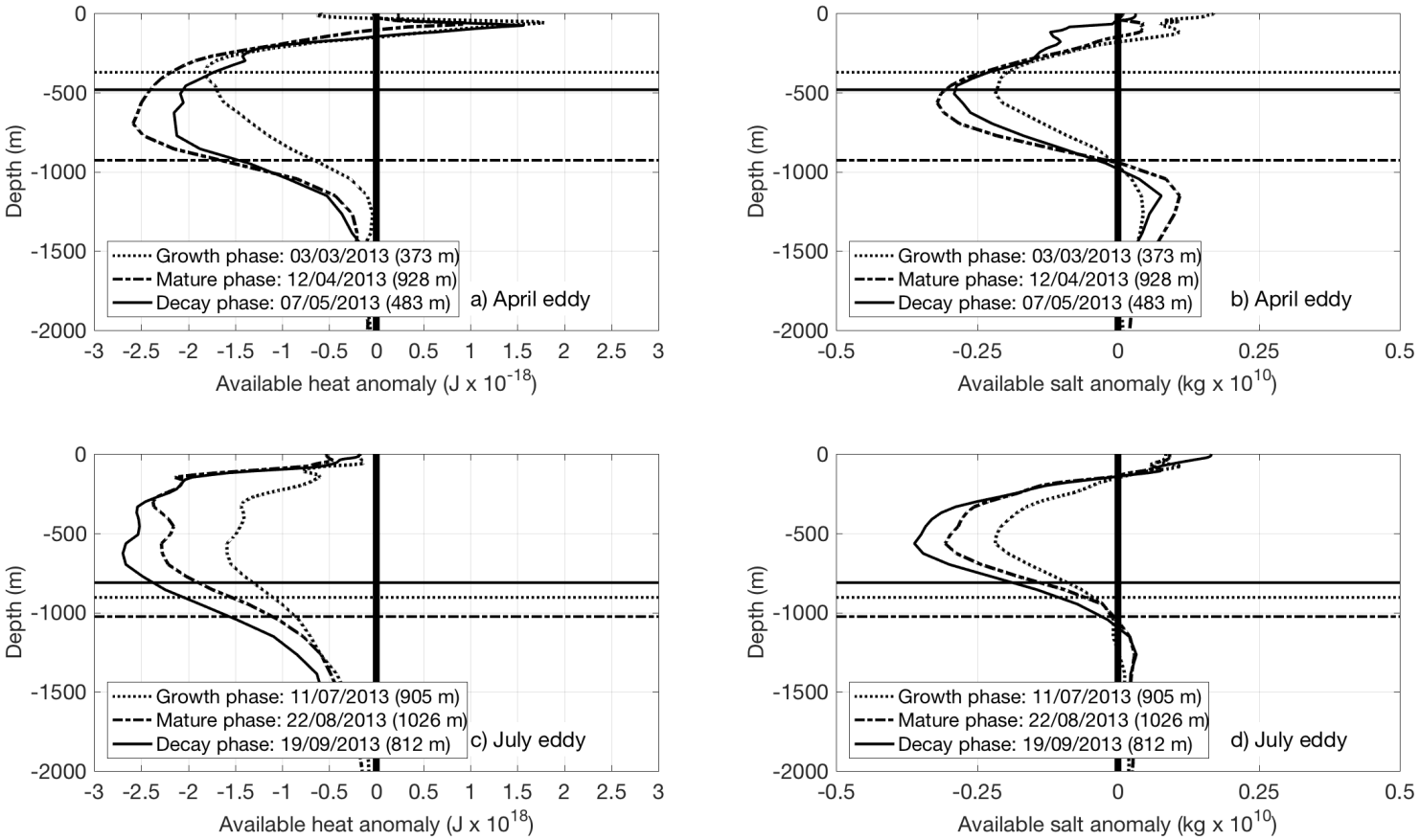

Figure 4.12: *(a,c) Available Heat Anomaly, AHA, and (b,d) Available Salt Anomaly, ASA, of the April and July eddies, respectively, for the eddy growth (dotted line), mature (dash-dot line) and decay (solid line) phases on the same selected dates as shown in Figures 4.9– 4.11. See legend for dates and trapped water depth.*

The vertical distribution of available heat (AHA) and salt anomaly (ASA) contents is shown in Figure 4.12 following the growth, mature and decay phases of each eddy. The structure of AHA and ASA for both eddies was similar with a single negative maximum subsurface centered around 400–700 m and 500 m, respectively. Near the surface, a shallow positive anomaly in ASA occupied the upper 100 m of the water column for both the April and July eddies ASA while the same applied for the AHA of the April eddy (Fig. 4.12a, b, d).

For the April eddy, an increase in AHA and ASA occurred from the growth to the mature phase, followed by a decrease from the mature to the decay phase. Differently, this latter decrease from the mature to the decay phase was absent for the July eddy and, instead, both AHA and ASA increased. This was attributed to the larger eddy radius exhibited by the July eddy during the date selected within its decay phase, as compared to its mature phase (Table 4.3). The mean vertically integrated AHA (ASA) of the April eddy was -58.8 $\times$ 10^{18} $\pm$ 65.1 $\times$ 10^{18} J (-145.5 $\times$ 10^{10} $\pm$ 158.8 $\times$ 10^{10} kg), and the July eddy was -151.7 $\times$ 10^{18} $\pm$ 83.7 $\times$ 10^{18} J (-336.7 $\times$ 10^{10} $\pm$ 189.6 $\times$ 10^{10} kg). These averaged estimates of total AHA and ASA (Table 4.3) were larger than those found for cyclonic eddies in the Peru-Chile Current System (-5.9 $\times$ 10^{18} J and -14.7 $\times$ 10^{10} kg, respectively Chaigneau et al. (2011)), and in the Western and Eastern Indian Ocean for subsurface cyclonic eddies (-5.1 $\times$ 10^{18} J and -25.6 $\times$ 10^{10} kg, Dilmahamod et al. (2018)). However, it must also be noted that estimates in these previous works are based on smoother vertical structures of the eddies since they were constructed from averaging Argo profiles over large areas to provide climatological views. It is likely expected that estimates for non-climatological eddies will present and carry much larger anomalies given then individual eddies can display peak radius that will consequently increase the heat and salt anomaly contents. Furthermore, trapping depths in Chaigneau et al. (2011) and Dilmahamod et al. (2018) are calculated from geostrophic velocities assuming a level of no motion at a given depth. This might also lead to some underestimation when computing the nonlinearity with depth, resulting in shallower trapping depths for vertical integration of the total AHA and ASA. While in this study the absolute model velocities were used and these might be leading, on the other hand, to some overestimation of the trapping depths (and therefore of AHA and ASA).

Lastly, estimates of heat and freshwater fluxes as the eddies evolved across the southern Mozambique Channel allow for a better understanding of how these fluxes vary in time along the eddy lifespan and to what extent these will eventually reach and enter the Agulhas Current system (Table 4.3). Heat and freshwater fluxes of the April (July) eddy vary from -0.02 PW (-0.07 PW) and 0.003 Sv (0.04 Sv) during the growth phase to -0.1 PW (-0.2 PW) and 0.09 Sv (0.14 Sv) during the mature phase and -0.04 PW (-0.2 PW) and 0.04 Sv (0.10 Sv) towards the decay phase. It was observed for both eddies, peak heat and freshwater fluxes were reached during the growth phase, except for the July eddy which retains high heat fluxes also during the decay phase. The magnitude of the heat and salt fluxes were up to one order of magnitude higher during the mature phase than during the growth phase, occasionally decreasing towards a lower order of magnitude during the decay phase, as it occurs for heat fluxes of the April eddy. These results highlight the importance of studies characterizing the Lagrangian evolution of cyclonic eddies in the southern Mozambique Channel to properly assess their actual contribution as cool and freshwater source waters to the Agulhas Current.

Interestingly, estimates of heat fluxes driven by Madagascar cyclonic eddies approached values reported for Agulhas Rings (anticyclonic eddies) using Argo floats and satellite data reaching up to 0.07 PW (Souza et al., 2011); whereas freshwater fluxes driven by the April and July eddies fall within the same order of magnitude as those reported for surface and subsurface cyclonic eddies in the South Indian Ocean, which ranged along -0.4, -0.02 and 0.8 Sv (Dilmahamod et al., 2018).

The analyses of the Lagrangian evolution of Madagascar cyclonic eddies show Madagascar cyclonic eddies continuously change over their lifespan, which will have impacts on their potential contributions to the Western Boundary Current system. In this regard, this study is the first one on attempting such an approach, providing a quantitative description of the time-evolving changes experienced by the available heat and salt anomaly contents, and fluxes, that ultimately will feed into the Agulhas Current.

4.4 Concluding Remarks

4.4.1 Summary and Conclusions

This Chapter has characterized for the first time the 3D Lagrangian evolution of two non-concomitant Madagascar cyclonic eddies based on *ad hoc* Argo experiments undertaken in April and July 2013. The set of Argo floats were configured to measure temperature and salinity at high temporal resolutions (daily and five-daily experiments) and at varying park depths (300 m, 500 m, 650 m and 1000 m) to test their retention within the eddy dynamics. These *in situ* measurements were complemented with altimetry data and the output of an eddy-permiting (1/4°) ocean general circulation model (GLORYS2v4). Statistics for near-surface eddy properties were derived from application of an eddy detection and tracking algorithm (Penven et al., 2005; Halo et al., 2014b) to both altimetry and model data. The agreement among the complementary data sources reveals a number of insightful features.

The April and July eddies propagated westward from South West Madagascar, where the South East Madagascar Current separates from the continental shelf, with a moderate poleward deflection. After a propagation of 130–137 days (ca. 5 months) the eddies interacting with the Agulhas Current at the KwaZulu-Natal Bight. The mean propagation speed of the April and July eddies was high, 13–15 cm s^{-1}, likely enhanced through advection of the eddies in the southern Mozambique Channel by favouring strong background currents. These propagation speeds are about two times the phase speed of nondispersive baroclinic Rossby waves for the range of latitude of Madagascar eddies (5–6 cm s^{-1} at 25–30° S), exceeding the prediction from theories for nonlinear vortices (McWilliams and Flierl, 1979; Cushman-Roisin, 1994; Chelton et al., 2011).

As long-lived mesoscales features, the observed April and July Madagascar eddies evolved in time, and over space, through three well defined phases. Along its growth phase, the eddies increased in radius from relatively small initial sizes towards a mature stage, where the eddy radius' remained nearly stable over time. The mature stage ended when the eddies started to decrease and approached their initial size along the so-called, decay phase. The time-varying relationship between the eddy radius, amplitude and rotational speed was tight for both eddies, following each other in parallel when the eddies propagated southwestward without complex interactions with other mesoscales features and / or physical boundaries. Generally, the observed July eddy presented a larger radius (89 km), amplitude (-27 cm) and stronger rotational speeds (69 cm s^{-1} than the April eddy (65 km, 16 cm and 57 cm s^{-1}, respectively). In both cases, mean rotational speeds derived from altimetry data exceeded their mean propagation speed, thus supporting their capability to transport ocean properties within their interior while travelling across the southern Mozambique Channel. The latter occurs when the ratio of the rotational speed to the propagation speed exceeds 1, indicating that the eddy is nonlinear (McWilliams and Flierl, 1979; Robinson, 1983; Chelton et al., 2011).

The analyses of water masses based on Argo floats retained within the eddies indicated Madagascar cyclonic eddies displayed the highest variability along its lifespan in the upper ∼100 m of the water column and below 900 m. These changes

near the surface were attributed to direct and rapid ocean-atmosphere interactions acting over the 5 months of travel. This is seen with Tropical Surface Water (TSW: σ_Θ<25.5 kg m^3; Beal et al. (2006)) becoming cooler and saltier over time as the eddy propagates southwestward. The significant water mass changes occurring deeper than 900 m are here attributed to the effective trapping vertical extent of the eddies. As the floats sampling the eddy travel southwestward, a progressive decrease in diluted Red Sea Water was observed, which originated further north, and increase in Antarctic Intermediate Water, which originated further south. This is likely a response to Argo floats sampling local waters along its excursions through the water column at the time of profiling, rather than sampling water retained within the eddy from its area of origin. At 150–200 m, all eddy profiles presented a subsurface salinity maximum approaching 35.65, characteristic for Subtropical Surface Water, (STSW Gründlingh et al. (1991)); and, below, a rather less variable domain of South Indian Central Water between 300–900 m (SICW: 8–14°C, 34.6–35.4 g kg^{-1}; Emery (2001)). When compared to an Argo profile sampling the Agulhas Current, the profiles within the eddy exhibit a distinctive cooler and fresher vertical distribution of ocean properties highlighted as negative temperature and salinity anomalies which extended through the water column down to 900 m, except for a relatively shallow and weak positive salinity anomaly within the upper 200 m. These negative temperature and salinity anomalies were as large as -2°C (0–900 m) and -0.2 g kg^{-1} (200-900 m), respectively, and support the potential of Madagascar cyclonic eddies to transport large temperature and salinity anomalies effectively from Madagascar to South East Africa, from the surface down to about 900 m.

The good agreement between model and observed eddy characteristics and Lagrangian evolution, allow the extension of the analyses towards model-based calculations of time-varying trapping depths and associated eddy-driven fluxes. Results highlight the importance of studies characterizing time-evolving changes experienced by the available heat and salt anomaly contents that ultimately will feed into the Agulhas Current. In this context, a distinct pattern was observed where eddy retention increases from initially shallower values to deepest trapping depths approaching 1000 m as the eddies grew and reached their mature stage, when rotational speeds are stronger and deep-reaching. In both cases this situation reversed towards the decay phase of the eddies, when trapping depths started to decrease following shallower strong rotational speeds. Overall the model April (July) eddy showed mean trapping water depths of 595 $\pm$ 294 m (914 m $\pm$ 107 m), volume transport about 13.4 $\pm$ 5.2 Sv (21.2 $\pm$ 9.1 Sv), heat flux of -0.07 $\pm$ 0.06 PW (-0.2 $\pm$ 0.09 PW) and freshwater flux of 0.04 $\pm$ 0.04 Sv (0.09 $\pm$ 0.05 Sv). These results evidence the role of Madagascar cyclonic eddies as transporters of cooled and freshened source waters into the Agulhas Current, demanding further investigation by combination of Argo dedicated experiments, remotely sensed data and, particularly, of direct measurements of velocity at different stages of the eddy lifespan when possible. The latter is crucial to enable the evaluation of model-based estimates on time-varying eddy-driven fluxes so as to assess the accuracy of these estimates against the real ocean.

4.4.2 Potential of Argo dedicated experiments

Results from this study complement a series of other works conducted in this region which investigate general eddy dynamics from altimetry and model data,

pursuing to uncover the characterization of the eddy demography, its energetic balances, generation mechanisms and potential links to climate variability (Halo et al., 2014b; Ridderinkhof et al., 2013; Dilmahamod et al., 2018). From a different perspective, the work in De Ruijter et al. (2004) represents to the most complete description of a Madgascar cyclonic eddy based on direct measurements of temperature, salinity and velocity. However, these measurements characterised the eddy only at the time of the survey, while located in the middle of the southern Mozambique Channel, being beyond the scope of their research to describe its time-varying vertical structure. These results add to previous works new knowledge, focusing on the Lagrangian characterisation of Madagascar cyclonic eddies from its generation site towards the Western Boundary Current, combining observations and model data to provide a robust view of the time-varying vertical structure and associated volume, heat and freshwater fluxes of these eddies.

The different configurations of the Argo floats used in this study evidence the trapping capabilities of the April and July eddies, suggesting that the most suitable configuration (among tested options) to capture eddy dynamics is daily profiling with park depths between 300–650 m. The park depth at 1000 m appeared to exceed the vertical extent of the April eddy while shallower park depths resulted in floats drifting over longer periods of time within both the April and July eddies. On the other hand, the Argo trajectories revealed by daily profiling floats suggest the presence of some rapid secondary circulation patterns through the convergence/divergence of the floats towards/from the eddy core over time, which demand further investigation.

The experimental design of the two Argo dedicated experiments presented here illustrates the benefits of *ad hoc* Argo configurations for the study of 3D Lagrangian eddy dynamics in combination with a 'state-of-the-art' ocean model and remotely sensed data. No single experiment will likely fit all regions of mesoscale eddy turbulence, and Argo floats were never designed to answer all the questions posed by the oceanographic community (Morris et al., 2019). However, dedicated experiments like these are valuable to be complemented with other data sources, validating further models and enabling a better understanding of the subsurface Lagrangian evolution of eddies not easily surveyed at different stages of their lifespan using research vessels.

Chapter 5

Downstream evolution of hydrographic properties and fluxes of the Agulhas Current

Preface:

Following on from the cyclonic eddy evolution and input into the Agulhas Current of cooler, fresher waters in Chapter 4, this Chapter explores the downstream evolution of hydrographic properties and fluxes of the Agulhas Current. This work shows that Argo floats deployed on daily profiling provide a valuable quasi-synoptic tool to study Western Boundary Currents. This Chapter has been submitted to the Journal of Geophysical Research: Oceans and is currently under review. The Chapter has been laid out in this format.

Morris T., Aguiar-González, B. Lamont, T. and Hermes, J. In Review. Downstream evolution of hydrographic properties and fluxes of the Agulhas Current. Submitted to Journal of Geophysical Research: Oceans.

This chapter addresses the third key question listed in Section 1.3:

Can Argo floats be used to capture the downstream evolution of fluxes in the Agulhas Current?

Abstract

The downstream evolution of Agulhas Current volume, heat and salt fluxes, was investigated using Argo floats, in combination with output from an eddy-resolving ocean general circulation reanalysis model. A dedicated experiment was undertaken in August 2017, whereby six floats were deployed along a perpendicular transect offshore of Port Edward (31° S), profiling from 1000 m to the surface on daily frequencies. We find the floats exited the Agulhas Current within 9 - 12 days at mean speeds of 0.51 - 0.76 m s^{-1}. The Argo and model data agree well in terms of volume transport (16.76 - 38.18 Sv; 17.70 - 32.51 Sv respectively), heat (0.85 - 1.79 PW; 0.99 - 1.91 PW respectively) and salt (0.60 - 1.37 x 10^{12} kg s^{-1}; 0.63 - 1.17 x 10^{12} kg s^{-1} respectively) fluxes, increasing in value from north to south. Model transects extended to full depth and 240 km offshore were used to calculate volume (54.17 - 121.79 Sv), heat (2.88 - 5.98 PW) and salt (1.96 x 10^{12} kg s^{-1} - 4.40 x 10^{12} kg s^{-1}) fluxes and showed the southward evolution of increasing fluxes. Argo floats on high profiling resolutions have been shown to be beneficial to the study of Western Boundary Currents, given their standard 10-daily profiles would almost completely bypass the Agulhas Current. This study illustrates the first near-real time survey of the Agulhas Current, and a potential method of quasi-synoptic surveys using Argo float technology.

5.1 Introduction

The Agulhas Current is the Western Boundary Current of the South West Indian Ocean sub-gyre and is comparable to the Kuroshio and Gulf Stream of the Northern Hemisphere (Bryden et al., 2005). The Agulhas Current is sourced from three regions: 1) mesoscale eddies travelling polewards through the Mozambique Channel (Ternon et al., 2014; Halo et al., 2014a), 2) westward propagating mesoscale eddies formed south of Madagascar at the termination of the South East Madagascar Current (De Ruijter et al., 2004; Morris et al., 2019) and 3) the recirculation of the South West Indian Ocean sub-gyre itself (Stramma and Lutjeharms, 1997; Hermes et al., 2007). The Agulhas Undercurrent flows northwards underneath the Agulhas Current with peak speeds of 0.9 m s^{-1} at 1400 m and the capacity to transport 4.2 $\pm$ 5.2 Sv of water (Beal, 2009). A schematic of the greater Agulhas Current region is shown in Figure 5.1, highlighting key features discussed.

Natal Pulses are large meanders of the Agulhas Current propagating along the east coast of South Africa (Pivan et al., 2016; Rouault and Penven, 2011) and are considered to be generated from the varability associated with offshore mesoscale eddies in the northern Agulhas Current region (Tsugawa and Hasumi, 2010). Natal Pulses are irregularly generated every 50-150 days (Ruijter et al., 1999) with one to two of these large pertubations propagating all the way to the Agulhas Bank region of the southern Agulhas Current (Rouault and Penven, 2011). Using isopycnal Lagrangian floats, observations from within a Natal Pulse show the pertubation to extend to 1000 m and significantly influenced the cross-shelf exchange of water masses along its pathway southwestwards (Pivan et al., 2016). Increased eddy activity within the Agulhas Current over the last 30 years has also resulted in the current broadening instead of intensifying as climate models and linear dynamical theory would suggest (Beal and Elipot, 2016).

The Agulhas Current terminates south of South Africa after moving offshore along the edge of the Agulhas Bank until it retroflects back on itself into the South Indian Ocean (Le Bars et al., 2012; Lutjeharms and Van Ballegooyen, 1988). Agulhas Rings are shed from the retroflection region and propagate northwestwards into the South Atlantic Ocean (Dencausse et al., 2010). This transport of warm and salty waters from the Indian to the Atlantic Ocean, via the Agulhas Current, is critical to the global thermohaline circulation and in particular the climate of the Northern Hemisphere (Beal et al., 2011).

Direct measurements of the volume, heat and salt transport of the Agulhas Current have been undertaken sporadically over the last four decades. Eight dedicated research cruises were completed at 31° S from 1975 to 1978 and a volume transport was determined from overside Conductivity, Temperature and Depth (CTD) instrument measurements to be 62 Sv polewards (1 Sv = 10^6 m^3 s^{-1}) for the upper 1000 m (Gründlingh, 1980). Furthermore, the study suggested that the volume transport should increase downstream by 6 Sv every 100 km (Gründlingh, 1980), which would equate to an increase of 27 Sv, totalling 89 Sv polewards over roughly 450 km; the distance from Durban to Port Alfred.

A trans-basin section across the South Indian Ocean was undertaken in 1987 by means of 106 full-depth CTD stations. The transect crossed the Agulhas Current

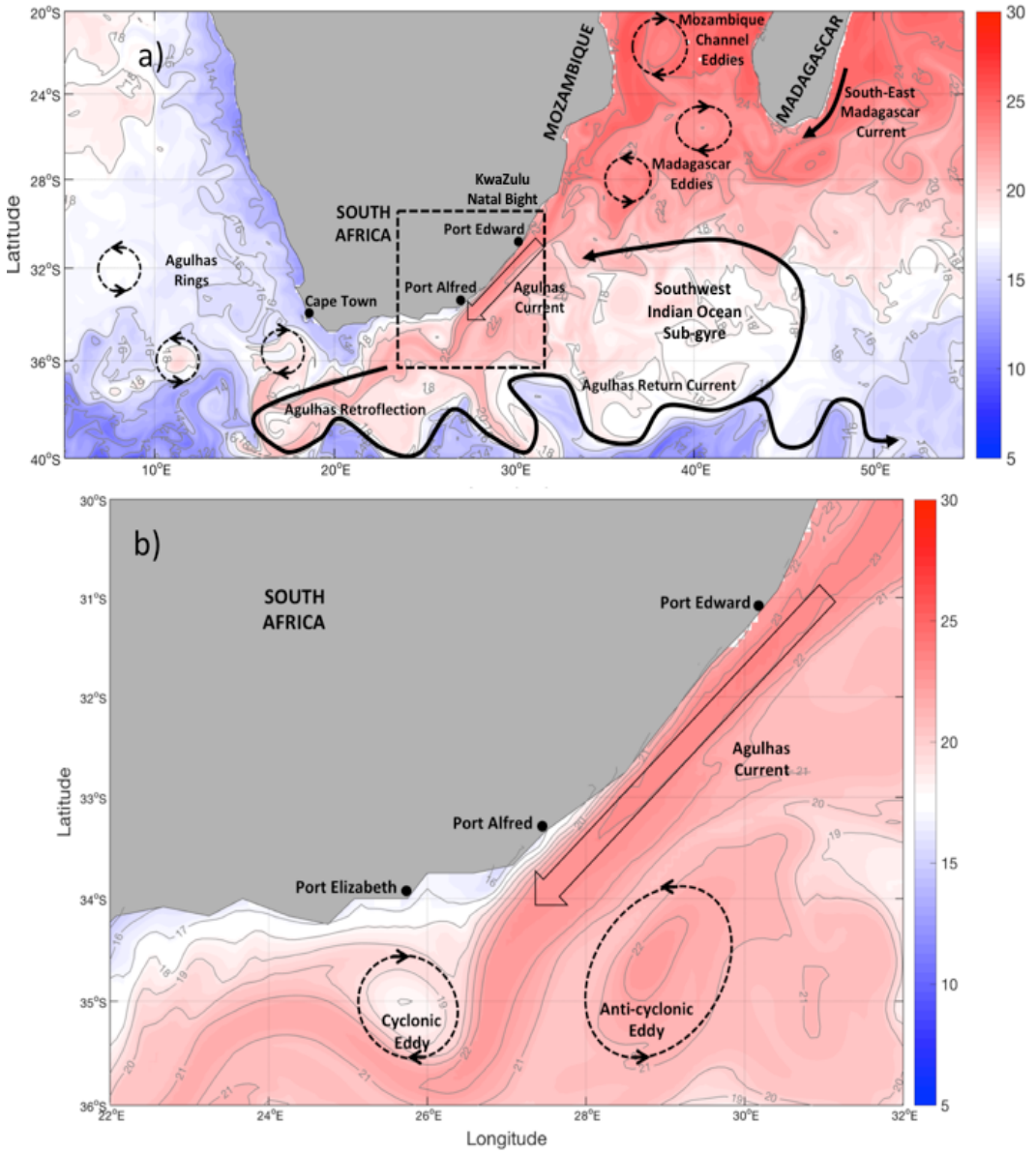

Figure 5.1: *(a) Map of sea surface temperature (°C) for the greater Agulhas Current region for 10 August 2017 (day of float deployment). Highlighted along the east coast of South Africa, prominently between Port Edward and Port Alfred, is the Agulhas Current (black large arrow). Sea surface temperature data was obtained from the GLORYS12V1 Reanalysis product. (b) Zoomed in map (from black dashed box in Fig. 5.1a) highlighting the anti-cyclonic eddy offshore of the Agulhas Current in the south, and the cyclonic eddy positioned over the shelf edge and eastern Agulhas Bank.*

between 31° and 32° S and the estimated volume transport was determined to be 85 Sv polewards (Toole and Warren, 1993). This was found to be 16% greater than a second full-depth estimate made at 32° S given the Agulhas Undercurrent had not been measured previously and thus not factored in to volume transport calculations (Beal and Bryden, 1999). Considerable analysis based on 15 full-depth lowered acoustic Doppler current profiler (LADCP) and CTD stations across the transect at 32° S resulted in a volume transport of 73 Sv polewards, a heat flux of 4.13 PW (1 PW = 10^{15} W) or 73 Sv at 13.82° C, and a salt flux of 2.64 x 10^{12} kg s^{-1} or 73 Sv at a salinity of 35.190 (Beal and Bryden, 1999). Finally, the Agulhas Current was calculated to warm and freshen by 0.08 PW and 0.03 x 10^{9} kg s^{-1} for every 10 Sv of volume transport increase across 32° S (Bryden and Beal, 2001), and vice versa. A strengthening (weakening) in the volume flow will result in a warming (cooling) and increase (decrease) of heat and salt flux within the Agulhas Current.

In order to evaluate volume transport over time, arrays of moorings acquiring current data at various depths, integrated spatially, are required. One such array was deployed at 31° S from February 1995 to April 1996 (Bryden et al., 2005). An average total transport for the Agulhas Current was calculated as 69.7 Sv polewards over a fixed region from the surface to 2400 m, and from the coast to 203 km offshore (or where the average currents were zero or close to zero) (Bryden et al., 2005). A minimum, 8.9 Sv, and maximum, 121.9 Sv, total volume transport polewards was recorded during the deployment, illustrating the extremes in volume transport the Agulhas Current is capable of (Bryden et al., 2005).

Using an inverse model to calculate net mass transport from an LADCP and CTD survey undertaken from 14 February to 17 March 2003, the following total cross-section estimates were determined: 100 $\pm$ 9 Sv at 32° S, 50 $\pm$ 11 Sv at 34° S and 96 $\pm$ 11 Sv at 36° S (Casal et al., 2009). The estimate at 32° S in particular was higher than anticipated, but still within the range of volume transports (9 - 121 Sv) observed for this region (Bryden et al., 2005). The apparent inconsistency from a very high (100 $\pm$ 9 Sv) to an average (50 $\pm$ 11 Sv) to once again a high (96 $\pm$ 11 Sv) volume transport with downstream evolution in the Agulhas Current was attributed to the quasi-synoptic nature of the survey over one month and the influence of mesoscale eddies offshore of East London and Port Elizabeth at the time of the survey.

Later estimates of volume transport were focused at 34° S making use of synoptic surveys as well as moored arrays. The first of these used two independent synoptic surveys to look at the difference in volume transport during a meander event and found the net volume transport during a meander (101 $\pm$ 1.4 Sv) to be very similar to that observed during a non-meander (119 $\pm$ 0.9 Sv) (Leber and Beal, 2014). Notably, these full-depth surveys were undertaken to 300 km offshore, and thus the full transport of the Agulhas Current was captured.

More recently, two consecutive moored arrays have been deployed at 34° S; the Agulhas Current Time-series (ACT) from 2010-2013 (Beal et al., 2015) and the Agulhas System Climate Array (ASCA) from 2015-2018 (Morris et al., 2017). ACT only acquired current meter data, while ASCA deployed MicroCAT instruments to additionally collect temperature and salinity data at discrete depths. From the ACT dataset, and in addition to a 22-year proxy of currents from altimetry data, a new method of volume transport estimation was established (Beal et al., 2015). This

allowed for a measurement at each time step out to the maximum of the vertically integrated velocity, beyond the half-width of the mean jet (Beal et al., 2015). This resulted in a volume transport estimate of 84 $\pm$ 11 Sv (large standard deviation as a result of standard error along with instrument error), (Beal et al., 2015).

Instrumenting moored arrays and undertaking synoptic surveys, while essential, are expensive and increasingly difficult to maintain. Furthermore, to look at the evolution of the Agulhas Current, multiple moored arrays or temporally-limited synoptic surveys would need to be undertaken. We thus look to opportunistic, yet strategic, autonomous robots deployments to understand the downstream evolution of the Agulhas Current, and couple these observations with numerical model outputs to extend the results further. For this paper, we used Argo floats sampling at a daily resolution, along with a reanalysis model product, to determine whether these methods may be used to investigate the downstream evolution of volume, heat and salt flux of a Western Boundary Current.

In this work the velocity and thermohaline structure of the Agulhas Current, and associated fluxes, is investigated based on the combined use of observations and output from an eddy-resolving ocean general circulation reanalysis model. The observations originate from an Argo dedicated experiment carried out in August 2017, hereafter referred as to the August Experiment. This experiment consisted of the deployment of six daily profiling floats to sample the downstream evolution of hydrographic properties of the Agulhas Current.

The Chapter is organized as follows. Section 5.2 describes the data and methods. Section 5.3 presents the observational results from the August Experiment. In Sections 5.3.1 and 5.3.2 the observed velocity and thermohaline structure of the Agulhas Current are investigated. In Section 5.4, the Argo observations are combined with model data to provide a joint view of the Agulhas Current velocity (Section 5.4.1) and thermohaline structure (Section 5.4.2) during the August Experiment. Lastly, in Section 5.5 the volume, heat and salt fluxes are assessed under the context of the August experiment and based on both Argo-derived and model-based estimates. The main findings are summarized in Section 5.6.

5.2 Data and Methods

Six Argo floats, equipped with temperature and conductivity sensors, were donated by the Euro-Argo MOCCA Project for this study (www.euro-argo.eu/EU-Projects/MOCCA-2015-2020). These floats were deployed in the Agulhas Current, with amended profiling settings (Table 5.1), in August 2017 (Fig. 5.1) in order to study the downstream evolution of the Agulhas Current and its water masses. The Argo float deployments were described in Chapter 3. A detailed description of data and methods follows.

5.2.1 Argo-Based Observations

The six floats (WMO numbers: 1917, 1912, 1914, 1915, 1913, 1916) were deployed along a transect perpendicular to the coastline offshore of Port Edward on 10 August 2017 (Fig. 5.2). The floats were deployed approximately 10 nm apart. The floats were set up to undertake daily profiling from a park and profile depth of 1000 m. The average time taken for the floats to descend to a park depth of 1000 m from the surface was 9 $\pm$ 2 hours. The floats spent 10 $\pm$ 3 hours at park depth, and a further 3 $\pm$ 0.7 hours ascending to the surface acquiring data. Two-way communication was possible with the floats through Iridium telecommunications, thus allowing the floats to be reconfigured to the standard Argo profiling mission once they had exited the Agulhas Current into the adjacent Atlantic and Indian Oceans. Mission parameters for the experiment are summarized in Table 5.1.

Table 5.1: *Setup parameters of the Argo floats during the August Experiment.*

Mission Parameter	**Float details**
No. of Floats	6
Communication	Iridium (2-way)
Profiling Frequency	Daily
Profiling Depth (m)	1000
Park Depth (m)	1000
Hours for float decent	9 ± 2
Hours at park depth	10 ± 3
Hours for float ascent	3 ± 0.7

A Sea Bird 911+ CTD reference cast was undertaken prior to each float deployment to verify the float data, beginning at the offshore station and moving inshore. The deployment transect, with CTD reference casts, took 10.5 hours to complete. Only these six stations were undertaken along this transect and the transect was only done once. The CTD data was post processed to international standards (Russo et al., 2019) and plotted alongside the first profile from each Argo float (Fig. 5.3). Float data extends to the park and profile depth of 1000 m, while the CTD casts were undertaken to approximately 1400 m. Figure 5.3 shows a tight relationship between the CTD casts (solid lines) and the first profile of the floats (open circles) for the Tropical Surface Waters (TSW), Sub-tropical Surface Waters (STSW) and South Indian Central Water (SICW) water masses. The variability at the intermediate water mass level represented in this region by Antarctic Intermediate Water (AAIW) and Red Sea Water (RSW) was only partially captured by the float data, while no deep water layers were captured by either instrument.

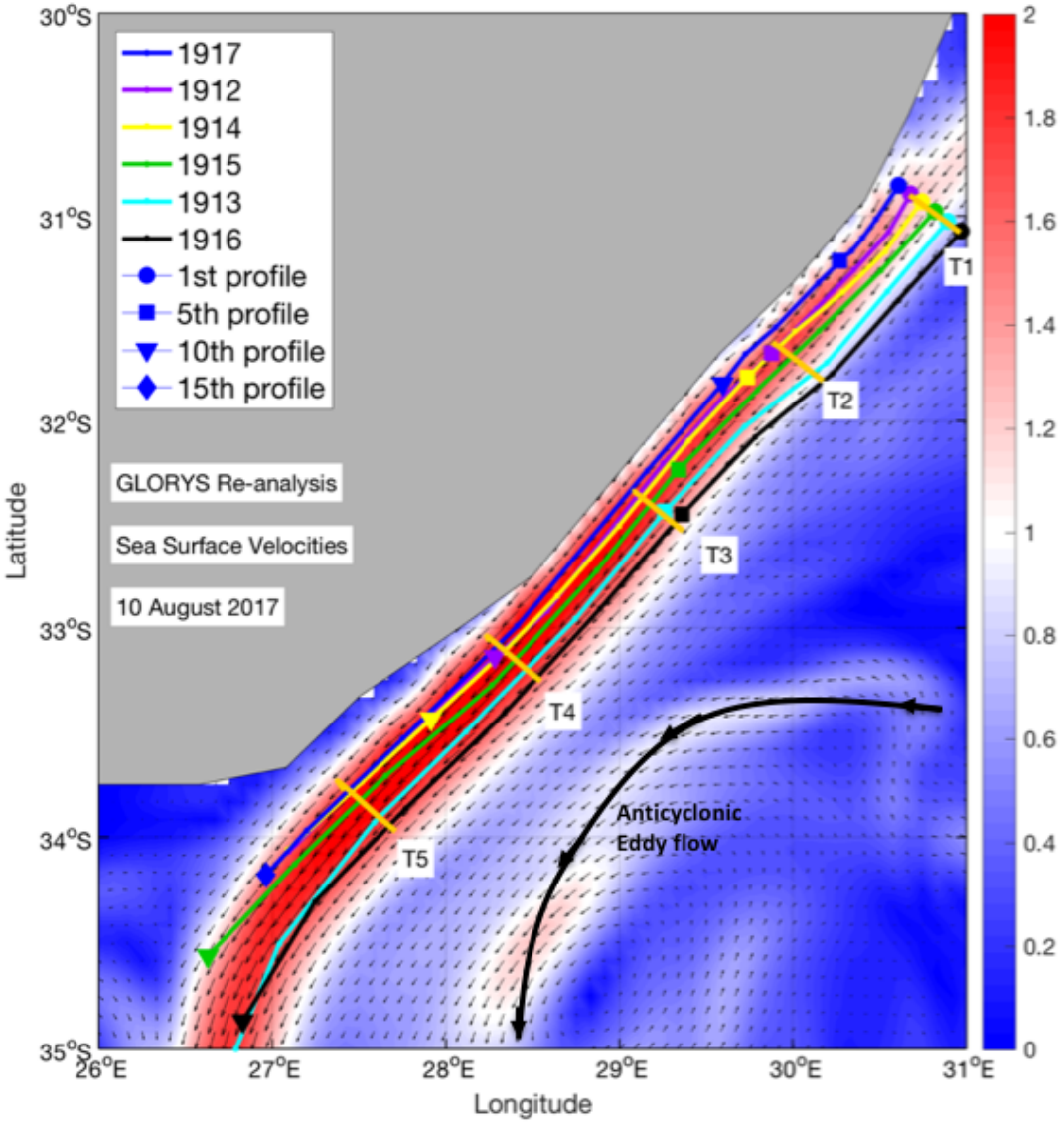

Figure 5.2: *Map of sea surface velocities* ($\mathrm{m\,s^{-1}}$) *for 10 August 2017 (day of float deployment). The Argo float trajectories are overlaid. The 1st, 5th, 10th and where applicable 15th profiles are marked with a circle, square, inverse triangle and diamond symbols respectively. Perpendicular transects across the Agulhas Current used for volume, heat and salt transport calculations are numbered from north (T1) to south (T5). Sea surface velocity data was obtained from the GLORYS12V1 Reanalysis product. Arrows represent unit vectors parallel to the vector velocity field.*

For each float, conservative temperature (°C), absolute salinity ($g\,kg^{-1}$) and the potential density anomaly (reference pressure 0 dbar, kg m^3) were calculated using TEOS-10 formulae. For the model, the conservative temperature, absolute salinity and potential density anomaly were calculated from extracted model variables (temperature and practical salinity) in order to compare to the Argo data efficiently. Only for Section 5.5.2, where we compare the model to historical *in situ* data, are the potential temperature and practical salinity values used. The Gibbs Seawater Toolbox developed for Matlab (version 3.06.11) was used for these calculations.

All Argo data were collected and made freely available by the International Argo Program and the national programs that contribute to it (http://www.argo.ucsd.edu, http://argo.jcommops.org) (Argo, 2000). The Argo Program is part of the Global Ocean Observing System (GOOS).

5.2.2 Numerical Model Output: GLORYS12V1

The GLORYS12V1 model, available from http://marine.copernicus.eu, was used to complement *in situ* measurements and extend the analyses towards a 3D view of the thermohaline and horizontal velocity structure of the Agulhas Current. This global reanalysis product has a 1/12° horizontal resolution, approximately 8 km. GLORYS12V1 is generated using the NEMO ocean model and is forced by ECMWF ERA-Interim reanalysis at the surface. The model has 50 vertical levels, and spans over the period 1993–2018. A multi-data and multivariate reduced order Kalman filter technique, based on the Singular Extended Evolutive Kalman (SEEK) filter formulation, is applied to the assimilation of ocean observations in the ocean model. Ocean observations used for the assimilation include Sea Level Anomalies (SLA) and Sea Surface Temperature (SST) satellite data, and *in situ* temperature and salinity profiles extracted from the Coriolis Ocean database for ReAnalysis (CORA) 4 database. These profile data are obtained from all possible instrumentation sources, such as Argo floats, CTD profiles, Expendable Bathythermography (XBT) profiles and satellite tracked drifters (Cabanes et al., 2013). It has been demonstrated that data assimilation improved the GLORYS12V1 product to be consistent with observations, and that these assimilated data constrained the model and reduced biases (Gasparin et al., 2018).

This reanalysis model product has not been used in Western Boundary Current studies, but has been shown to be useful for process studies globally and regionally for steric sea level changes and to study topographic Rossby waves at the Pacific Yap-Marina Junction (Storto et al., 2019; Ma et al., 2019). A number of studies have used the model at a 1/4° horizontal resolution to capture mesoscale eddy dynamics in the source water region of the Agulhas Current (Morris et al., 2019; Ramanantsoa et al., 2018b; Ramanantsoa et al., 2018a) as well as the South Indian Ocean Countercurrent (Menezes et al., 2016). This study provides the first evaluation of this reanalysis model product for the Agulhas Current.

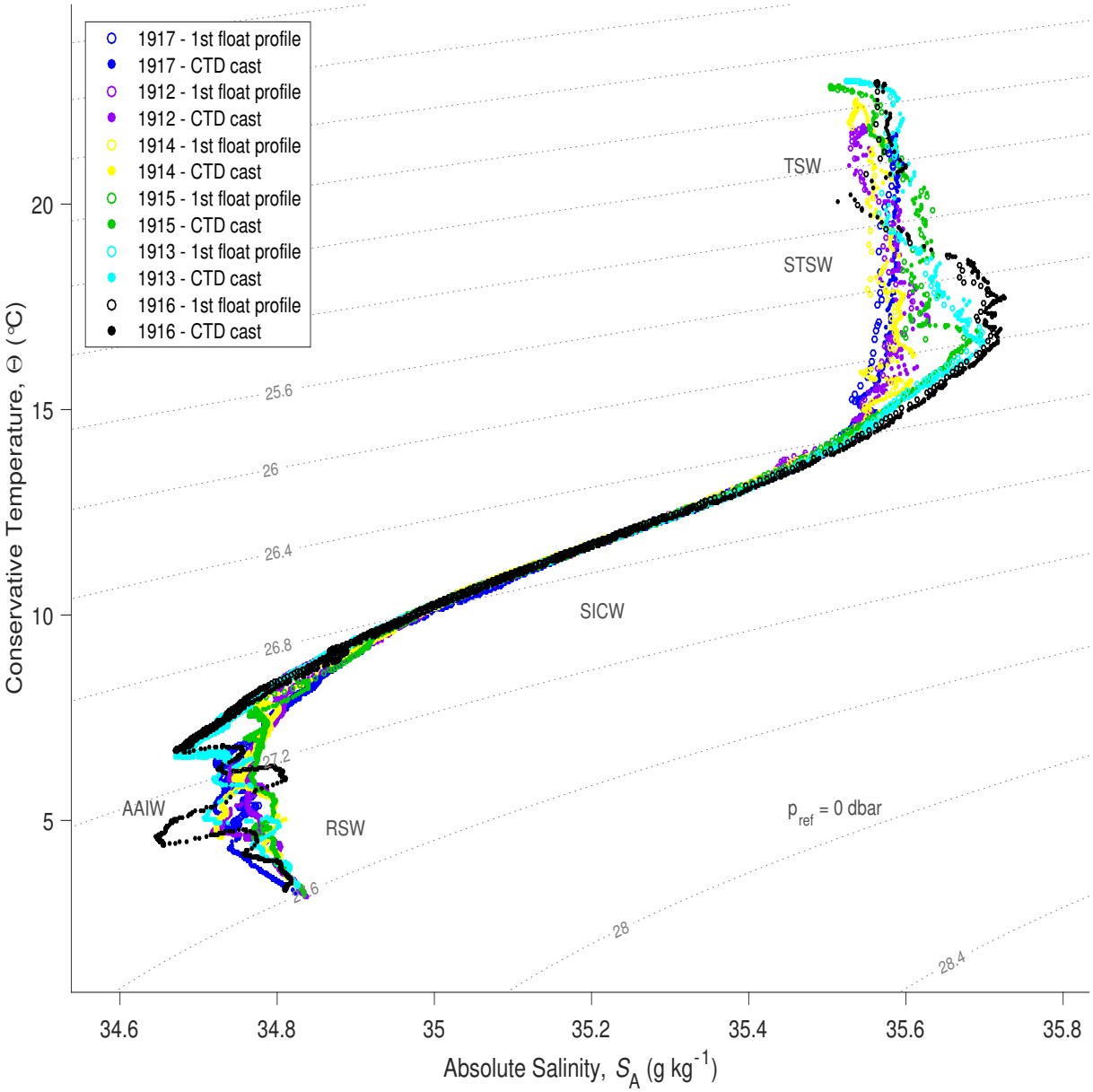

Figure 5.3: *A conservative temperature (°C) and absolute salinity ($\mathrm{g\,kg^{-1}}$) diagram of the first profile from each of the Argo floats (circles) compared to the CTD profile undertaken prior to each Argo float deployment (solid lines). The depth of the Argo float profiles (1000 m) were not as deep as the CTD casts (approximately 1400 m), thus the intermediate water masses were not as well represented by the Argo floats.*

5.3 August Experiment: Downstream evolution from Argo daily profiling

In this section the structure of the Agulhas Current based on the August Experiment is addressed, where six daily profiling Argo floats were deployed along a perpendicular section crossing the Agulhas Current. In Section 5.3.1 the horizontal velocity structure revealed by Argo-derived speeds is investigated. In Section 5.3.2 the thermohaline structure and water mass evolution as captured by downstream propagating floats is discussed.

5.3.1 Argo-derived velocity structure

The Agulhas Current exhibited a stable regime with no meandering for this experiment along the east coast of South Africa between Port Edward and Port Alfred (Fig. 5.1). An anticyclonic eddy was centered at 35° S; 28.5° E, offshore of the Agulhas Current and south of Port Alfred (Fig. 5.1 and 5.2), and a cyclonic eddy was situated over the shelf edge and eastern Agulhas Bank (35° S; 25.5° E). These two mesoscale eddies directed the Agulhas Current around their peripheries as the current diverged offshore (Fig. 5.1b). The focus of this Chapter is the jet-like portion of the Agulhas Current adjacent to the continental shelf.

Float 1917, the 'coastal' float, deployed last and closest to the coast, remained within the Agulhas Current for 15 days, recording a mean speed of 0.42 ± 0.39 m s^{-1} (Fig. 5.2: blue trajectory and Table 5.2). Floats 1912 and 1914 were deployed within the inshore edge of the Agulhas Current, both requiring 12 days to propagate as far as 34° S. The floats measured similar mean speeds of 0.51 ± 0.23 and 0.51 ± 0.10 m s^{-1} respectively (Fig. 5.2: purple and yellow trajectories and Table 5.2).

The three offshore floats were deployed within the Agulhas Current itself. Float 1915, with a mean speed of 0.71 ± 0.16 m s^{-1}, was classified (based on this mean speed) as deployed inshore of the Agulhas Current core. Float 1916, with a mean speed of 0.72 ± 0.11 m s^{-1}, was classified as deployed offshore of the Agulhas Current core. Both of these floats took 10 days to exit the Agulhas Current. The Agulhas Current core float (1913), with a marginally greater mean speed of 0.76 ± 0.15 m s^{-1}, left the Agulhas Current after only 9 days (Fig. 5.2: green, black and cyan trajectories and Table 5.2). It must be highlighted that float speeds, calculated as the distance between two positions in a 24 hour period, were considerably less than the peak surface speeds (1.8 m s^{-1}) of the Agulhas Current Beal et al., 2015. This is due to the descending and ascending nature of the float and that the float spends nearly a third of its daily mission cycle at 1000 m (Table 5.1).

To illustrate the relative position of the floats' deployment within the Agulhas Current, the mean float speed for the first three profiles of each float, and the mean float speed over the entire duration of the floats within the Agulhas Current, along with their standard deviations, are given in Table 5.2. A clear trend of increasing float speed from the first deployment at 18 km (1917) to the fifth float deployment at 51.5 km (1913) was found for the first three profiles and the full trajectory of the floats, with a slight decrease offshore to float 1916 (60.5 km). There was also a clear increase of the mean float speeds from 33.5 km offshore (1914) to 42.5 km offshore (1915), capturing the Agulhas Current core floats (1915, 1913, 1916) to those inshore

Table 5.2: *Argo float trajectory dynamics within the Agulhas Current for the August Experiment.*

Float trajectory	**1917**	**1912**	**1914**	**1915**	**1913**	**1916**
Distance deployed offshore (km)	18	26	33.5	42.5	51.5	60.5
No. of days to exit Agulhas Current	15	12	12	10	9	10
Mean speed ($m\,s^{-1}$) for full trajectory	0.42 $\pm$ 0.39	0.51 $\pm$ 0.23	0.51 $\pm$ 0.10	0.71 $\pm$ 0.16	0.76 $\pm$ 0.15	0.72 $\pm$ 0.11
Mean speed ($m\,s^{-1}$) over first three profiles	0.17 $\pm$ 0.07	0.31 $\pm$ 0.03	0.38 $\pm$ 0.01	0.52 $\pm$ 0.02	0.61 $\pm$ 0.04	0.61 $\pm$ 0.02
Position within Agulhas Current	Coastal	Inshore of Agulhas Current	Inshore of Agulhas Current	Inshore of Agulhas Current core	Agulhas Current core	Offshore of Agulhas Current core

of the core (1912, 1914) and the coastal float (1917).

The Agulhas Current core has been found to be 20 km from the coast along the east coast of South Africa, and approximately 70 km wide (Beal and Bryden, 1999). However, the current is subjected to a number of meanders annually (Leber and Beal, 2014; Krug and Tournadre, 2012), with 1.6 of these meanders maintaining their structure to offshore of Port Elizabeth per year (Rouault and Penven, 2011). The core of the current has been shown to be variable in its distance from the coast. From a 267-day mooring array at 32° S, the core was within 20 - 30 km of the coast 79% of the time, was found 62 km from the coast 8% of the time, 102 km off the coast 11% of the time, and 150 km offshore for less than 2% of the entire mooring deployment (Bryden et al., 2005). While a month-long survey of the east coast showed the Agulhas Current core to be 75 km offshore off of Port Elizabeth, 20 km offshore off of East London and Port St. Johns and 50 km offshore of Richards Bay (Casal et al., 2009). The float speeds calculated for this experiment places the core approximately 51.5 km offshore.

5.3.2 Argo-derived thermohaline structure

As noted in earlier classifications of water masses for the Agulhas Current region (Beal et al., 2006; Stramma and Lutjeharms, 1997; Emery, 2001), five distinctive upper and intermediate water masses are present: Tropical Surface Water (TSW, $\leq$ 25.5 γ), Sub-tropical Surface Water (STSW, 25.5 - 26.4 γ), South Indian Central Water (SICW, 26.4 - 27.0 γ), Red Sea Water (RSW, 27.25 - 27.7 γ) and Antarctic Intermediate Water (AAIW, 27.2 - 27.4 γ). As shown in Section 5.3.1, the floats

propagated along the Agulhas Current with no interactions (i.e. inshore mesoscale eddies causing meandering of the current) and were classified based on their mean speeds and deployment locations across the Agulhas Current. In this section, we look at the north-south gradient (southward propagation) of the Agulhas Current to determine the evolution of water masses.

Given the trajectories of the floats described in Section 5.3.1, three classifications were assumed: the coastal float (1917), floats deployed along the inshore edge of the Agulhas Current (1912 and 1914) and three floats within the Agulhas Current itself (1915, 1913 and 1916). In order to analyze the evolution of water masses over distance downstream, a series of conservative temperature-absolute salinity profile diagrams were plotted, where the 1st (black solid line), 5th (cyan solid line), 10th (green solid line) and, where applicable, 15th (orange solid line) profiles are shown (Fig. 5.4). For all six floats, SICW remains unchanged profile-to-profile as the floats propagated southwestwards. The SICW is represented by a wide range of temperatures and salinities in the Agulhas Current (8 - 15° C, 34.6 - 35.6, Stramma and Lutjeharms (1997)), and exhibits a water mass with homogeneous properties spread over a large area, with no downstream variation of properties. Analysis will be focused on the upper (TSW and STSW) and intermediate (RSW and AAIW) water masses.

Float 1917, the coastal float, was the only float with 15 profiles within the Agulhas Current, due to its slower mean speed. Very little change occurred in the surface waters (Fig. 5.4a), with profiles 5, 10 and 15 exhibiting more variability than profile 1. The float propagated southwestwards relatively slowly, since it was outside of the core of the current, with profile 1 off 31° S, and profile 10 (10 days later) only 1° further south (Fig. 5.2). Profile 1, but more so profiles 5 and 10, showed a trend of RSW at its lower ranges (5-14° C, 34.8 to 35.4 for salinity, Emery (2001)), which freshens by 0.33 g kg^{-1} and cools by 0.78° C towards an AAIW (at 27.3 kg m^3) by profile 15 over a distance of 505 km.

The evolution of water masses for float 1912 (Fig. 5.4b) was very similar to float 1917, however there was much greater variability in the surface waters with a trend towards freshening (0.10 g kg^{-1} for TSW at 25 kg m^3 and 0.09 g kg^{-1} for STSW at 26 kg m^3) and cooling (0.67° C for STSW) as the float propagated south over a distance of 222 km between profiles 5 and 10. The greater variability between fresher and saltier waters for float 1912 may be attributed to the proximity of the float to the edge of the Agulhas Current, with exchange of waters likely occurring between the Agulhas Current and the inshore coastal waters. The intermediate water masses were shown to freshen by 0.06 g kg^{-1} and cool by 0.30° C from RSW towards AAIW at 27.3 kg m^3 over 338 km from profile 1 to 10.

Float 1914 (inshore of Agulhas Current) was unique from all the other floats (Fig. 5.4c) as it showed an increase in salt in the surface waters (0.14 g kg^{-1} for TSW at 25 kg m^3 and 0.08 g kg^{-1} for STSW at 26 kg m^3), along with a less obvious warming trend from profile 5 to profile 10 (0.41° C for TSW at 25 kg m^3 and 0.23° C for STSW at 26 kg m^3). This occurred over a distance of 250 km. At the intermediate water mass level, there appeared a very slight cooling and freshening, but not pronounced enough to trend towards AAIW.

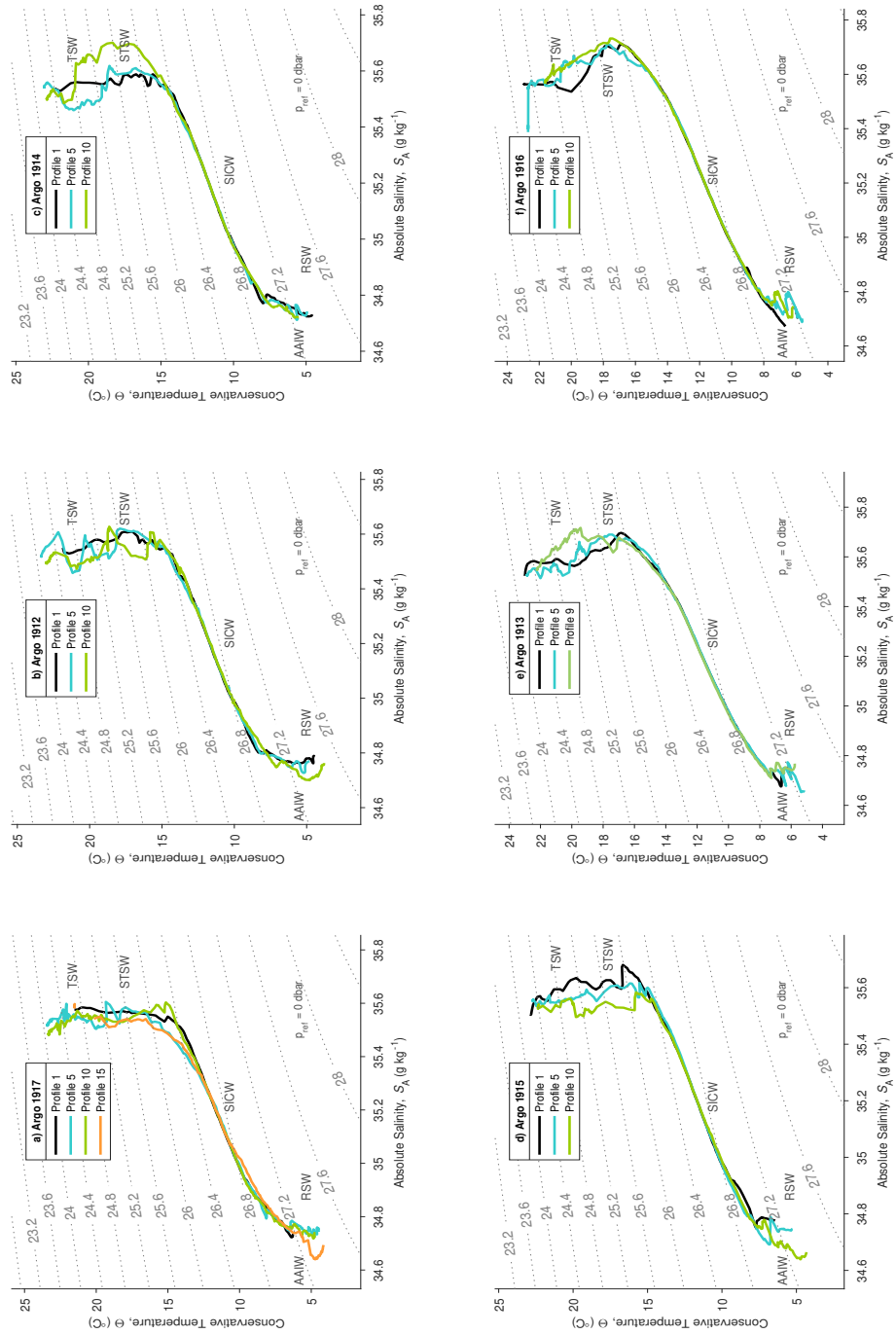

Figure 5.4: *Conservative temperature (°C) and absolute salinity (g kg^{-1}) plots for each Argo float, (a) 1917, (b) 1912, (c) 1914, (d) 1915, (e) 1913, (f) 1916. Only profiles 1, 5, 10 and where applicable, 15 are shown in order to illustrate the evolution of the water masses as the floats propagate southwestwards with the Agulhas Current.*

Float 1915 (Fig. 5.4d), the float deployed inshore of the Agulhas Current core, showed the same trend as 1917 and 1912 with freshening (0.11 g kg^{-1} for TSW at 25.2 kg m^3, 0.15 g kg^{-1} for STSW at 26 kg m^3 and 0.10 g kg^{-1} for RSW and AAIW at 27.3 kg m^3) and cooling (0.41° C for TSW at 25.2 kg m^3, 0.23° C for STSW at 26 kg m^3 and 0.62° C for RSW and AAIW at 27.3 kg m^3) in the surface and intermediate water masses as the float progressed south. The surface waters (TSW and STSW) changes were shown between profiles 1 and 10, a distance of 560 km, while the intermediate water mass change occurred over 360 km from profile 5 to 10. This float also propagated completely isolated from the other floats (Fig. 5.2), where some degree of overlap was noted for the inshore floats. It was thus interesting that float 1915 showed a similar trend to the inshore floats as it propagated faster than both 1917 and 1912.

Finally the two offshore floats (1913 and 1916) showed an increase of salt (0.10 and 0.08 g kg^{-1} for TSW at 25.2 kg m^3 for 1913 and 1916, and 0.06 and 0.03 g kg^{-1} for RSW and AAIW at 27.2 kg m^3 and 27.0 kg m^3 respectively for 1913 and 1916), accompanied by a slight warming (0.18° C and 0.35° C for 1913 and 1916 for TSW at 25.2 kg m^3, and 0.13° C and 0.17° C for 1913 and 1916 for RSW and AAIW at 27.2 kg m^3 and 27.0 kg m^3 respectively), over space (600 km for 1913 and 575 km for 1916 for the surface waters and 380 km and 360 km for intermediate water masses) and time (Fig. 5.4e and f). The increase in salt in the surface layers was not as great as for float 1914, but still notable, given the shape of their first profiles, and showed a large value for salt (35.73 g kg^{-1}) at a density of 26 kg m^{-3}. Float 1913 was deployed within the actual Agulhas Current core given its trajectory speed (0.76 ± 0.15 m s^{-1}) was greater than all five of the other floats.

However, evaporation at the ocean-atmosphere interface cannot account for the increase in salinity in the STSW water mass layer for floats 1914, 1913 and 1916 within the Agulhas Current given its 1.8 m s^{-1} surface velocity (Beal et al., 2015) and the depth at which STSW sits within the water column (roughly below 130 m). A more likely explanation is the recirculation of the Agulhas Current around the South West Indian Ocean sub-gyre (Lutjeharms, 2006; Hermes et al., 2007) and, at times, mesoscale eddy influence from the interior of the Indian Ocean (Nauw et al., 2008; Dilmahamod et al., 2018). By far the greatest influence to the Agulhas Current in terms of its three sources is the Agulhas Current Recirculation, which is loosely defined as meriodinally restricted to the region south of Madagascar (Lutjeharms, 2006). While variability within the flow of the Agulhas Current Recirculation exists, it likely predominantly influences the Agulhas Current south of 32°S. Modeling work has shown a significant relationship for volume flux for the Agulhas Current Recirculation and the Agulhas Current on interannual times scales, most notably for late austral summer (Hermes et al., 2007). The recirculation also provided considerable heat flux to the Agulhas Current, but was cooler than what was contributed from mesoscale eddies through the Mozambique Channel and South-West Madagascar (Hermes et al., 2007). Unfortunately the model study did not look at salt flux influencing the Agulhas Current through recirculation, but we argue that the Agulhas Current Recirculation is a likely source of influence for the offshore edge of the Agulhas Current, inclusive of salt fluxes, particularly in the absence of offshore mesoscale eddies visible at the time of this study (Fig. 5.2).

5.4 Combining Argo and model data

Through this section the joint view of combining Argo data from the August Experiment with output from an eddy-resolving ocean general circulation reanalysis model is assesses. In Section 5.4.1 the velocity structure of the AC is addresses. In Section 5.4.2 the thermohaline structure of the AC is investigated.

5.4.1 Velocity structure

Studies along 31° and 32° S, using CTD and, where available, Lowered-Acoustic Doppler Current Profiler (L-ADCP) casts used a level of no motion (2000 db) to calculate geostrophic velocity (Toole and Warren, 1993; Beal and Bryden, 1999). Argo profiles less than 1000 db do not capture this level of no motion, nor the northward flowing Agulhas Undercurrent (Beal and Bryden, 1999), and thus were not used determine geostrophic velocities from these data. For the volume, heat and salt calculations (Section 5.5), the August Experiment and model-derived speeds along each transect were used, described further within this section.

To evaluate the current from north to south, transects (T1 - T5) were extracted perpendicular to the coastline across the Agulhas Current (Fig. 5.2), roughly one degree apart. Argo float data was interpolated along each floats' trajectory southwestwards every kilometer, thus allowing for standardization of distance between transects. Variables interpolated along the Argo trajectories were conservative temperature, absolute salinity, potential density relative to the surface, and the speed of the float. Float speed was calculated as the distance from one surface position to the next over 24 hours. It thus may be seen as the integrated speed from 1000 m to the surface, given the floats' decent and ascent through the water column. Float 1917 was excluded from the calculations of speed and volume, heat and salt flux in Section 5.5, as it was not representative of Agulhas Current waters given the floats' proximity to the coast. The coordinates of these five transects were then used to extract data from the model to 1000 m. Variables included temperature and salinity (later converted to conservative temperature and absolute salinity), total u- and v- components. The cross-shore (u') and alongshore (v') components were rotated 127.5° for the coastline.

These five transects for the August Experiment and the model are plotted in Figure 5.5a and 5.5b respectively, with distance from the coast along the x-axis representing inshore on the left; offshore on the right. For both data sets, there was an increase in speed across the transect from T1 in the north to T5 in the south. The transects show a decrease in speed offshore, more so in the model data compared to the August Experiment, indicative of transects capturing the offshore extent of the Agulhas Current. For the August Experiment, the Agulhas Current core was at 50 km offshore on T1 - T3, 55 km offshore at T4 and approximately 60 km offshore at T5. The model exhibited the same trend of Agulhas Current core moving between 50 km offshore in the north to 60 km offshore in the south. This agrees well with the Argo-derived velocity data, indicating the Agulhas Current core being roughly 51.5 km offshore (Section 5.3.1).

5.4.2 Thermohaline structure

The model conservative temperature, absolute salinity and potential density anomaly (reference pressure 0 dbar) were plotted at the same positions as for profile 1 for the August Experiment. Conservative temperature and absolute salinity vertical sections, overlaid with the potential density anomaly and Argo deployment positions, are shown for the August Experiment (Fig. 5.6a and c respectively) and the model (Fig. 5.6b and d respectively).

The vertical distribution shown by the August Experiment and the model agree well at the first profile position. Isotherms were uplifted closer inshore, particularly illustrated at depth, while warmer surface temperatures were evident over the offshore three profiles. Isohalines were also shown shoaling towards the coast for the August Experiment and the model, while a pool of higher salinity water (35.6) was visible subsurface (100 - 300 m) from offshore in both sections. This high salinity input has been described using the conservative temperature-absolute salinity diagrams in Figure 5.4 and Section 5.3.2.

The key difference between the August Experiment and the model lies in the variability (or lack thereof for the model) across isolines illustrated in the vertical sections. The August Experiment conservative temperature vertical section exhibited cooler surface temperatures inshore, and a smaller pool of 23° C water offshore. The greatest difference lies around the 27 kg m^{-3} potential density anomaly isopycnal (associated with intermediate water masses), which upwelled more substantially for the August Experiment (to 600 m inshore from 900 m offshore) compared to the model (upwelled to 650 m inshore from 800 m offshore). Isotherms for the August Experiment showed variability within the SICW thermocline region, between 10° C and 7° C, exhibiting a large lens of 9° C water from 33.5 km to 51.5 km from the coast, with a very narrow 8° C lens. The 5° C isotherm also extended deeper than 1000 m, 33.5 km from the coast. By comparison, the model exhibited more uniform spacing between isotherms.

Similarly, absolute salinity for the August Experiment showed greater variability than the model, with the 27 kg m^{-3} potential density anomaly isoline following the 34.8 isohaline from the inshore to offshore profiles. For the model vertical section, the 27 kg m^{-3} potential density anomaly isopycnal and 34.8 isohaline are approximately 150 m apart throughout.

From this description the greatest variability for the August Experiment lies within the TSW and STSW water masses (extending from 24.7 to 26.4 kg m^{-3} as per Donohue and Toole (2003)) and the intermediate water masses (centered around the 27 kg m^{-3} as per Tomczak and Godfrey (1994)).

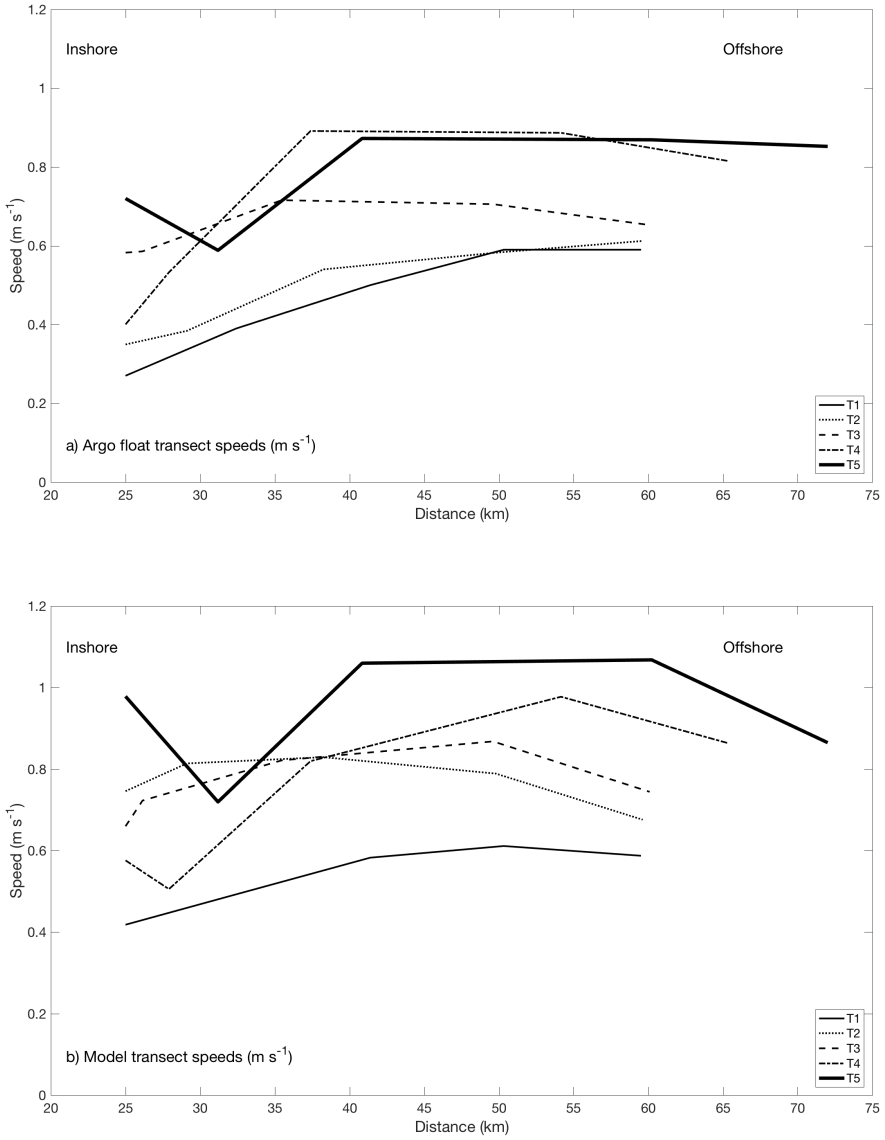

Figure 5.5: *a) Argo transect speeds (m s^{-1}) and b) Model transect speeds (m s^{-1}). T1 = Transect 1 (solid thin line), T2 = Transect 2 (dotted line), T3 = Transect3 (dashed line), T4 = Transect 4 (dot-dash line), T5 = Transect 5 (solid thick line). Distance is given as relative to the coast but only shown for the actual transect.*

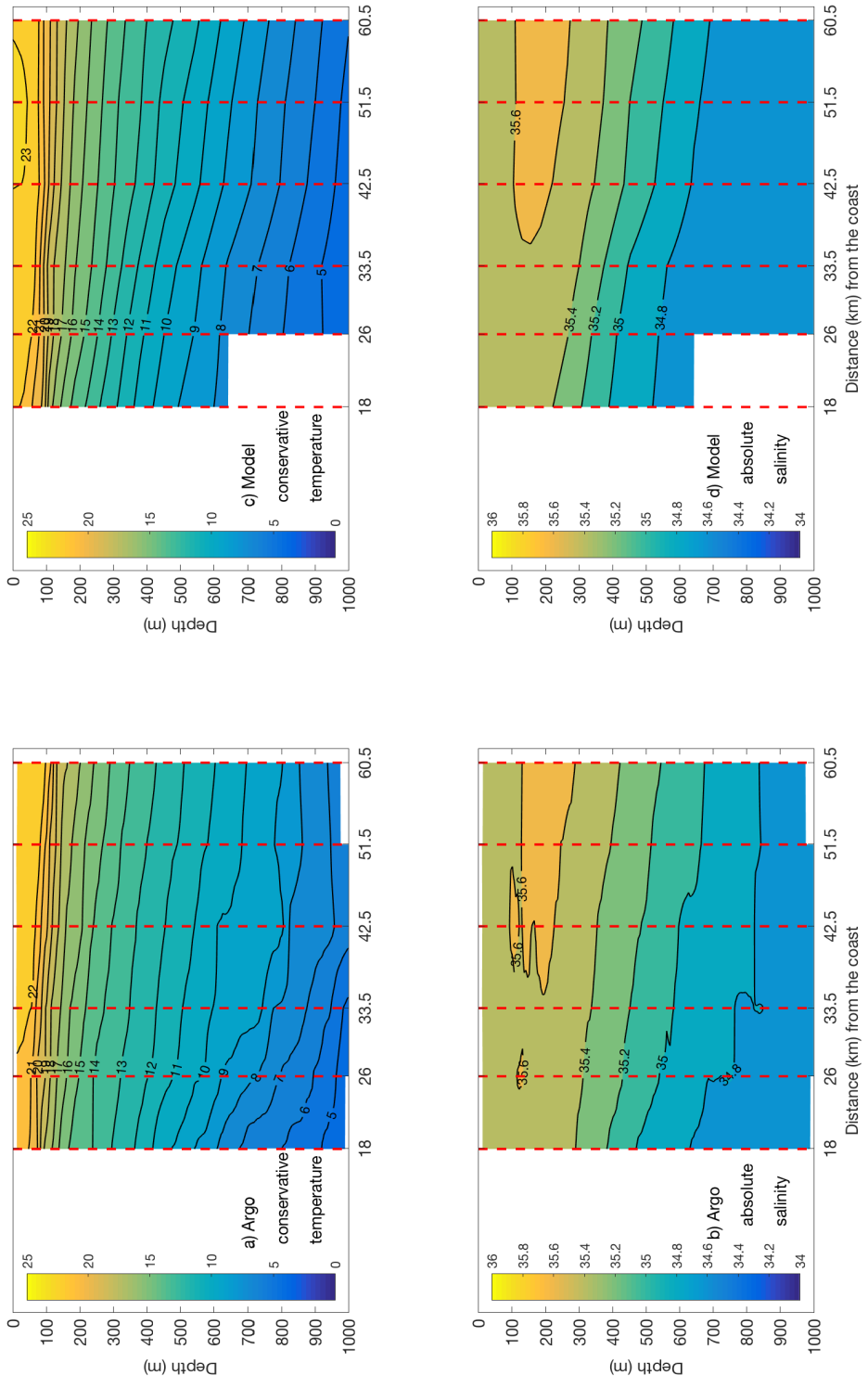

Figure 5.6: *(a) August Experiment conservative temperature vertical section from the coast to 61 km offshore, (b) August Experiment absolute salinity vertical section from the coast to 61 km offshore, (c) Model conservative temperature vertical section from the coast to 61 km offshore, (d) Model absolute salinity vertical section from the coast to 61 km offshore.*

5.5 Volume, heat and salt fluxes

In this section the downstream evolution of volume, heat and salt fluxes from the surface to 1000 m, computed and discussed through the combined use of Argo and model data is assessed. Thereafter, water mass fluxes from Argo-derived data are presented (Section 5.5.1). In Section 5.5.2 the model-based estimates of volume, heat and salt fluxes through the full extent of the AC are calculated and discussed; hereafter referred as to Extended Transects (down to the seabed).

The volume, heat and salt flux equations (Beal and Bryden, 1999) are given below:

$$V_e = \int_z^0 \int_x^0 V \, dz \, dx \tag{5.1}$$

$$Q_h = \int_z^0 \int_x^0 \rho_0 \, C_p \, \Theta \, V \, dz \, dx \tag{5.2}$$

$$Q_s = \int_z^0 \int_x^0 \rho_0 \, S_A \, V \, dz \, dx \tag{5.3}$$

where,
ρ_0 = 1026 kg m^{-3}
C_p = 4000 J Kg^{-1} °C^{-1}
Θ (°C) and S_A (g kg^{-1}) = the mean conservative temperature and absolute salinity calculated across each transect
V = is speed in m s^{-1}
z = depth in meters
x = distance in meters

5.5.1 August Experiment: Argo-derived and model-based fluxes

Using the same transects extracted from interpolated August Experiment trajectories in Section 5.4.1, the volume, heat and salt flux were derived for both the August Experiment and model data sets, with results to 1000 m summarized in Table 5.3, and water mass flux results summarized in Table 5.4.

Most notably, the distance across the transects (i.e. from float 1912 to 1916 offshore) were fairly narrow, ranging from 34.53 km along T1 to 47.04 km along T5 (Table 5.3). The depth to which the calculations were made was 1000 m; the profiling depth of the floats. Both the August Experiment and model transects exhibited an increase in speed moving southwards (as described in Section 5.4.1). Similarly, the volume transport for the August Experiment transects increased from north to south, and ranged from 16.76 Sv (T1) to 38.18 Sv (T5). Ultimately the volume transport for the model transects increased from 17.70 Sv on T1 to 32.51 Sv on T5, but volume transports decreased from T2 (23.45 Sv) through T3 (20.00 Sv) and T4 (19.98 Sv), before increasing to T5 again.

For the August Experiment, an increase of heat flux transported southwards was captured with 0.85 PW on T1 through to 1.79 PW on T5. For the model data, a similar trend as for model volume transport was captured with an increase from T1 (0.99 PW) to T2 (1.31 PW), before decreasing slightly to 1.23 PW on T3 (1.25 PW on T4) and increasing substantially to 1.91 PW on T5 again. A very similar trend was

shown for the salt flux, with an increase in salt transported from north to south for the August Experiment (0.60 x 10^{12} kg s^{-1} at T1 to 1.37 x 10^{12} by T5). The model data showed the same trend again as for heat flux, from 0.63 x 10^{12} kg s^{-1} at T1 to 0.84 x 10^{12} kg s^{-1} at T2, decreasing to 0.72 x 10^{12} kg s^{-1} at T3 and T4, before increasing again to 1.17 x 10^{12} kg s^{-1} at T5 (Table 5.3).

Historically, not many observations of the heat and salt flux within the AC have been made (Beal and Bryden, 1999; Bryden and Beal, 2001). Most recently, the Agulhas System Climate Array moorings have made advances in capturing the heat and salt variability within the AC over approximately 25 months at 34°, but these results are still being prepared for publication (McMonigal et al., 2020). The results from this work also only represented the upper 1000 m of the water column, and did not capture the full extent of the current and lower water masses, which would alter these results. With the Argo profiles, only the upper layer of the intermediate water mass was captured which, as shown in the conservative temperature-absolute salinity diagrams (Fig. 5.4), appeared to be dominated by RSW which has a higher salinity value than AAIW. However, the results show with the August Experiment an increase of speed, volume, heat and salt fluxes with southward propagation. The model transects showed a similar increase in terms of values between T1 and T5 to the August Experiment, but showed variability in the results between T2 and T4. Interestingly, the transport weighted temperature and salinity for each of the August Experiment transects showed a decrease in value (12.52° C to 11.46° C; 35.19 to 35.11) from T1 to T5 (Table 5.3), while the model transported temperature and salinity showed an increase in values (13.68° C to 14.43° C; 35.23 to 35.30). These values represent the temperature and salinity values at the location of maximum transport, and the most representative temperature and salinity for the 1000 m water columns (Tillinger and Gordon, 2010). Given temperature decreases with depth it can be assumed for the August Experiment the maximum location of transport decreased from north to south, while for the model, this maximum location (i.e. depth) of transport increased.

Table 5.3: *August Experiment and model transect calculations for volume, heat and salt flux.*

Transect	**Distance (km)**	**Volume Transport (Sv)**	**Heat Flux (PW)**	**Salt Flux (x10^{12} kg s^{-1})**	**Transport weighted temperature (°C)**	**Transport weighted salinity (g Kg^{-1})**
T1: Argo	34.53	16.76	0.85	0.60	12.52	35.19
T2: Argo	34.65	18.11	0.88	0.65	11.98	35.16
T3: Argo	35.11	23.90	1.15	0.86	11.76	35.14
T4: Argo	40.32	32.47	1.57	1.17	11.84	35.14
T5: Argo	47.04	38.18	1.79	1.37	11.46	35.11
T1: Model	34.53	17.70	0.99	0.63	13.68	35.23
T2: Model	34.65	23.45	1.31	0.84	13.70	35.25
T3: Model	35.11	20.00	1.23	0.72	15.08	35.37
T4: Model	40.32	19.98	1.25	0.72	15.32	35.37
T5: Model	47.04	32.51	1.91	1.17	14.43	35.30

It was shown in Section 5.4.2 that the greatest variability for the August Experiment lay within the TSW and STSW water masses, while the SICW remained consistent from north to south. For TSW, the mean layer thickness across the five transects

was 131.4 ± 8.4 m, from the surface, with volume transport increasing from 2.19 Sv (T1) to 5.00 Sv (T5). The heat and salt fluxes remained consistent over T1 and T2 for TSW (0.18 and 0.17 PW respectively, 0.07 x 10^{12} kg s^{-1}) before increasing to 0.37 PW and 0.15 x 10^{12} kg s^{-1} by T5 (Table 5.4). STSW, with a mean thickness of 215.6 ± 11.5 m below TSW, and SICW with a mean thickness of 609.8 ± 51.6 m, exhibited the same trends as TSW; increasing in volume, heat and salt fluxes from north to south with the Agulhas Current. For SICW, there appeared a minimal decrease in heat and salt flux between T1 and T2, before increasing southwards, though no decrease in volume transport was calculated (Table 5.4). Noticeably, SICW carried the greatest volume of heat and salt southwards, having the largest area of the three water masses analysed in this work, but also representative of the thermocline for the Agulhas Current. The transport-weighted temperature and salinity ranged between 12.52 - 11.46° C for the August Experiment, 13.68 - 14.43° C for the model and 35.19 - 35.11 x 10^{12} kg s^{-1} for the August Experiment and 35.23 - 35.30 x 10^{12} kg s^{-1} for the model. Transport-weighted parameters represent the region within the water column at which the transport is most heavily weighted Tillinger and Gordon, 2010. The ranges calculated for the 1000 m data-sets fit squarely within the SICW range of temperature and salinities as shown in Figures 5.3 and 5.4. This further supports the findings of greater variability in the upper water mass levels (TSW and STSW) as would be expected with a fast moving current, while the bulk of the transport lies in the water mass range associated with the thermocline.

Table 5.4: *Estimates of volume, heat and salt flux for the Tropical Surface Water (TSW), Subtropical Surface Water (STSW) and South Indian Central Water (SICW) water masses using the August Experiment data.*

Transect	Volume Transport (Sv)	Heat Flux (PW)	Salt Flux (x10^{12} kg s^{-1})
T1: TSW	2.19	0.18	0.07
T2: TSW	2.37	0.17	0.07
T3: TSW	3.13	0.23	0.09
T4: TSW	4.25	0.31	0.12
T5: TSW	5.00	0.37	0.15
T1: STSW	3.62	0.16	0.08
T2: STSW	3.91	0.15	0.08
T3: STSW	5.16	0.19	0.10
T4: STSW	7.01	0.26	0.14
T5: STSW	8.24	0.27	0.15
T1: SICW	10.21	0.35	0.29
T2: SICW	11.03	0.31	0.26
T3: SICW	14.55	0.39	0.32
T4: SICW	19.77	0.53	0.44
T5: SICW	23.25	0.57	0.49

5.5.2 Extended transects for August Experiment: Model-based fluxes

A transect undertaken in February and March 1995 using full-depth CTD and L-ADCP profiles perpendicular to the coastline from 31° S, determined a heat flux of 4.13 PW, a salt flux of 2.64 x 10^{12} kg s^{-1} for 73 Sv of volume transport (Beal and

Bryden, 1999). For this comparison to the Beal and Bryden (1999) transect, temperature extracted from the model was converted to potential temperature and not to conservative temperature as for the rest of the manuscript's flux calculations. Salinity was kept as practical salinity units.

Data was extracted from the model (27 February - 6 March 1995) at the same positions as for Beal and Bryden (1999). A volume transport of 82.57 Sv, a heat flux of 4.41 PW and a salt flux of 2.97 x 10^{12} kg s^{-1} was obtained. With an over-estimation of the model data compared to the published *in situ* results of 10 Sv (7.3%), 0.28 PW (6.7%) and 0.33 x 10^{12} kg s^{-1} (12.5%). A transport weighted temperature of 13.06° C compared to 13.82° C was obtained, with a transport weighted salinity of 35.11 compared to 35.19. The model agrees very well with the *in situ* data given an overestimation of less than 10% on average and transport weighted parameters less than one degree for temperature and within one decimal place for salinity. It can be argued that model data improves with successive assimilations of observed data, and given the model was run from 1993, with this transect extracted from 1995, there is confidence in the close relationship of these results (Storto et al., 2019).

For the Agulhas Undercurrent, a volume transport of 2.73 Sv northwestwards along the shelf edge was calculated (within 100 km of the coast), with a total equatorward transport for the transect of 3.72 Sv. Values of 6 $\pm$ 1 Sv (Beal and Bryden, 1997) and 5 Sv within 80 km of the coast (with a total equatorward transport of 13 Sv), (Beal and Bryden, 1999) have been found along the 31° S transect. Additional Agulhas Undercurrent transport calculations have been made offshore of Port Elizabeth (4.2 $\pm$ 0.9 Sv) and Richards Bay (2.8 $\pm$ 2.1 Sv) during a month long survey of the east coast of South Africa (Casal et al., 2009), indicating the range of transport applicable for the Agulhas Undercurrent. While the value determined was low in comparison to literature for this work, the model has captured the Agulhas Undercurrent in its correct geographical position (Fig. 5.7) and within an acceptable value. Plotted in Figure 5.7 is the model vertical section for velocity, red being southwestward (Agulhas Current) and blue being northeastward (Agulhas Undercurrent along the shelf) in direction. The vertical section agrees well with Figure 6a of Beal and Bryden (1999) which shows the same structure for the Agulhas Current.

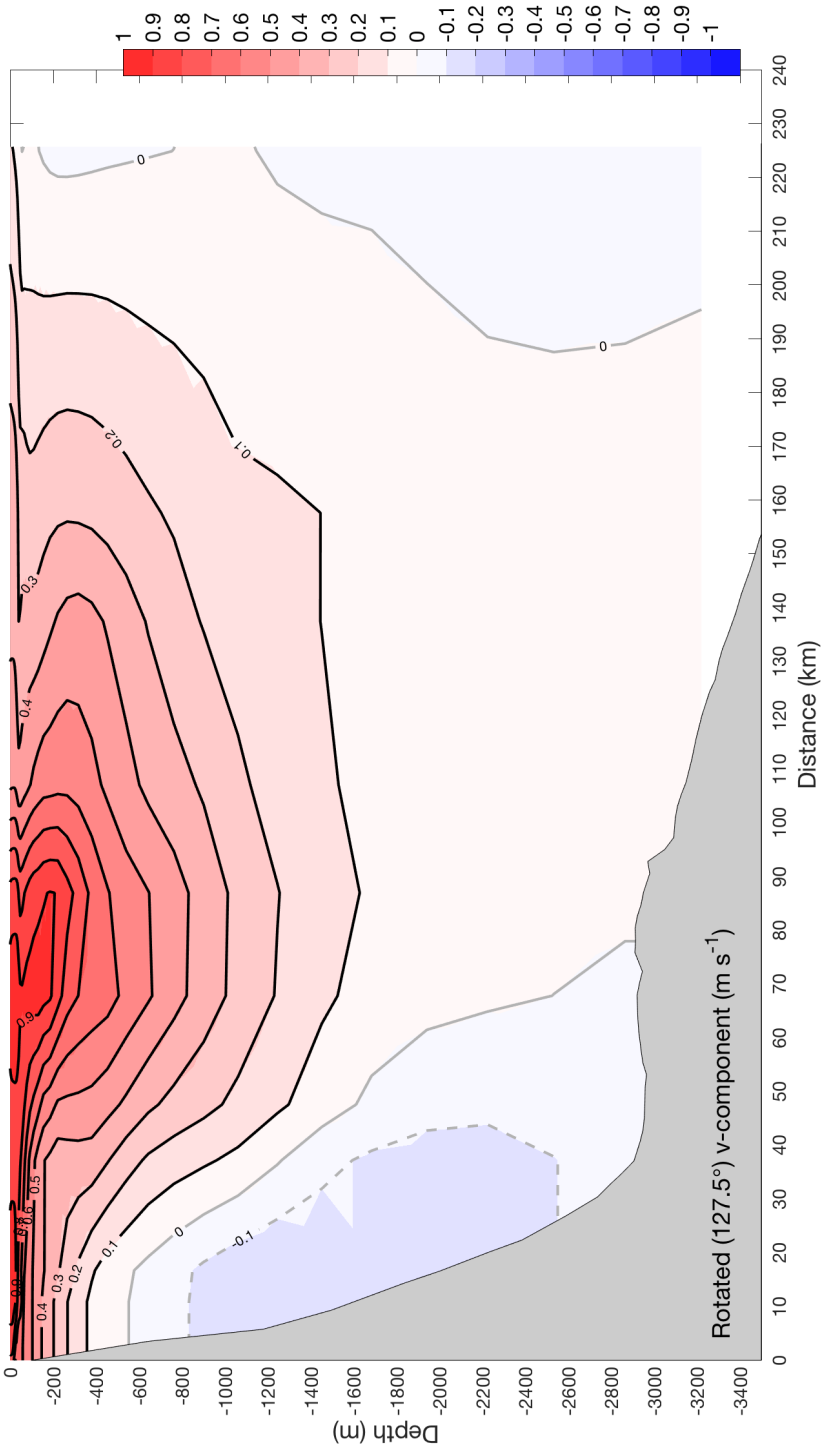

Figure 5.7: *Vertical section of model velocity data (m s^{-1}) for the 32° transect Beal and Bryden, 1999 for 27 February to 6 March 1995. Red contours show the Agulhas Current propagating polewards, and blue represents equatorward Agulhas Undercurrent flow.*

In order for a representation of the full water column for the August Experiment to be obtained, in the absence of full-depth Argo profiles, the study had to rely on the model further. Using the same five transects, data was extracted for the same day, from the same start position (on float 1912) to 240 km offshore and to the full depth of the water column (Table 5.5).

The volume transport for the five transects increased from north (49.75 Sv) to south (126.32 Sv) as was expected, and as shown for both the August Experiment and 1000 m model data sets (Section 5.5.1). The range of volume transport, 9 - 121 Sv, proposed at 32° S (Bryden et al., 2005) should logically increase to approximately 21 - 133 Sv given the estimate of 6 Sv per 100 km suggested by Gründlingh (1980), illustrating the model estimate to be within the range of volume transport anticipated for the Agulhas Current.

The heat flux values from T1 to T5 showed an increase with southward propagation, increasing from 2.88 PW (T1) to 5.98 PW (T5). The salt flux increased from 1.96 x 10^{12} kg s^{-1} at T1 to 4.40 x 10^{12} kg s^{-1} at T5. The estimated volume (74.5 Sv) and salt flux (2.69 x 10^{12} kg s^{-1}) calculations at T2, closely resemble the results found by Beal and Bryden (1999), while the heat flux of 3.81 PW was lower than previously estimated. The August Experiment took place in the middle of austral Winter, while the Beal and Bryden (1999) survey took place in March, the end of the austral Summer. Thus the heat flux obtained in late austral Summer was determined to be closer to the expected maximum for this region (Beal and Bryden, 1999). While the heat flux was less than previously measured, these estimates are within range for the Agulhas Current.

From these extended transects and subsequent volume, heat and salt calculations, further confidence that the model replicated the Agulhas Current in comparison to published literature was acquired. Further, given the 1000 m model and Argo data sets agreed well, confidence in the upper water column assessment of the Agulhas Current was obtained for the August Experiment. Given these data replicated the realistic variability of the Agulhas Current (Section 5.4.2), it has been shown that Argo floats, if deployed strategically across the Agulhas Current, are able to make a realistic synoptic assessment of the volume, heat and salt flux of the current. Furthermore, this study is the first to show a near-real time (approximately 10 - 12 days) evolution of volume, heat and salt transport of the Agulhas Current.

Table 5.5: *Extended model transects (full depth, 240 km offshore) calculations for volume, heat and salt flux.*

Extended model transect	**Volume Transport (Sv)**	**Heat Flux (PW)**	**Salt Flux (x10^{12} kg s^{-1})**	**Transport weighted temperature (°C)**	**Transport weighted salinity (g Kg^{-1})**
T1	54.17	2.88	1.96	13.00	35.26
T2	74.50	3.81	2.69	12.51	35.28
T3	64.09	3.42	2.32	13.06	35.34
T4	86.96	4.45	3.14	12.53	35.25
T5	121.79	5.98	4.40	12.01	35.26

5.6 Concluding Remarks

This Chapter has captured the evolution of the Agulhas Current in terms of volume, heat and salt fluxes in a near-real time (10-12 days) survey for the first time. Six Argo floats, acquiring temperature and salinity, were programmed to undertake daily profiling from 1000 m to the surface and were deployed along a perpendicular transect offshore of Port Edward, roughly 31° S. These data were complemented with output from an eddy-resolving global general ocean reanalysis model (GLORYS12V1), and obtained a number of insightful results.

The floats captured a 'stable' version of the Agulhas Current, devoid of mesoscale eddy influence at the time of the survey, allowing propagation from northeast to southwest with minimal interruption. The floats were classified in relation to the Agulhas Current according to their speeds as coastal (1917), the inshore edge of Agulhas Current (1912, 1914), inshore of Agulhas Current core (1915), the Agulhas Current core itself (1913) and offshore of the Agulhas Current core (1916). The coastal float (1917) was the only float to exhibit a slower trajectory, likely interacting physically with the continental slope. The remaining five floats exited the fast-flowing Western Boundary Current in 9 - 12 days at mean speeds ranging from 0.51 ± 0.23 m s^{-1} to 0.76 ± 0.15 m s^{-1}. For this work the Agulhas Current core was found to be between 50 km (in the north) and 60 km (in the south) offshore of the coast.

Analysis of the conservative temperature-absolute salinity diagrams for each float highlighted three phenomena. The first was the increase in salinity at the very surface of the TSW water mass for floats 1917, 1912 and 1914, which was attributed to rainfall. These three inshore floats likely captured the Agulhas Current's influence on convective rainfall (Nkwinkwa Njouodo et al., 2018) along the southeastern coastline, which experiences year-round rainfall (Tyson and Preston-Whyte, 2000). The second phenomenon was the input at the STSW water mass of higher salinity waters from the offshore float (1916) for roughly 25 km shoreward. This was attributed to the influence of the Agulhas Current Recirculation given the latitude of the influence (31° S), but more so the absence at that time of any mesoscale eddies offshore. Finally there was found to be no variability within the SICW water mass. The assessment of the intermediate water masses was cursory at best given the floats only profiled from 1000 m, whereas intermediate water masses in this region can extend to 1500 m (Beal et al., 2006; Emery, 2001).

The August Experiment data was integrated along each downstream transect, and five cross-current transects were extracted, nominally 1° apart. Flux calculations were applied to the individual water mass levels and the volume transport, heat and salt fluxes for each water mass were found to increase from north to south, showing evolution along the Agulhas Current. The bulk of the transport was also found to occur within the SICW water mass; the thermocline range. The August Experiment and model-derived speeds were compared, as well as the volume, heat and salt flux, by matching the coordinates in the model data (to 1000 m) to those of the August Experiment cross-current transects. An increase in all three fluxes with southward propagation was found for both the August Experiment and model data when comparing the initial and ultimate transects (T1 and T5 respectively), with model data showing variability in results along T2 - T4.

In order to expand on the August Experiment results and ensure that they agree with what has been reported on in literature, the GLORYS reanalysis model was further relied upon. Firstly the model data was compared for the same period to the Beal and Bryden (1999) transect and results were found to be very similar (varying by less than 10%) and within one degree and one decimal place for the transport-weighted temperature and salinity respectively. To ensure the results were accurately capturing the Agulhas Current, the model was extended to 240 km offshore, and to the full depth of the water column. A large range for the volume (54.17 - 121.79 Sv), heat (2.88 PW - 5.98 PW) and salt (1.96×10^{12} kg s^{-1} - 4.40×10^{12} kg s^{-1}) fluxes was obtained. The heat and salt flux estimates are believed to be within the accepted range for the Agulhas Current, given the survey took place in austral Winter.

Argo floats have been used in this experiment as a novel, near-real time, approach to capturing the evolution of the Agulhas Current. The value in the near-real time assessment of the Agulhas Current allows for a higher-resolution evaluation of the transport within the current. The survey by Casal et al. (2009) took one month to complete which allowed for change to take place in the system. Time and again, the cost of dedicated research vessel surveys and subsurface moored observations have been shown to be exorbitant. And while these data are, and always will be, invaluable, newer technologies such as Argo, and the adaption of their mission profiles to daily sampling through energetic Western Boundary Currents, need to be tabled as possible solutions to assist in understanding these fast-flowing currents.

Chapter 6

General Discussion and Concluding Remarks

Preface:

This chapter brings together the evolution of the cyclonic mesoscale eddies and the Agulhas Current experiments. Section 6.1 looks at the methodology of the experiments and suggestions are given on how to replicate high resolution Argo float experiments in the Greater Agulhas Current System, and indeed turbulent and Western Boundary Current systems in general. The concluding remarks of the two scientific experiments are highlighted (Sections 6.2 and 6.3) as well as the impacts and benefits these studies may have on the Argo Program and data acquisition within the Indian Ocean (Section 6.4). Finally, the focus of where further exploration of the Greater Agulhas Current System should be, is investigated in Section 6.5.

This chapter discusses the first three key questions (Section 1.3) addressed in Chapters 2, 4 and 5, as well as the final key question in Section 1.3:

What are the impacts and benefits of altered Argo mission parameters on data acquisition in the Indian Ocean?

6.1 Can Argo floats be used to study mesoscale eddies in the southern Mozambique Channel and the Agulhas Current? (Chapter 2)

Over the course of five years (2013-2017), Argo floats were deployed from five research cruises in the Greater Agulhas Current region. The Argo floats were made available for the experiments by Woods Hole Oceanographic Institution (WHOI) in the United States, The United Kingdom Meteorological Office, the Commonwealth Scientific and Industrial Research Organisation (CSIRO) in Australia and the Euro-Argo Monitoring the Oceans and Climate Change with Argo (MOCCA) project. These Argo float teams also agreed to allow an altered profiling mission during the experiments to test these research questions (Section 1.3). Argo floats were deployed in two cyclonic eddies spawned from southwest Madagascar (Chapter 4), an anti-cyclonic eddy (not analyzed further in the thesis), and for two experiments within the Agulhas Current. Only the latter of these two Agulhas Current experiments was analyzed, as the first was concentrated offshore of the Agulhas Current and associated with an offshore cyclonic eddy. A recall of these five cruises and their Argo float deployments are shown in Figure 2.1.

The Indian Ocean is notoriously under-sampled and understudied (Hood et al., 2016) and yet, according to recent studies, the Indian Ocean has been warming basin-wide over the last century (Roxy et al., 2014). The tropical Indian Ocean has increased by more than 1° C at the surface, which is roughly 50 - 60% greater than other tropical regions, exceeding natural variability (Hu and Fedorov, 2019). These waters are exported polewards by currents such as the Leeuwin Current, the East Madagascar Current and the Agulhas Current; the latter contributing to the Atlantic Meridional Overturning Circulation through the Agulhas Retroflection (Beal et al., 2011). Arguably then, a comprehensive understanding of the Greater Agulhas Current System, the mesoscale eddies that contribute volume, heat and salt to the Agulhas Current, the dynamics of the northern extent of the Agulhas Current and the evolution of the Agulhas Current itself, is critical.

The work in this thesis (Chapter 2) has shown the increase of Argo profiles for the experiments (red bars, Fig. 2.2b, 2.3b) over the standard profiles (blue bars, Fig. 2.2b, 2.3b). This was more pronounced in the southern Mozambique Channel, but shows valuable input into the Greater Agulhas Current System. The increases were as a direct result of altering of the profiling missions to capture the turbulence of mesoscale eddies and the fast-flowing Agulhas Current for this work. The Argo float setups were modified per experiment, and while not all setups will suit all turbulent regions globally, the is suggested following for the Greater Agulhas Current System:

- Ideally, Argo floats should be fitted with two-way telemetry communication to allow for the re-programming of Argo floats during their mission within the region of turbulence or fast-flowing current, and to revert back to standard profiling once this mission is complete.
- For mesoscale eddies in the southern Mozambique Channel, both daily and five-daily profiling was found to be effective in allowing the Argo floats to remain trapped within these systems, though daily profiling allowed for a better definition of eddy loops and tracking. This will of course depend on

the Argo float teams' battery considerations, and potentially Argo floats should be equipped with additional lithium batteries if possible. Park depths of 500 - 650 m would be the most suitable for this region, given the depth of the eddy cores found for this region. Profiles from 1000 m seemed to capture the mesoscale eddy. However, it is advised to do a profile to 2000 m for validation purposes every 10 profiles or so.

- The Argo float experiment along the Agulhas Current was too shallow. A park depth of 1000 m would be optimal, but with profiles from 2000 m to the surface in order to capture the full structure of the Agulhas Current and allow for geostrophic calculations. Daily profiles would be ideal.

Following this discussion on the Argo float experimental set up, the dedicated scientific results obtained from the experiments are given in Sections 6.2 and 6.3 below.

6.2 By using Argo floats on high-resolution profiling missions, can the knowledge of the vertical structure, geometric properties and fluxes of Madagascar cyclonic eddies be improved? (Chapter 4)

The deployment of eight Argo floats on altered missions within two cyclonic mesoscale eddies formed off southwest Madagascar provided a unique opportunity to study these anomalies subsurface. Very little is known of these mesoscale eddies, much less their contribution to the Agulhas Current. The majority of physical oceanographic understanding of these mesoscale eddies comes from model studies (Ridderinkhof et al., 2013; Halo et al., 2014b) augmented with satellite observations, with limited papers on subsurface oceanographic parameters from in situ observations (De Ruijter et al., 2004; Barlow et al., 2017; Noyon et al., 2018).

Using Argo float data and output from the eddy-permitting (1/4°) GLORYS ocean general circulation model, the following key insights of Madagascar cyclonic mesoscale eddies were made:

- The eddies propagated across the Mozambique Channel in approximately five months from southwest Madagascar to the KwaZulu-Natal Bight. Their propagation speed (13 - 15 cm s^{-1}) exceeded the theoretical prediction for dispersion of nonlinear vortices (Chelton et al., 2011; Cushman-Roisin, 1994; McWilliams and Flierl, 1979).

- The eddies exhibited clear growth, maturity and decay phases when they were unhindered in their propagation by external forcings (i.e. other eddies). They also remained non-linear for their entire lifespan, with trapped depths ranging from 373 m to 1026 m, dependent on phase. Thus these mesoscale cyclonic eddies were capable of transporting material (such as water masses, pollutants and biological organisms) across the Mozambique Channel.

- Madagascar cyclonic eddies contribute Tropical Surface Water, Sub-tropical Surface Water, South Indian Central Water, Red Sea Water and Antarctic Intermediate Water to the Agulhas Current (for the upper 1000 m where the Argo profiling took place). The April (July) eddy contributions included trapped water to 595 $\pm$ 294 m (914 $\pm$ 107 m), volume transports of 13.4 $\pm$ 5.2 Sv (21.2 $\pm$ 9.1 Sv), heat fluxes of -0.07 $\pm$ 0.06 PW (-0.2 $\pm$ 0.09 PW) and freshwater fluxes of 0.04 $\pm$ 0.04 Sv (0.09 $\pm$ 0.05 Sv).

Studying mesoscale eddies at sea is challenging - the timing of ship activities with a developing or mature mesoscale eddy (depending on the research question) being one of the trickiest details. To study the evolution of a mesoscale eddy would require ships time of at least one month, ideally three to four months, which is incredibly expensive, both in terms of cost and carbon footprint. This study thus highlights an ideal method of undertaking such a synoptic survey by means of mission-altered Argo floats. Ideally, the study of mesoscale eddies in such a way would greatly benefit from biogeochemical floats being used to investigate in addition to the standard parameters, dissolved oxygen, nitrate, pH, chlorophyll *a* (using fluorescence), suspended particles (using optical backscatterance) and downwelling irradiance (by means of a radiometer).

Furthermore simultaneous deployments within the cyclonic and anticyclonic lobes of a dipole eddy would enhance the understanding of this train of features propagating across the southern Mozambique Channel at a rate of four to six per year (Ridderinkhof et al., 2013). The deployment of two Argo floats within an anti-cyclonic eddy (independent of the two cyclonic eddy experiments) in December 2013 (Fig. 2.1) illustrated how quickly the floats dissipated out of the anticyclonic eddy (roughly 15 days). This experiment was not described further for the thesis, but to deploy floats across both lobes of the dipole remains a valuable experiment. Particularly if floats were to move across the interstitial jet between the anti-cyclonic and cyclonic eddies, highlighting a mixing of physical properties.

6.3 Can Argo floats be used to capture the downstream evolution of fluxes in the Agulhas Current? (Chapter 5)

Six Argo floats, profiling daily from 1000 m to the surface, were deployed across the Agulhas Current in August 2017. The aim of the synoptic survey was to study the north-south evolution of hydrographic properties and fluxes downstream of the Agulhas Current. A number of studies have been undertaken to study these dynamics of the Agulhas Current using single transects (Gründlingh, 1980; Toole and Warren, 1993; Beal and Bryden, 1999; Bryden and Beal, 2001; Leber and Beal, 2014), mooring arrays (Bryden et al., 2005; Beal et al., 2015), with one month-long survey of four transects crossing the Agulhas Current (Casal et al., 2009). This work represents the first to study the dynamics of the Agulhas Current using Argo floats with output from an eddy-resolving ocean general circulation reanalysis model. A number of key results were determined:

- The Agulhas Current core was found to be between 50 km (in the north) and 60 km (in the south) offshore from the coast during this study of a 'stable', non-meandering, version of the Agulhas Current. This was determined by making use of the downstream trajectory speeds of the Argo floats and positioning in relation to sea surface velocities on the day of deployment.

- An evolution of volume transport, heat and salt fluxes was determined for the Argo August Experiment and the matching geographical positions within the model. Using model transects extended both with depth and distance offshore to capture the full Agulhas Current also exhibited evolution from north to south in volume transport (54.17 - 121.79 Sv), heat flux (2.88 - 5.98 PW) and salt flux (1.96 - 4.40 x 10^{12} kg s^{-1}).

Undertaking surveys across the Agulhas Current is time-consuming and changes can take place within the system (Casal et al., 2009). Two recent surveys of the Transkei shelf extending from Port Shepstone to Port Elizabeth, whereby 38 transects were undertaken from depths of 20 km for the shallowest station to the 1000 m isobath, took 30 days to complete (Russo et al., 2019; Barlow et al., 2020). The Argo floats deployed for this experiment exited the non-meandering section of the Agulhas Current in 9 - 12 days, capturing profiles of the water column from 1000 m to the surface, providing the first near-real time synoptic survey of the Agulhas Current. Making use of this method of surveying the Agulhas Current, along with detailed multi-disciplinary CTD casts in month-long surveys or by means of moored arrays (all of which greatly relies on research funding), would greatly augment the current understanding of the Agulhas Current.

An additional recommendation to improve this type of surveying is further suggested:

- Argo floats should ideally be set to park and profile from 2000 m to the surface instead of 1000 m on a daily profiling frequency (as stated previously). This would mean that Argo floats would not capture the shelf region along the east coast of South Africa, and the Agulhas Current core is known to be as little as 20 km from the coast at times (Bryden et al., 2005; Beal et al., 2015). Thus shelf propagating Argo floats, either set to very shallow park and profile depths or floats especially designed for shelf work, would need to be deployed in tandem to standard profiling floats to capture the full dynamics of the Agulhas Current.

Finally, if this method of surveying the Agulhas Current is considered a viable possibility, Argo floats should be deployed at least every three months to capture dynamics across all the seasons. This may seem like an exorbitant cost in terms of instrumentation, data transfer and the fact that Argo floats are lost from the Agulhas Current system in 10 - 15 days. A survey of the Transkei coastline off the east coast of South Africa using a research vessel (Russo et al., 2019) would cost in the region of R 5.25 million (35 days at roughly R 150 000 per day). To undertake this full survey every three months would amount to R 21 million per year. In comparison, six standard Argo floats cost approximately R 1.8 million and 24 floats for the four surveys would total R 7.2 million. Even with data transfer costs, data processing through an Argo data center, and the use of a small boat operating out of Durban for roughly three days per survey to deploy these 24 floats, the costs would not exceed R 10 million, more than half what the vessel surveys would cost. If biogeochemical floats are considered instead of standard floats (hence doubling the cost of floats), the costs would still not exceed those of the vessel surveys. Notably, it is not as straight forward as a basic costing given Argo floats will never replace the multi-disciplinary value a research vessel undertaking work 24 hours a day is able to produce. However, careful and innovative ways of studying the Agulhas Current need to be considered if we ever hope to fully appreciate and understand this current and how it is changing over time.

6.4 What are the impacts and benefits of altered Argo mission parameters on data acquisition in the Indian Ocean?

The Argo Program was initiated in 1999, with the first floats deployed the same year (Riser et al., 2016), providing full global coverage of the oceans since 2006 (Roemmich et al., 2019). The original objective of the program was to systematically monitor the global oceans in real-time, to understand the change occurring within the system, and its subsequent impacts on the global climate (Riser et al., 2016). Fast forward nearly 20 years and the Argo program has become the most successful of all the global ocean observation systems, accumulating over 2 million profiles in a little over 18 years (Riser et al., 2016; Roemmich et al., 2019). A World Ocean Database assessment of subsurface profiles of temperature and salinity to at least 1000 m amounted to just over half a million profiles in 100 years. The Argo program quadrupled this work in a fifth of the time taken, providing global coverage without regional bias. Naturally some regions remain understudied, such as the winter ice-covered regions, marginal seas less than 2000 m deep, the deep oceans beyond 2000 m and the equatorial regions where Argo floats on standard profiling missions of 10 days are quickly moved away from the equator due to Coriolis forcing (Roemmich et al., 2019).

Many global ocean observing systems have looked to the Argo program's success to improve their own systems as was noted at the recent Ocean Obs '19 conference. The Argo Program is also looking at increasing its capabilities with a number of initiatives including incorporating biogeochemical sensors onto floats, developing floats with a capacity of 4000 m and 6000 m to start exploring the abyssal ocean and increased observations in Western Boundary Currents and Marginal Seas (Roemmich et al., 2019). The most efficient way of doing the latter would be to alter the profiling mission of the Argo floats to shallower park and profile depths and higher resolution of profiling. This thesis has shown the success of using an altered profiling mission to study cyclonic mesoscale eddies and the Agulhas Current.

This is relatively easy to implement for countries with healthy economies who are able to support ocean research within their own territorial waters as well as extend observations for the greater good of global climate science to the open ocean and regions of interest. This is far more difficult for countries whose primary focus is poverty alleviation, deadly virus eradication such as malaria, AIDS and cholera, and with a focus on coastal and shelf regions where subsistence fishers focus daily to feed their families. This is largely the case for the entire of the Indian Ocean rim countries with the exception of Australia, and South Africa and India to some degree. The Indian Ocean has also been shown to be the fastest warming ocean on the planet (Roxy et al., 2014), with an increase in devastating CAT5 tropical cyclones making landfall (Fitchett, 2018) as was the case in March and April 2019 with Cyclone Idai and Cyclone Kenneth destroying large swaths of the Mozambican coastline six weeks apart from one another.

Arguably, in order to support coastal communities against devastating cyclonic storms resulting storm surges and extreme events, work with fishing communities to find healthy stocks of fish and protect the livelihoods of millions of people residing in coastal communities around the Indian Ocean, a much greater

understanding of the Indian Ocean is desperately required. Additional concerns such as pirates, intense weather systems and the sheer size of the Indian Ocean pose great difficulties to undertaking this work. This is where Argo float technology, adapted for turbulent regions and Western Boundary Currents where required, with deep and biogeochemical measurements to augment the suite of measurements being made and even developments in to coastal floats to allow for shelf measurements, would assist in the solution.

No singular ocean observing system will hold all the answers, and nor should any project, regional ocean observing system or country assume otherwise. The incredible demands on data archiving, processing and dissemination systems would attest to this. However, looking to multiple systems, each with their own unique capabilities at addressing problems, would be ideal and should be implemented globally.

6.5 Future work within the Greater Agulhas Current System

This thesis has shown the evolution of physical properties of cyclonic mesoscale eddies, spawned off South West Madagascar and propagating westwards across the southern Mozambique Channel (Chapter 4). However, the subsurface interaction of these cyclonic eddies with the shelf edge prior to the fluxes joining up with the Agulhas Current remains a gap. From the two cyclonic eddies studied and the eight Argo floats deployed, one of these floats remained within a cyclonic eddy, to interact with the shelf region and propagate southwestwards with the Agulhas Current. Using theoretical studies on eddy interactions with meridional boundaries (Nof, 1999) and surface tracking studies already undertaken in this region (Braby et al., 2016), the subsurface shelf region interaction of cyclonic eddies with the Agulhas Current using this one float should be explored further.

While the thesis concentrated on Argo floats deployed in two Madagascar cyclonic eddies, similar float deployments into both cyclonic and anticyclonic eddies simultaneously would enhance the understanding of subsurface eddy dynamics propagating across the Mozambique channel from Madagascar (as described in Section 6.2). Additionally, seeding Argo floats into eddies propagating southwards through the Mozambique Channel would also increase the understanding of these source water region eddies to the Agulhas Current.

The work in this thesis has also shown the evolution of physical properties along the Agulhas Current (Chapter 5) and the downstream evolution of fluxes and properties of the Agulhas Current during a non-meandering situation. Future work could look at how these fluxes change during a meander event, should deployment in to a successful Natal Pulse (i.e. one that maintains its structure as far south as Port Elizabeth) be achieved. Recent surveys of a meandering and non-meandering state of the Agulhas Current indicated that the volume transport of the Agulhas Current remains constant (Leber and Beal, 2014) at 34° S. Though how this meandering impacts the heat and salt fluxes and the evolution of the volume transport and fluxes from north to south could be explored further.

Finally, with regular monitoring of the Agulhas Current using Argo floats, a climatology of near-real time data can be built up which would assist with trend analysis, particularly for rainfall, over the east coast of South Africa. This current is intimately connected to the atmosphere in this region, which has direct impacts on rainfall, leading river and estuarine flooding (or lack thereof), which in turn impacts subsistence fishers and communities along the Transkei coast. Argo float data are assimilated into global coupled-climate forecast models in near-real time, providing immediate benefit to forecast systems. Thus, ocean robots, extremely remote to the real-life hardships of poverty alleviation, could be the very connections needed to solving very real world problems.

Bibliography

Argo (2000). "Argo float data and metadata from Global Data Assembly Centre (Argo GDAC)". In: *SEANOE*. DOI: http://doi.org/10.17882/42182.

Backeberg, B. C. and C. J. C. Reason (2010). "A connection between the South Equatorial Current north of Madagascar and Mozambique Channel eddies". In: *Geophys. Res. Lett.* 37.4.

Barceló-Llull, B. et al. (2017). "Anatomy of a subtropical intrathermocline eddy". In: *Deep-Sea Res. I* 124, pp. 126–139.

Barlow, R. et al. (2017). "Phytoplankton communities and acclimation in a cyclonic eddy in the southwest Indian Ocean". In: *Deep-Sea Res. I* 124, pp. 18–30. DOI: 10.1016/j.dsr.2017.03.013.

Barlow, R. et al. (2020). "Phytoplankton adaptation and absorption properties in an Agulhas Current ecosystem". In: *Deep Sea Research Part I: Oceanographic Research Papers*, p. 103209.

Beal, L.M. (2009). "A time series of Agulhas Undercurrent transport". In: *Journal of Physical Oceanography* 39.10, pp. 2436–2450.

Beal, L.M. and H.L. Bryden (1997). "Observations of an Agulhas undercurrent". In: *Deep-Sea Res. I* 44.9-10, pp. 1715–1724.

— (1999). "The velocity and vorticity structure of the Agulhas Current at 32 S". In: *Journal of Geophysical Research: Oceans* 104.C3, pp. 5151–5176.

Beal, L.M. and S. Elipot (2016). "Broadening not strengthening of the Agulhas Current since the early 1990s". In: *Nature* 540.7634, pp. 570–573.

Beal, L.M. et al. (2006). "The sources and mixing characteristics of the Agulhas Current". In: *J. Phys. Oceanogr.* 36.11, pp. 2060–2074.

Beal, L.M. et al. (2011). "On the role of the Agulhas system in ocean circulation and climate". In: *Nature* 472.7344, pp. 429–436.

Beal, L.M. et al. (2015). "Capturing the transport variability of a western boundary jet: Results from the Agulhas Current Time-Series Experiment (ACT)". In: *Journal of Physical Oceanography* 45.5, pp. 1302–1324.

Beron-Vera, F.J. et al. (2013). "Objective detection of oceanic eddies and the Agulhas leakage". In: *J. Phys. Oceanogr.* 43.7, pp. 1426–1438.

Biastoch, A. et al. (1999). "The importance of flow in the Mozambique Channel to seasonality in the greater Agulhas Current system". In: *Geophys. Res. Lett.* 26.21, pp. 3321–3324.

Braby, L. et al. (2016). "Observed eddy dissipation in the Agulhas Current". In: *Geophys. Res. Lett* 43.15, pp. 8143–8150.

Bryden, H.L. and L.M. Beal (2001). "Role of the Agulhas Current in Indian Ocean circulation and associated heat and freshwater fluxes". In: *Deep Sea Research Part I: Oceanographic Research Papers* 48.8, pp. 1821–1845.

Bryden, H.L., L.M. Beal, and L.M. Duncan (2005). "Structure and transport of the Agulhas Current and its temporal variability". In: *J. Phys. Oceanogr.* 61.3, pp. 479–492.

Cabanes, C. et al. (2013). "The CORA dataset: validation and diagnostics of in-situ ocean temperature and salinity measurements". In: *Ocean Sci.* 9.1, pp. 1–18.

Casal, T.G.D. et al. (2009). "Structure and downstream evolution of the Agulhas Current system during a quasi-synoptic survey in February–March 2003". In: *Journal of Geophysical Research: Oceans* 114.C3.

Casanova-Masjoan, M. et al. (2017). "Characteristics and evolution of an Agulhas ring". In: *J. Geophys. Res.: Oceans* 122.9, pp. 7049–7065.

Celliers, L. and M.H. Schleyer (2002). "Coral bleaching on high-latitude marginal reefs at Sodwana Bay, South Africa". In: *Mar. Pollut. Bull.* 44.12, pp. 1380–1387.

Chaigneau, A., G. Eldin, and B. Dewitte (2009). "Eddy activity in the four major upwelling systems from satellite altimetry (1992–2007)". In: *Prog. Oceanogr.* 83.1-4, pp. 117–123.

Chaigneau, A. et al. (2011). "Vertical structure of mesoscale eddies in the eastern South Pacific Ocean: A composite analysis from altimetry and Argo profiling floats". In: *J. Geophys. Res.* 116.C11.

Chelton, D. B. et al. (1998). "Geographical variability of the first baroclinic Rossby radius of deformation". In: *J. Phys. Oceanogr.* 28.3, pp. 433–460.

Chelton, D. B., M. G. Schlax, and R. M. Samelson (2011). "Global observations of nonlinear mesoscale eddies". In: *Prog. Oceanogr.* 91.2, pp. 167–216.

Collins, C., J. C. Hermes, and C. J. C. Reason (2014). "Mesoscale activity in the Comoros Basin from satellite altimetry and a high-resolution ocean circulation model". In: *J. Geophys. Res.* 119.8, pp. 4745–4760.

Cushman-Roisin, B. (1994). *Introduction to Geophysical Fluid Dynamics*. Englewood Cliffs: Prentice-Hall.

De Ruijter, W. P. M. et al. (2002). "Observations of the flow in the Mozambique Channel". In: *Geophys. Res. Lett.* 29.10, pp. 140–1.

De Ruijter, W. P. M. et al. (2004). "Eddies and dipoles around South Madagascar: formation, pathways and large-scale impact". In: *Deep-Sea Res. I* 51.3, pp. 383–400.

Dencausse, G., M. Arhan, and S. Speich (2010). "Routes of Agulhas rings in the southeastern Cape Basin". In: *Deep Sea Research Part I: Oceanographic Research Papers* 57.11, pp. 1406–1421.

Desbruyeres, D. et al. (2017). "Global and full-depth ocean temperature trends during the early twenty-first century from Argo and repeat hydrography". In: *Journal of Climate* 30.6, pp. 1985–1997.

Dilmahamod, A.F. et al. (2018). "SIDDIES Corridor: A Major East-West Pathway of Long-Lived Surface and Subsurface Eddies Crossing the Subtropical South Indian Ocean". In: *J. Geophys. Res.* 123.8, pp. 5406–5425.

Dong, C. et al. (2014). "Global heat and salt transports by eddy movement". In: *Nature Communications* 5.

Donohue, K.A. and J.M. Toole (2003). "A near-synoptic survey of the Southwest Indian Ocean". In: *Deep-Sea Res. II* 50.12-13, pp. 1893–1931.

Duacs/AVISO (2014). "A New Version of Ssalto/Duacs Products Available in April 2014, Version 1.1, CNES". In:

Emery, W.J. (2001). "Water types and water masses". In: *Encyclopedia of Ocean Sciences* 6, pp. 3179–3187.

Fine, R.A. (1993). "Circulation of Antarctic intermediate water in the South Indian Ocean". In: *Deep-Sea Res. I* 40.10, pp. 2021–2042.

Fitchett, J.M. (2018). "Recent emergence of CAT5 tropical cyclones in the South Indian Ocean". In: *South African Journal of Science* 114.11-12, pp. 1–6.

Frajka-Williams, E. et al. (2019). "Atlantic Meridional Overturning Circulation: Observed transports and variability". In: *Frontiers in Marine Science* 6, p. 260.

Gasparin, F. et al. (2018). "A large-scale view of oceanic variability from 2007 to 2015 in the global high resolution monitoring and forecasting system at Mercator Océan". In: *Journal of Marine Systems* 187, pp. 260–276.

Gründlingh, M. L., R. A. Carter, and R. C. Stanton (1991). "Circulation and water properties of the southwest Indian Ocean". In: *Prog. Oceanogr.* 28.4, pp. 305–342.

Gründlingh, M.L. (1980). "On the volume transport of the Agulhas Current". In: *Deep Sea Research Part A. Oceanographic Research Papers* 27.7, pp. 557–563.

Haller, G. and F.J. Beron-Vera (2013). "Coherent Lagrangian vortices: The black holes of turbulence". In: *J. Fluid Mech.* 731.

Halo, I. et al. (2014a). "Eddy properties in the Mozambique Channel: A comparison between observations and two numerical ocean circulation models". In: *Deep-Sea Res. II* 100, pp. 38–53.

Halo, I. et al. (2014b). "Mesoscale eddy variability in the southern extension of the East Madagascar Current: Seasonal cycle, energy conversion terms, and eddy mean properties". In: *J. Geophys. Res.* 119.10, pp. 7324–7356.

Hermes, J. C., C. J. C. Reason, and J. R. E. Lutjeharms (2007). "Modeling the variability of the greater Agulhas Current system". In: *J. Climate* 20.13, pp. 3131–3146.

Hood, R.R. et al. (2016). "The 2nd International Indian Ocean Expedition (IIOE-2): Motivating New Exploration in a Poorly Understood Basin." In: *Limnology and Oceanography Bulletin* 25.4, pp. 117–124.

Hu, S. and A.V. Fedorov (2019). "Indian Ocean warming can strengthen the Atlantic meridional overturning circulation". In: *Nature Climate Change* 9.10, pp. 747–751.

Inoue, R. et al. (2016a). "Western north Pacific integrated physical-biogeochemical ocean observation experiment (INBOX): part 1. Specifications and chronology of the S1-INBOX floats". In: *J. Mar. Res.* 74.2, pp. 43–69.

Inoue, R. et al. (2016b). "Western North Pacific Integrated Physical-Biogeochemical Ocean Observation Experiment (INBOX): Part 2. Biogeochemical responses to eddies and typhoons revealed from the S1 mooring and shipboard measurements". In: *J. Mar. Res.* 74.2, pp. 71–99.

Kouketsu, S. et al. (2016). "Mesoscale eddy effects on temporal variability of surface chlorophyll a in the Kuroshio Extension". In: *J. Oceanogr.* 72.3, pp. 439–451.

Krug, M and Jean Tournadre (2012). "Satellite observations of an annual cycle in the Agulhas Current". In: *Geophys. Res. Lett.* 39.15.

Lamont, T., M.A. Van Den Berg, and R.G. Barlow (2016). "Agulhas Current Influence on the Shelf Dynamics of the KwaZulu-Natal Bight". In: *Journal of Physical Oceanography* 46.4, pp. 1323–1338.

Law, C.S. et al. (2001). "A Lagrangian SF6 tracer study of an anticyclonic eddy in the North Atlantic: Patch evolution, vertical mixing and nutrient supply to the mixed layer". In: *Deep-Sea Res. II* 48.4-5, pp. 705–724.

Le Bars, D., W.P.M. De Ruijter, and H.A. Dijkstra (2012). "A new regime of the Agulhas Current retroflection: Turbulent choking of Indian–Atlantic leakage". In: *Journal of Physical Oceanography* 42.7, pp. 1158–1172.

Leber, G.M. and L.M. Beal (2014). "Evidence that Agulhas Current transport is maintained during a meander". In: *J. Geophys. Res.: Oceans* 119.6, pp. 3806–3817.

Lee, S-K. et al. (2015). "Pacific origin of the abrupt increase in Indian Ocean heat content during the warming hiatus". In: *Nature Geoscience* 8.6, p. 445.

Lewis, J.K., A.D. Kirwan Jr, and G.Z. Forristall (1989). "Evolution of a warm-core ring in the Gulf of Mexico: Lagrangian observations". In: *J. Geophys. Res.: Oceans* 94.C6, pp. 8163–8178.

Li, C. et al. (2017). "A statistical study on the subthermocline submesoscale eddies in the northwestern Pacific Ocean based on Argo data". In: *J. Geophys. Res.* 122.5, pp. 3586–3598.

Lutjeharms, J. R. E. (1988). "Remote sensing corroboration of retroflection of the East Madagascar Current". In: *Deep-Sea Res. II* 35.12, pp. 2045–2050.

Lutjeharms, J.R.E. (2006). *The Agulhas Current*. Vol. 2. Springer.

Lutjeharms, J.R.E. and R.C. Van Ballegooyen (1988). "The retroflection of the Agulhas Current". In: *Journal of Physical Oceanography* 18.11, pp. 1570–1583.

Ma, Q. et al. (2019). "Intensified Deep Ocean Variability Induced by Topographic Rossby Waves at the Pacific Yap-Mariana Junction". In: *Journal of Geophysical Research: Oceans* 124.11, pp. 8360–8374.

McMonigal, K. et al. (2020). "The impact of meanders, deepening and broadening, and seasonality on Agulhas Current temperature variability". In: *Journal of Physical Oceanography* In review.

McWilliams, J. C. and G. R. Flierl (1979). "On the evolution of isolated non-linear vortices". In: *J. Phys. Oceanogr.* 9, pp. 1155–1182.

Menezes, V.V. et al. (2016). "Interannual variability of the South Indian Countercurrent". In: *J. Geophys. Res.: Oceans* 121.5, pp. 3465–3487.

Morris, T. (2009). *Physical oceanography of Sodwana Bay and its effect on larval transport and coral bleaching*. MTech Thesis, Cape Peninsula University of Technology.

Morris, T., T. Lamont, and M.J. Roberts (2013). "Effects of deep-sea eddies on the northern KwaZulu-Natal shelf, South Africa". In: *Afr. J. Mar. Sci.* 35.3, pp. 343–350.

Morris, T. et al. (2017). "The importance of monitoring the Greater Agulhas Current and its inter-ocean exchanges using large mooring arrays". In: *S. Afr. J Sci.* 113.7-8, pp. 1–7.

Morris, T. et al. (2019). "Lagrangian evolution of two Madagascar cyclonic eddies: Geometric properties, vertical structure, and fluxes". In: *Journal of Geophysical Research: Oceans*.

Nauw, J. J. et al. (2008). "Observations of the southern East Madagascar Current and undercurrent and countercurrent system". In: *J. Geophys. Res.* 113.C8, p. C08006.

New, A. L. et al. (2007). "On the circulation of water masses across the Mascarene Plateau in the South Indian Ocean". In: *Deep-Sea Res. I* 54.1, pp. 42–74.

Ning, J. et al. (2019). "Impact of Cyclonic Ocean Eddies on Upper Ocean Thermodynamic Response to Typhoon Soudelor". In: *Remote Sens.* 11.8, p. 938.

Nkwinkwa Njouodo, A.S. et al. (2018). "Atmospheric signature of the Agulhas Current". In: *Geophysical Research Letters* 45.10, pp. 5185–5193.

Nof, D. (1999). "Strange encounters of eddies with walls". In: *Journal of Marine Research* 57.5, pp. 739–761.

Noyon, M. et al. (2018). "Plankton distribution within a young cyclonic eddy off south-western Madagascar". In: *Deep-Sea Res. II*.

Ockhuis, S. et al. (2017). "The 'suitcase hypothesis': Can entrainment of meroplankton by eddies provide a pathway for gene flow between Madagascar and KwaZulu-Natal, South Africa?" In: *Afr. J. Mar. Sci.* 39.4, pp. 435–451.

Okubo, A. (1970). "Horizontal dispersion of floatable particles in the vicinity of velocity singularities such as convergences". In: *Deep Sea Research and Oceanographic Abstracts*. Vol. 17. 3. Elsevier, pp. 445–454.

Palastanga, V. (2007). "Oceanic variability around Madagascar: connections to the large-scale Indian Ocean circulation and its forcing". PhD thesis. Utrecht University.

Pegliasco, C., A. Chaigneau, and R. Morrow (2015). "Main eddy vertical structures observed in the four major Eastern Boundary Upwelling Systems". In: *J. Geophys. Res.* 120.9, pp. 6008–6033.

Penven, P. et al. (2005). "Average circulation, seasonal cycle, and mesoscale dynamics of the Peru Current System: A modeling approach". In: *J. Geophys. Res.* 110.C10.

Pérez, J.J.S. (2003). "Evolution of the open-sea eddy ALGERS'98 in the Algerian Basin with Lagrangian trajectories and remote sensing observations". In: *J. Mar. Syst.* 43.3-4, pp. 105–131.

Pivan, X., M. Krug, and S. Herbette (2016). "Observations of the vertical and temporal evolution of a Natal Pulse along the Eastern Agulhas Bank". In: *Journal of Geophysical Research: Oceans* 121.9, pp. 7108–7122.

Ponsoni, L. et al. (2016). "The East Madagascar Current: Volume transport and variability based on long-term observations". In: *J. Phys. Oceanogr.* 46.4, pp. 1045–1065.

Qiu, B. and S. Chen (2005). "Eddy-induced heat transport in the subtropical North Pacific from Argo, TMI, and altimetry measurements". In: *J. Phys. Oceanogr.* 35.4, pp. 458–473.

Quadfasel, D.R. and J.C. Swallow (1986). "Evidence for 50-day period planetary waves in the South Equatorial Current of the Indian Ocean". In: *Deep-Sea Res.* 33.10, pp. 1307–1312.

Quartly, G. D. and M. A. Srokosz (2004). "Eddies in the southern Mozambique Channel". In: *Deep-Sea Res. II* 51.1-3, pp. 69–83.

Quartly, G.D. et al. (2006). "Eddies around Madagascar – The retroflection re-considered". In: *J. Mar. Syst.* 63.3, pp. 115–129.

Ramanantsoa, J.D. et al. (2018a). "Coastal upwelling south of Madagascar: Temporal and spatial variability". In: *J. Mar. Syst.* 178, pp. 29–37.

Ramanantsoa, J.D. et al. (2018b). "Uncovering a new current: The Southwest MAdagascar coastal current". In: *Geophys. Res. Lett.* 45.4, pp. 1930–1938.

Rao, S.A. et al. (2012). "Why is Indian Ocean warming consistently?" In: *Climatic change* 110.3-4, pp. 709–719.

Renault, L., J.C. McWilliams, and P. Penven (2017). "Modulation of the Agulhas Current retroflection and leakage by oceanic current interaction with the atmosphere in coupled simulations". In: *Journal of Physical Oceanography* 47.8, pp. 2077–2100.

Rhein, M. et al. (2013). "Observations: Ocean". In: *Climate Change 2013: The Physical Science Basis. Contribution of Working Group I to the Fifth Assessment Report of the Intergovernmental Panel on Climate Change*.

Ridderinkhof, W. et al. (2013). "Dipoles of the south east Madagascar Current". In: *Geophys. Res. Lett.* 40.3, pp. 558–562.

Riser, S. C. et al. (2016). "Fifteen years of ocean observations with the global Argo array". In: *Nat. Clim. Change* 6.2, p. 145.

Roberts, M.J. et al. (2006). "Oceanographic environment of the Sodwana Bay coelacanths (Latimeria chalumnae), South Africa". In: *S. Afr. J Sci.* 102.9-10, pp. 435–443.

Roberts, M.J. et al. (2010). "Shelf currents, lee-trapped and transient eddies on the inshore boundary of the Agulhas Current, South Africa: their relevance to the KwaZulu-Natal sardine run". In: *Afr. J. Mar. Sci.* 32.2, pp. 423–447.

Robinson, A. R. (1983). "Overview and summary of eddy science". In: *Eddies in marine science*. Springer, pp. 3–15.

Roemmich, D. et al. (2019). "On the future of Argo: A global, full-depth, multi-disciplinary array". In: *Frontiers in Marine Science* 6.

Rouault, M.J. and P. Penven (2011). "New perspectives on Natal Pulses from satellite observations". In: *J. Geophys. Res.: Oceans* 116.C7.

Roxy, M.K. et al. (2014). "The curious case of Indian Ocean warming". In: *Journal of Climate* 27.22, pp. 8501–8509.

Ruijter, W. P. M. de et al. (1999). "Indian-Atlantic interocean exchange: Dynamics, estimation and impact". In: *J. Geophys. Res.* 104.C9, pp. 20885–20910.

Russo, C.S. et al. (2019). "Hydrography of a shelf ecosystem inshore of a major Western Boundary Current". In: *Estuarine, Coastal and Shelf Science* 228, p. 13.

Samelson, R. M., M. G. Schlax, and D. B. Chelton (2014). "Randomness, symmetry, and scaling of mesoscale eddy life cycles". In: *J. Phys. Oceanogr.* 44.3, pp. 1012–1029.

Sangrà, P. et al. (2005). "Life history of an anticyclonic eddy". In: *J. Geophys. Res.* 110.C3.

Sangrà, P. et al. (2007). "On the nature of oceanic eddies shed by the Island of Gran Canaria". In: *Deep-Sea Res. I* 54.5, pp. 687–709.

Schott, F. et al. (1988). "The boundary currents east and north of Madagascar: 2. Direct measurements and model comparisons". In: *J. Geophys. Res.* 93.C5, pp. 4963–4974.

Schott, F. A. and J. P. McCreary (2001). "The monsoon circulation of the Indian Ocean". In: *Prog. Oceanogr.* 51.1, pp. 1–123.

Schott, F. A., S.-P. Xie, and J. P. McCreary (2009). "Indian Ocean circulation and climate variability". In: *Rev. Geophys.* 47.1, RG1002.

Schouten, M. W., W. P. M. de Ruijter, and P. J. van Leeuwen (2002). "Upstream control of Agulhas Ring shedding". In: *J. Geophys. Res.* 107.C8, pp. 23–1.

Siedler, G., M. Rouault, and J. R. E. Lutjeharms (2006). "Structure and origin of the subtropical South Indian Ocean Countercurrent". In: *Geophys. Res. Lett.* 33.24.

Siedler, G. et al. (2009). "Modes of the southern extension of the East Madagascar Current". In: *J. Geophys. Res.* 114.C1.

Souza, J. M. A. C. et al. (2011). "Estimation of the Agulhas Ring impacts on meridional heat fluxes and transport using ARGO floats and satellite data". In: *Geophys. Res. Lett.* 38.21.

Storto, A. et al. (2019). "Ocean reanalyses: recent advances and unsolved challenges". In: *Frontiers in Marine Science* 6, p. 418.

Stramma, L. and J. R. E. Lutjeharms (1997). "The flow field of the subtropical gyre of the South Indian Ocean". In: *J. Geophys. Res.* 102.C3, pp. 5513–5530.

Swallow, J., M. Fieux, and F. Schott (1988). "The boundary currents east and north of Madagascar: 1. Geostrophic currents and transports". In: *J. Geophys. Res.* 93.C5, pp. 4951–4962.

Talley, L.D. et al. (2011). *Descriptive physical oceanography: An introduction*. Academic press.

Ternon, J.F. et al. (2014). "In situ measured current structures of the eddy field in the Mozambique Channel". In: *Deep-Sea Res. II* 100, pp. 10–26.

Tillinger, D. and A.L. Gordon (2010). "Transport weighted temperature and internal energy transport of the Indonesian Throughflow". In: *Dynamics of Atmospheres and Oceans* 50.2, pp. 224–232.

Tomczak, M. and J.S. Godfrey (1994). *Regional Oceanography: an Introduction*. Pergamon.

Toole, J.M. and B.A. Warren (1993). "A hydrographic section across the subtropical South Indian Ocean". In: *Deep Sea Research Part I: Oceanographic Research Papers* 40.10, pp. 1973–2019.

Tsugawa, M. and H. Hasumi (2010). "Generation and growth mechanism of the Natal Pulse". In: *J. Phys. Oceanogr.* 40.7, pp. 1597–1612.

Tyson, P.D. and R.A. Preston-Whyte (2000). *Weather and climate of Southern Africa*. Oxford University Press.

Ullgren, J. E. et al. (2012). "The hydrography of the Mozambique Channel from six years of continuous temperature, salinity, and velocity observations". In: *Deep-Sea Res. I* 69, pp. 36–50.

Van Aken, H.M. et al. (2003). "Observations of a young Agulhas Ring, Astrid, during MARE in March 2000". In: *Deep-Sea Res. II* 50.1, pp. 167–195.

Weiss, J. (1991). "The dynamics of enstrophy transfer in two-dimensional hydrodynamics". In: *Physica D: Nonlinear Phenomena* 48.2-3, pp. 273–294.

Wyrtki, K. (1971). *Oceanographic atlas of the international Indian Ocean expedition*. National Science Foundation.

You, Y. (1998). "Intermediate water circulation and ventilation of the Indian Ocean derived from water-mass contributions". In: *J. Mar. Res.* 56.5, pp. 1029–1067.

Zhang, W-Z. et al. (2015a). "Dynamical processes within an anticyclonic eddy revealed from Argo floats". In: *Geophys. Res. Lett.* 42.7, pp. 2342–2350.

Zhang, Z. et al. (2015b). "Subthermocline eddies observed by rapid-sampling Argo floats in the subtropical northwestern Pacific Ocean in Spring 2014". In: *Geophys. Res. Lett.* 42.15, pp. 6438–6445.